AD-A060 120 MASSACHUSETTS INST OF TECH CAMBRIDGE LAB FOR MFG AND--ETC F/G 11/11
EFFECT OF ABRASIVE GRIT SIZE ON ABRASIVE WEAR.(U)
JUN 78 N P SUH, N SAKA, H SIN N00014-76-C-0068
UNCLASSIFIED NL

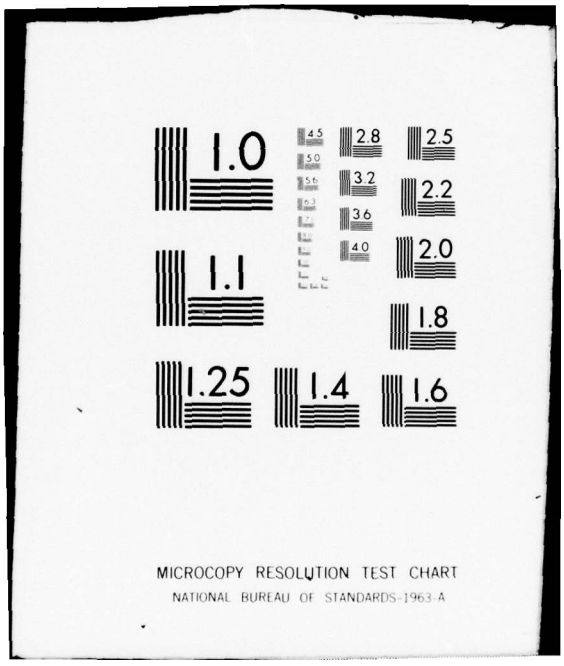
1.0
1.1
1.25
1.4
1.6
1.8
2.0
2.2
2.5
2.8
3.2
3.6
4.0
4.5
5.0
5.6
MICROCOPY RESOLUTION TEST CHART
NATIONAL BUREAU OF STANDARDS-1963-A

Effect of Abrasive Grit Size on Abrasive Wear

Progress Report to
The Advanced Research Projects Agency, DOD
Contract No. N00014-76-C-0068

Nam P. Suh
Nannaji Saka
Hyo-Chol Sin

Laboratory for Manufacturing and Productivity
School of Engineering
Massachusetts Institute of Technology
Cambridge, Massachusetts 02139

June 1978

(12)

EFFECT OF ABRASIVE GRIT SIZE ON ABRASIVE WEAR

Progress Report

to

The Advanced Research Projects Agency, DOD
Contract No. N00014-76-C-0068

Nam P. Suh

Nannaji Saka

Hyo-Chol Sin

Laboratory for Manufacturing and Productivity
School of Engineering
Massachusetts Institute of Technology
Cambridge, Massachusetts 02139

June 1978

Unclassified

SECURITY CLASSIFICATION OF THIS PAGE (When Data Entered)

REPORT DOCUMENTATION PAGE

READ INSTRUCTIONS BEFORE COMPLETING FORM

1. REPORT NUMBER ----------

2. GOVT ACCESSION NO. ---------- (9)

3. RECIPIENT'S CATALOG NUMBER ---------- Progress Rept.

4. TITLE (and Subtitle)

(6) Effect of Abrasive Grit Size on Abrasive Wear
Progress Report

5. TYPE OF REPORT & PERIOD COVERED
January 1, 1977-
December 31, 1977

6. PERFORMING ORG. REPORT NUMBER ---

7. AUTHOR(s)

(10) Nam P. Suh, Nannaji Saka and Hyo-Chol Sin

8. CONTRACT OR GRANT NUMBER(s)
(15) N00014-76-C-0068

9. PERFORMING ORGANIZATION NAME AND ADDRESS
Laboratory for Manufacturing and Productivity
~~School of Engineering~~ New
Massachusetts Institute of Technology

10. PROGRAM ELEMENT, PROJECT, TASK AREA & WORK UNIT NUMBERS
---

11. CONTROLLING OFFICE NAME AND ADDRESS
(11) Department of the Navy
Office of Naval Research
Arlington, Virginia 22217 N00014

12. REPORT DATE
June 1978

13. NUMBER OF PAGES
128

14. MONITORING AGENCY NAME & ADDRESS(if different from Controlling Office)
Office of Naval Research
M.I.T. Resident Representative
Room E19-628
Cambridge, Massachusetts 02139 (N66017)
(12) 129 p.

15. SECURITY CLASS. (of this report)
Unclassified

15a. DECLASSIFICATION/DOWNGRADING SCHEDULE
----

16. DISTRIBUTION STATEMENT (of this Report)

The distribution of this document is unlimited.

17. DISTRIBUTION STATEMENT (of the abstract entered in Block 20, if different from Report)

18. SUPPLEMENTARY NOTES

19. KEY WORDS (Continue on reverse side if necessary and identify by block number)

abrasive wear, grit size, groove formation, wear coefficient, real contact area, cutting, plowing, subsurface deformation, sliding wear, ductility

20. ABSTRACT (Continue on reverse side if necessary and identify by block number)

The purpose of the M.I.T. research on wear during the calendar year 1977 was to apply the delamination theory of wear in minimizing the wear rate of splines and door hinges. The technique explored was the use of thin soft metal coatings on hard substrates, which was shown in a prior study to increase the wear resistance by three orders of magnitude. One of the problems concerning the use of thin metal coatings in these appli-

DD FORM 1 JAN 73 1473 EDITION OF 1 NOV 65 IS OBSOLETE
S/N 0102-014-6601

Unclassified 410 897
SECURITY CLASSIFICATION OF THIS PAGE (When Data Entered)

(continuation of block 20)

cations was the possible removal of the coated material by oxides on splines and salts formed on door hinges. Therefore, two-pronged investigations were undertaken in collaboration with NADC and Foxboro/Trans-Sonics, Inc: the realistic evaluation of soft metal coatings and the role of abrasive wear in these applications. This report describes the work done on the basic abrasive wear mechanisms, in particular the size effect of abrasive particles on abrasive wear.

To examine the dependence of abrasive wear of materials on the grit size in detail, tests were conducted on polymethylmethacrylate (PMMA), commercially pure nickel, AISI 1095 steel and OFHC copper using pin-on-disk geometry. The groove formation process on PMMA specimen was directly observed in an optical microscope. Cutting tests with diamond conical tools on AISI 1095 steel were also conducted.

The wear coefficient was found to increase by a factor of 3 from 600 to 60 grit for all materials tested and it was found that the critical grit diameter was about 80 μm. The friction coefficient was found to vary in a similar fashion to the wear coefficient and increased with grit diameter by 20% for all materials. The groove width on PMMA specimens was found to be proportional to the grit size and the number of contacts was inversely proportional to the square of the grit diameter. Estimation of the real contact area from those measurements agreed fairly well with the hardness-applied load relationship.

Experimental data of friction coefficient in abrasion and cutting tests was compared with the theories for such simple shapes as sphere and cone. The composite geometry (cone and sphere) was found to explain the results. This model shows that the contacting part of abrasive will become relatively blunter with decreased grit size. By combining this with the criterion for the mechanical interaction at the specimen-particle interface, the grit size effect is discussed.

The seperation of total external energy into cutting, plowing and subsurface deformation energies is found to explain the grit size effect on abrasive wear semi-quantitatively; the wear coefficient in abrasion is the ratio of the cutting energy to the total external work done. The transition of wear mode from abrasion to sliding wear is discussed by considering the geometry change at the specimen-abrasive interface and the variations in the energy components with decreased abrasive grit size. It is found by estimation that when the grit size is less than about 1 μm the wear is controlled by sliding wear mechanisms. The dependence of the wear coefficient on ductility is also discussed.

There are two major practical implications of this work: First, in lubricated systems abrasive wear caused by hard particles can be eliminated by filtering particles more than 1 μm only. Filtration of abrasive particles smaller than 1 μm will not result in additional reduction wear rate. Conversely, when abrasion is used as a material removal process, the size of the abrasive particles should be greater than 80 μm for maximum productivity. Second, in designing two-phase materials for abrasion wear resistance the size of the hard strengthening phase should be kept below 1 μm to minimize abrasion due to strengthening phase itself. Most of the strengthening schemes fortunately follow this criterion automatically.

ABSTRACT

The purpose of the M.I.T. research on wear during the calendar year 1977 was to apply the delamination theory of wear in minimizing the wear rate of splines and door hinges. The technique explored was the use of thin soft metal coatings on hard substrates, which was shown in a prior study to increase the wear resistance by three orders of magnitude. One of the problems concerning the use of thin metal coatings in these applications was the possible removal of the coated material by oxides on splines and salts formed on door hinges. Therefore, two-pronged investigations were undertaken in collaboration with NADC and Foxboro/Trans-Sonics, Inc: the realistic evaluation of soft metal coatings and the role of abrasive wear in these applications. This report describes the work done on the basic abrasive wear mechanisms, in particular the size effect of abrasive particles on abrasive wear.

To examine the dependence of abrasive wear of materials on the grit size in detail, tests were conducted on polymethylmethacrylate (PMMA), commercially pure nickel, AISI 1095 steel and OFHC copper using pin-on-disk geometry. The groove formation process on PMMA specimen was directly observed in an optical microscope. Cutting tests with diamond conical tools on AISI 1095 steel were also conducted.

The wear coefficient was found to increase by a factor of 3 from 600 to 60 grit for all materials tested and it was found that the critical grit diameter was about 80 μm. The friction coefficient was found to vary in a similar fashion to the wear coefficient and increased with grit diameter by 20% for all materials. The groove width on PMMA specimens was found to be proportional to the grit size and the number of contacts was inversely proportional to the square of the grit diameter. Estimation of the real contact area from those measurements agreed fairly well with the hardness-applied load relationship.

Experimental data of friction coefficient in abrasion and cutting tests was compared with the theories for such simple shapes as sphere and cone. The composite geometry (cone and sphere) was found to explain the results. This model shows that the contacting part of abrasive will become relatively blunter with decreased grit size. By combining this with the criterion for the mechanical interaction at the specimen-particle interface, the grit size effect is discussed.

The separation of total external energy into cutting, plowing and subsurface deformation energies is found to explain the grit size effect on abrasive wear semi-quantitatively; the wear coefficient in abrasion is the ratio of the cutting energy to the total external work done. The transition of wear mode from abrasion to sliding wear is discussed by considering the geometry change at the specimen-abrasive interface and the variations in the energy components with decreased abrasive grit size. It is found by estimation that when the grit size is less than about 1 μm the wear is controlled by sliding wear mechanisms. The dependence of the wear coefficient on ductility is also discussed.

There are two major practical implications of this work: First, in lubricated systems abrasive wear caused by hard particles can be eliminated by filtering particles more than 1 μm only. Filtration of abrasive particles smaller than 1 μm will not result in additional reduction wear rate. Conversely, when abrasion is used as a material removal process, the size of the abrasive particles should be greater than 80 μm for maximum productivity. Second, in designing two-phase materials for abrasion wear resistance the size of the hard strengthening phase should be kept below 1 μm to minimize abrasion due to strengthening phase itself. Most of the strengthening schemes fortunately follow this criterion automatically.

ACKNOWLEDGEMENTS

The work reported in this report was sponsored by the Defense Advanced Research Projects Agency through the Office of Naval Research under contract N00014-76-C-0068. We are grateful to Dr. Edward van Reuth, Dr. Richard S. Miller and Lt. Comdr. William K. Petrovic for their personal support and guidance of our work.

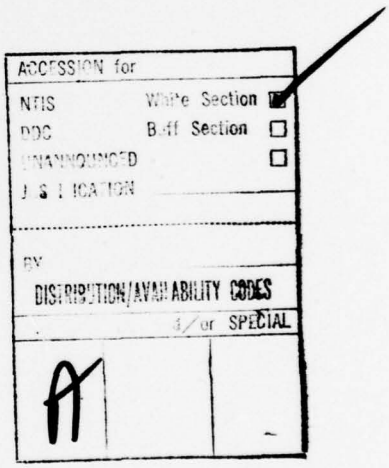

TABLE OF CONTENTS

LIST OF FIGURES

LIST OF FIGURES

LIST OF FIGURES

LIST OF FIGURES

I. INTRODUCTION

Abrasive wear may be caused by a hard rough surface sliding on a soft surface or by hard abrasive particles entrapped between soft sliding surfaces. In both cases surface is damaged by such mechanisms as cutting, plowing, and single or repeated plastic deformation which may lead to subsurface crack nucleation and propagation. While some abrasive particles remove material from the surface in the form of microchips, other contacting particles simply form grooves without removing material by the chip formation process.

For abrasive wear to take place by a cutting mechanism, the abrasive must be harder than the wearing material. Tabor (1) showed that for one material to scratch another it must be at least 20% harder. Richardson (2) showed that the wear resistance increases when the maximum hardness of the surface and the bulk hardness of the material exceed about 80% of the abrasive hardness.

An important characteristic of abrasion is the dependence of wear rate on the particle size. The volume wear increases with grit size up to some critical diameter and then only slowly increases with grit size (3-5) or remains constant (6-12). A great deal of work has been done to explain this size effect by many investigators and several theories have been proposed. These explanations can be classified into two large groups: one being that with decrease of grit size the deterioration (10, 13-16) and imbedding (15, 17) of the abrasive increase and the other that the geometry (8) and the distribution (12, 18) of small abrasive particles are different from those of larger particles.

Avient, Goddard and Wilman (10) studied the abrasion behavior of many materials and concluded that the clogging of the interstices between the finer abrasive grains by wear debris is responsible for the critical size effect. They feel that only a small front region of the specimen contacts the abrasive particles effectively and the remaining rear part slides over the clogged abrasive. Therefore, the friction coefficient and the wear rate decrease rapidly with decrease of the grit diameter. They concluded that this effect would be larger for larger sample sizes. However, according to the results of Larsen-Basse (13), who investigated the effect of the sample size, the difference between wear rates with the long specimen direction parallel and perpendicular to the sliding direction is only 10-30% for the finer grits.

In the study of 3-body abrasion, Rabinowicz (14) explained the effect, based on the surface energy criterion, to be due to the formation of large adhesive wear particles which clog the interstices and interfere with the abrasive action. The deterioration mechanism of the abrasive was studied extensively using the Scanning Electron Microscope (SEM) by Date and Malkin (16). With continued use, the rapid deterioration in performance with finer grits was accompanied by a buildup of metal caused by capping of the abrasive grain tips with metal chips and by clogging. They reported that numerous adhesive wear particles were found for finer grit sizes. Based on this observation, they postulated that the smaller abrasion rate with finer grits is due to abrasive grains making elastic contact with the specimen at loads insufficient for cutting.

The elastic contact hypothesis was first proposed by Larsen-Basse (18),

who measured the size and number of grooves formed on polished copper specimens when they were abraded by silicon carbide abrasive papers. The specimen was moved under load a distance of approximately 1mm, which is a similar technique to that used by Avient, Goddard and Wilman (10) and by Mulhearn and Samuels (8). He estimated the real contact area by summing up the square of the groove width. For the fine grits and the very coarse grit the results show large deviation. From this result and Kragelskii's criterion for the metal-abrasive interaction (19), he postulated that many fine grits have only elastic interaction with the surface. Furthermore, as it is unlikely that the abrasive grits gradually become more angular with increased size, it was speculated that the fraction of the load carried by particles in elastic contact increases with decreased grit size.

Mulhearn and Samuels (8) investigated the structure of silicon carbide abrasive papers and developed a theoretical model of the abrasion process. The shape of contacting particles, their topography in the abrasive paper, their deterioration with use, the fraction of contacting particles which cut a chip, and the rate of change of this factor with use of the paper were studied comprehensively. They concluded that the shapes of the abrasive particles are different for different grades of abrasive and for the fine grains the proportion of acicular particles is much larger and, therefore, the fine grains contain cracks even in the unused condition.

Johnson (17) studied the pickup of abrasive particles in annealed aluminum during abrasion by using electron probe microanalyser. He found that the pickup of abrasive particles by the wearing surface is greater by a factor of 200 for 600 grit than for 240 grit because the former deteriorates

more rapidly. Wilman and co-workers (3, 9-11) observed an increase in the friction coefficient during abrasion with sliding distance, which they attributed to the progressive pickup of emery abrasive.

Recently, Moore and Douthwaite (15) attempted to explain the size effect in terms of the plastic deformation at and below the worn surface. They estimated the equivalent plastic strain and the flow stress as a function of depth below the worn surface and evaluated the work done in deforming the material below the groove and the energy absorbed in plowing the surface. They concluded that the energy expended in plastic deformation of material from the grooves and below the surface accounts for almost all the external work done for all grit sizes in abrasion, and volume wear is dependent on the grit size probably because the deterioration and pickup of abrasive particles become more intense at small grit sizes. Larsen-Basse (13) concluded that the conditioning (such as removal of plastic coat and sharpening by initial fracture) and deterioration of fine grit abrasives is more predominant than for coarse grits; the wear rate will become independent of grit size when the effects of grit wear can be eliminated.

According to Malkin and co-workers (20-22), the total energy in grinding consists of chip formation, plowing, and sliding energies. Rubbing between wear flats on the abrasive grains and the workpiece is one type of sliding processes encountered in grinding. As abrasive grains wear by attrition, the forces and energy associated with this rubbing increase in proportion to the wear flat area. It was argued that the relatively flexible backing of the coated abrasive allows some of grains to come into elastic contact with the metal surface at a load per grain less than that

required to cause plowing or cutting. They concluded that this type of sliding and the increase of plowing energy with decrease of cutting depth, as seen from the experiments with spherical tools, are responsible for the size effect.

Studies of abrasive paper, subsurface deformation, and groove formation (8, 15, 18) show that the size and shape distribution of abrasive particles are similar for all grit sizes. Therefore, the interaction between abrasive particles and material surface also must be understood in terms of geometric similarity, if the packing condition is not different for different grit sizes. Assuming that the abrasive particles are spherical, simple calculation shows that groove geometries are similar and, therefore, the ratios of groove width to grit diameter are the same for all grit sizes. Because of this fact, the size effect cannot be explained clearly by the elastic contact hypothesis or by the plowing energy argument.

The idealized model of abrasion given by Rabinowicz and co-workers (6, 23) provides the theoretical basis for the abrasion, but this model does not predict the grit size effect. The physical interpretations of the wear coefficient K, (based on the ratio of the volume removed as wear particles to the volume deformed) by Shaw (24, 25) and energy argument by Suh (26), make it possible to express the wear coefficient in terms of the groove geometry and all components of energies associated with abrasion. By relating the hardness of material to the specific energy in metal cutting (27), the wear coefficient K is expressed as the ratio of the cutting energy to the total external work done. As will be discussed later in detail, the nature of the deformation process around abrasive particles and the partitioning of the

total energy into each component such as chip formation, plowing and sub-surface deformation energy determines K.

The physical interpretation of the wear coefficient K with relative fractions of the energies, and the observation of sliding wear particles strongly suggest that there is a possibility of the transition with decrease of grit size from cutting mode to sliding mode. The existing theories on the size effect provide only partial answers and some of them are based on incorrect assumptions. The purpose of this study is to understand the abrasive wear mechanisms by investigating the possible causes of grit size effect in abrasive wear and to explore the possibility of the transition from cutting wear to sliding wear as a function of the grit size.

II. EXPERIMENTAL

A. Materials

Polymethylmethacrylate (PMMA), commercially pure nickel, AISI 1095 steel and OFHC copper were chosen for study. The choice of the materials was based on several considerations. PMMA was chosen for its transparency for direct optical observation. Commercially pure nickel was chosen because it has a good work-hardening property. To get spherodized and annealed microstructures, AISI 1095 steel and OFHC copper were chosen. AISI 1095 steel was spherodized and OFHC copper was recrystallized. These materials cover a wide range of hardness and microstructures.

Samples were cut from 6.35 mm diameter rods of the materials. Before heat treatment of metal samples, ends of each sample were ground on abrasive papers to ensure uniform contact. Commercially pure nickel samples were encapsulated in Vycor tubes and then annealed at 800^{o}C for one hour. To get small grain size the cold-worked OFHC copper specimens were encapsulated and recrystallized at 500^{o}C for one hour. AISI 1095 steel was heat-treated at 900^{o}C for half an hour, then oil quenched and tempered at 400^{o}C for one hour to yield spherodized structure. The hardness and density of the materials are given in Table I and the microstructures are shown in Figure 1.

B. Abrasion Tests

Abrasion experiments were conducted on a pin-on-disk set-up shown in Figure 2. Specimens were abraded on commercial silicon carbide abrasive

TABLE I: EXPERIMENTAL MATERIALS

MATERIAL	TREATMENT	VICKERS HARDNESS (kg / mm^2)	DENSITY (g / cm^3)
PMMA	---	17.5	1.18
OFHC Cu	Recrystallized $500^{o}C$, 1 hr	44.0	8.90
Ni	Annealed $800^{o}C$, 1 hr	88.5	8.90
AISI 1095 Steel	Spherodized 900^{o} C, 30 min; oil quenched; $400^{o}C$, 1 hr	472.0	7.85

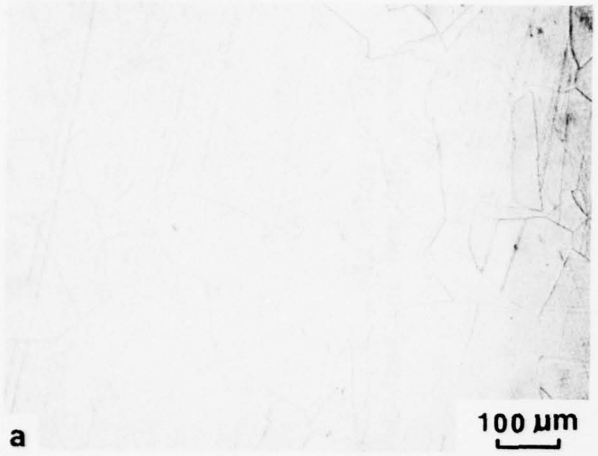

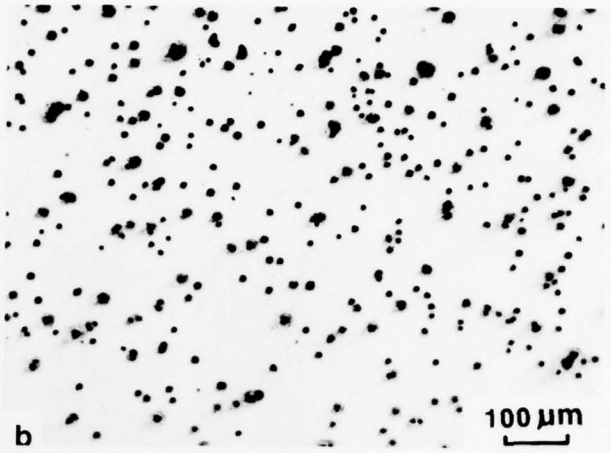

Figure 1: Microstructures of experimental materials: (a) nickel, (b) AISI 1095 steel, (c) OFHC copper.

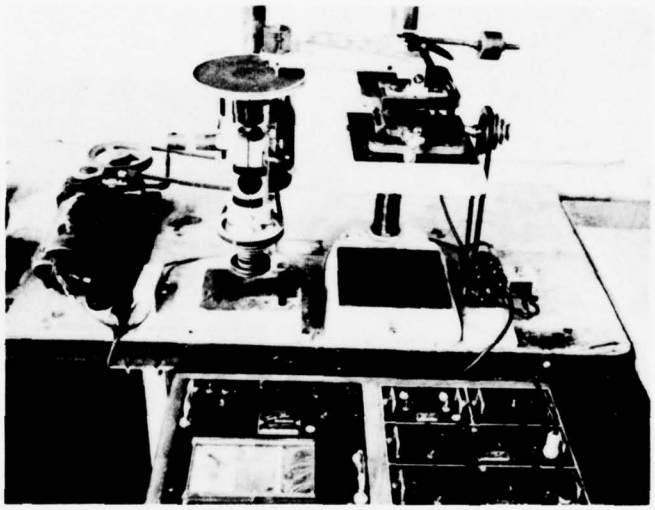

Figure 2: Experimental set-up used for abrasion tests. Specimen passes over the fresh abrasive along a spiral track.

papers. The specimen held in a loading arm followed a spiral track on a 20 cm diameter abrasive disk and therefore always passed over the fresh abrasive. The total distance slid on each disk was 4m. The normal load was applied by a dead-weight and the tangential force was measured by a dynamometer - Sanborn recorder assembly.

Grits 600, 320, 180, 120 & 60 were used and the normal load was varied between 4.9 N (0.5 kg) and 39.2 N (4 kg). The angular velocity of the disk was held constant so that the sliding velocity was varied from 2 to 6 cm/sec following the track. The specimens were weighed to an accuracy of 0.01 mg before testing. After testing, the specimens were brushed lightly and the weight was again measured. The weight loss and the tangential force were determined as an average of at least 4 measurements for each experimental condition. In case of OFHC copper and AISI 1095 steel, 4/0 and 3/0 emery papers were also used to investigate the wear behavior extensively.

After abrasion tests the surface of worn specimens were observed microscopically. Selected samples were electroplated with nickel to preserve edges and cut by a diamond saw parallel to the sliding direction and perpendicular to the worn surface. Then specimens were mounted, polished and eteched with standard etchants and observed in optical and scanning electron microscopes to determine the subsurface deformation. Wear particles were collected during the test and examined in an optical microscope.

C. Optical Observation of the Abrasion Process

PMMA samples were cut approximately 6 mm in length and their ends were mechanically polished on various papers and finally with 0.05 μm alpha

alumina powder. The specimen was loaded under the objective of the microscope, while abrasive paper was fixed on the stage. The stage was moved slowly and steadily, and grooves formed on the surface of the specimen were observed through the specimen directly. Figure 3 shows the experimental set-up. The displacement of the stage, therefore, the length of the grooves were carefully controlled. To prevent interference between grooves the stage was moved a distance of the order of the average spacing between contacting particles.

Abrasive papers of 5 grit sizes and loads between 4.9 N (0.5 kg) and 39.2 N (4 kg) were used. The total number of grooves formed on the surface was counted and their widths were measured. When the total groove number was large, at least 100 grooves were selected randomly and their widths were determined.

D. Tests With Conical Tools

In order to simulate abrasive action, experiments were conducted with single-point conical tools. A pin on cylinder type of apparatus was used, which is similar to the turning operation. A conical diamond tool was held in a dynamometer mounted on the carriage of a lathe. Normal and tangential forces were measured and monitored by a Sanborn recorder. The tests were carried out under the normal load of 4.4 N (0.45 kg) and at the cutting speed of about 1.6 cm/sec. Tool angles were varied between 70 and 140 degrees. Weight loss was determined, and cutting particles were collected and examined in an optical microscope.

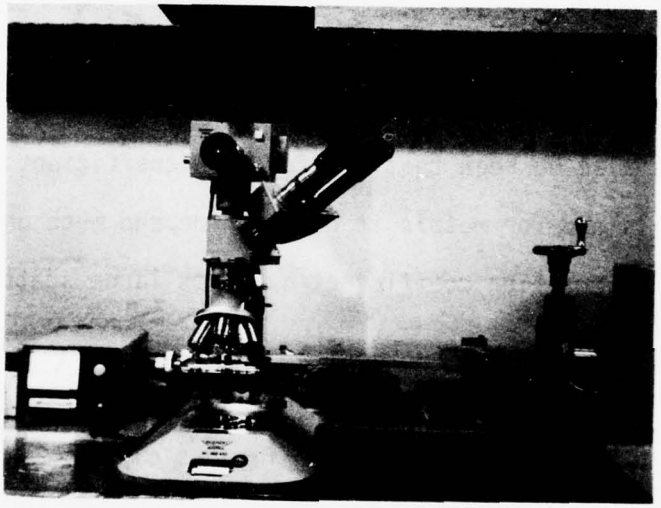

Figure 3: Experimental set-up used for optical observation of groove formation on the surface of PMMA sample.

III. RESULTS

A. Abrasion Tests

Figure 4 shows the friction coefficient as a function of the abrasive grit diameter D_g for the materials tested, sliding at 4.9 N (0.5 kg) to 39.2 N (4 kg) load on different grades of dry silicon carbide abrasive papers. It can be seen that the friction coefficient initially increases with grit diameter slightly, and later levels out and becomes substantially constant. It can also be seen that the friction coefficient does not vary much with materials and for metals it does not depend much on the applied load. For PMMA the friction coefficient exhibits large scatter compared to metals.

The wear rate and the wear coefficient as a function of the grit diameter are shown in Figures 5-8. These figures clearly show the influence of abrasive grit size on wear. As the abrasive grit diameter is increased, the wear rate increases rapidly until a critical grit size is reached and later becomes independent of grit diameter or increases only slowly. It can be seen that the slope of the latter stage depends on the material and the normal load. For PMMA with the applied load of 39.2 N (4 kg) the slope is quite large. The critical grit diameter for all the materials tested is about 80 μm.

Wear particles were collected during the test to investigate their size and shape. Figure 9 shows the collected wear particles. It can be seen that the abrasive particles as well as wear particles were removed during abrasion. The particles are essentially in the form of microchips

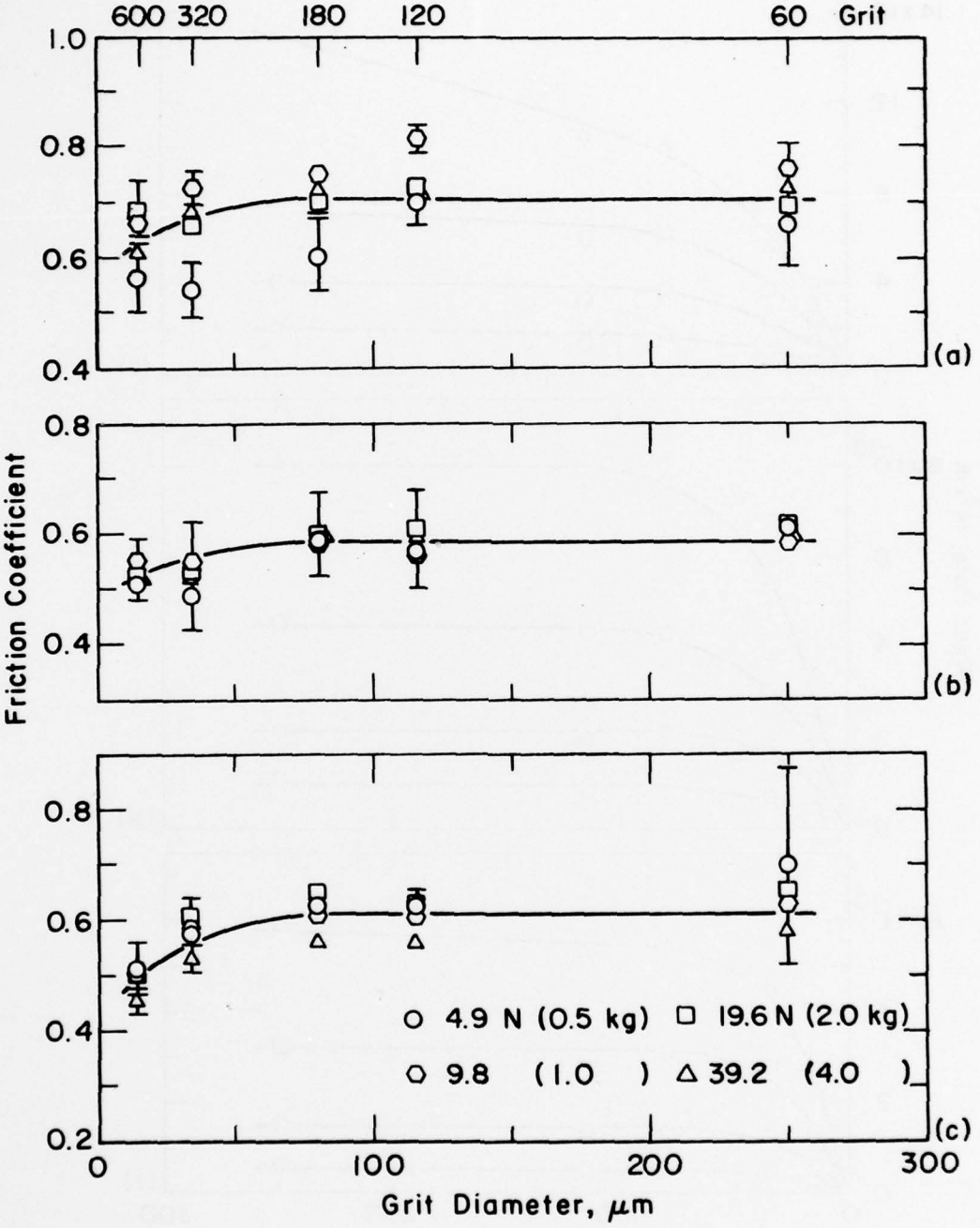

Figure 4: Friction coefficient as a function of the abrasive grit diameter for different normal loads: (a) PMMA, (b) nickel, (c) AISI 1095 steel.

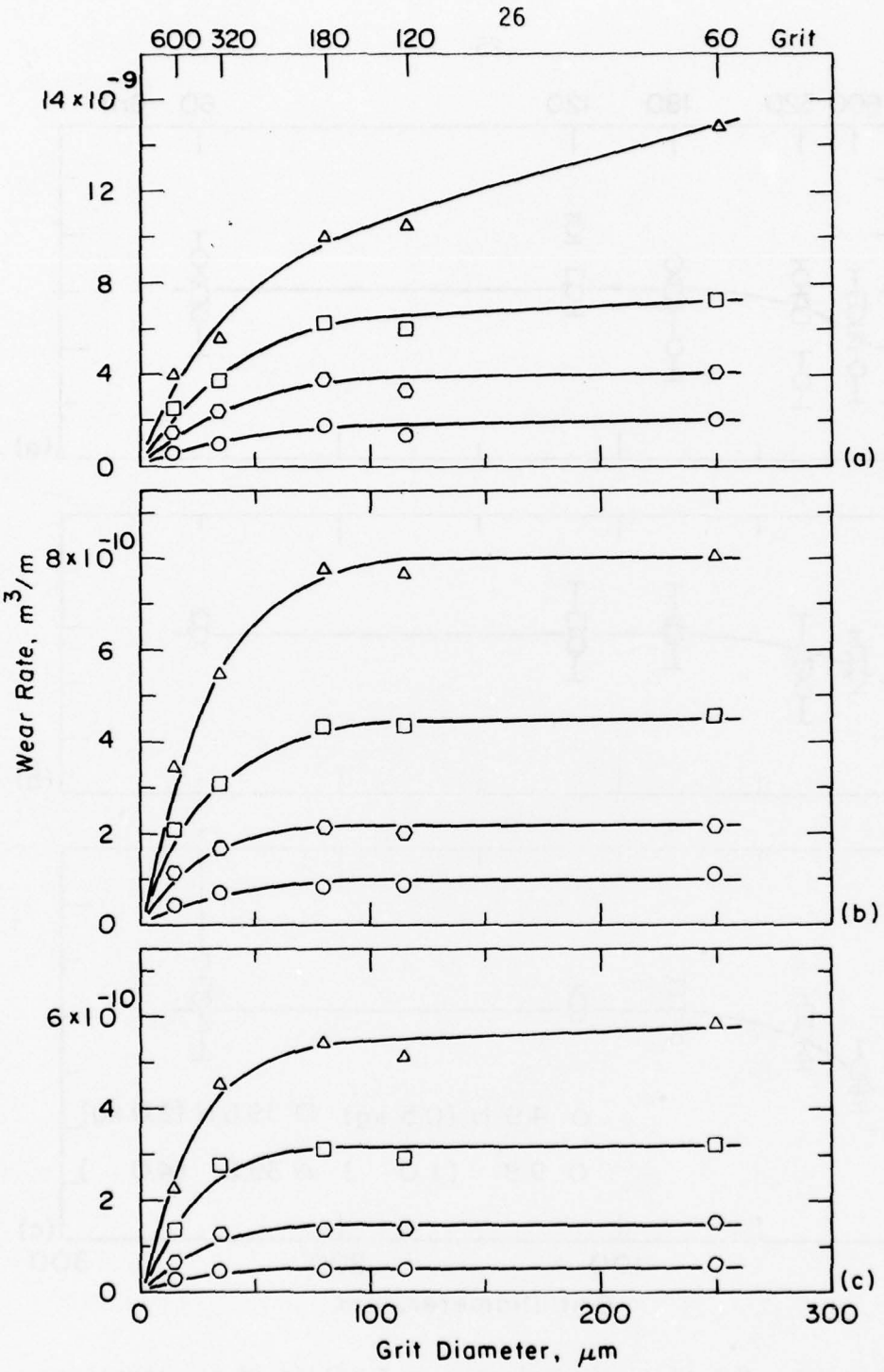

Figure 5: Wear rate as a function of the abrasive grit diameter for different normal loads (symbols are same as previous figure): (a) PMMA, (b) nickel, (c) AISI 1095 steel.

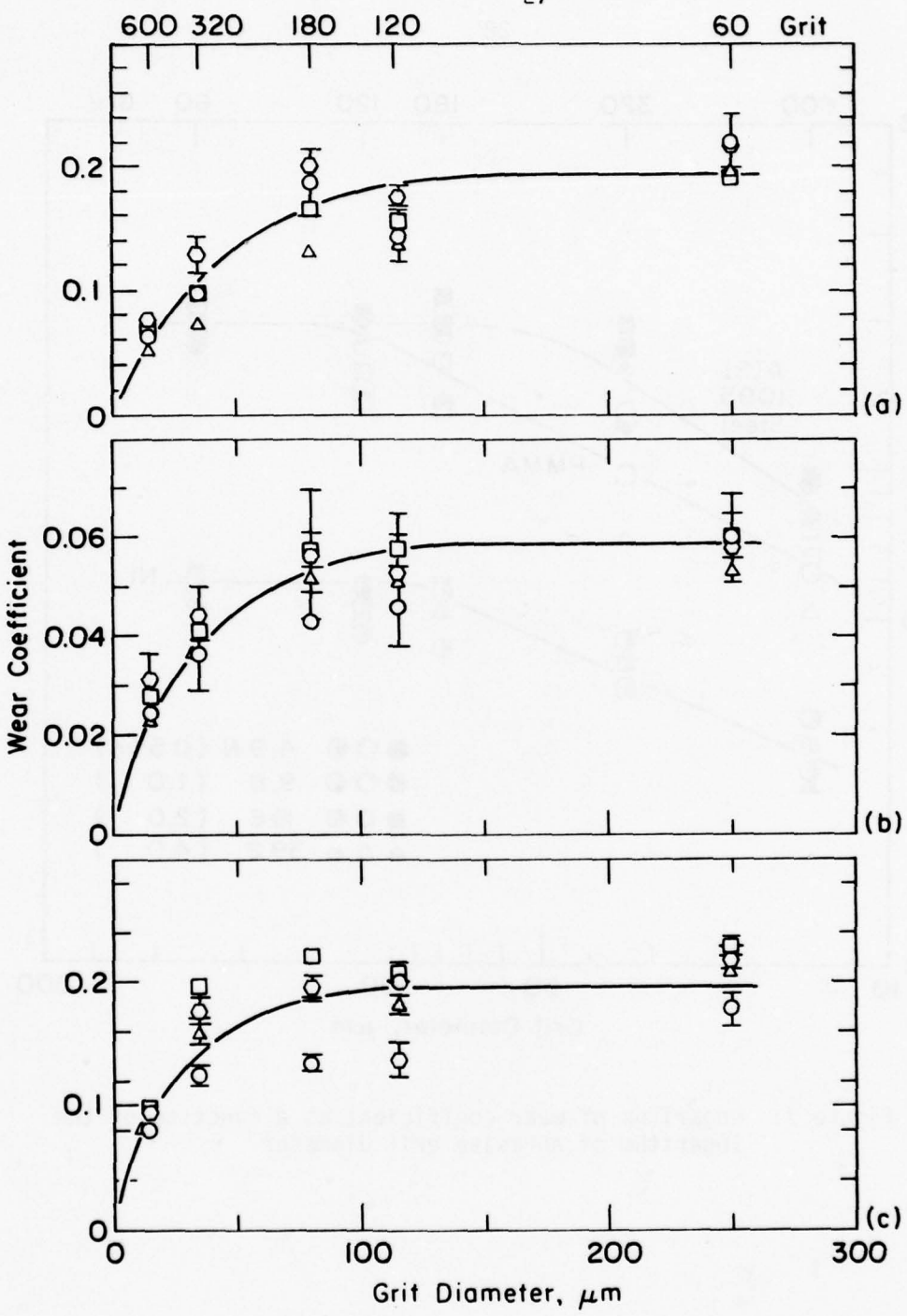

Figure 6: Wear coefficient versus abrasive grit diameter for different normal loads: (a) PMMA, (b) nickel, (c) AISI 1095 steel.

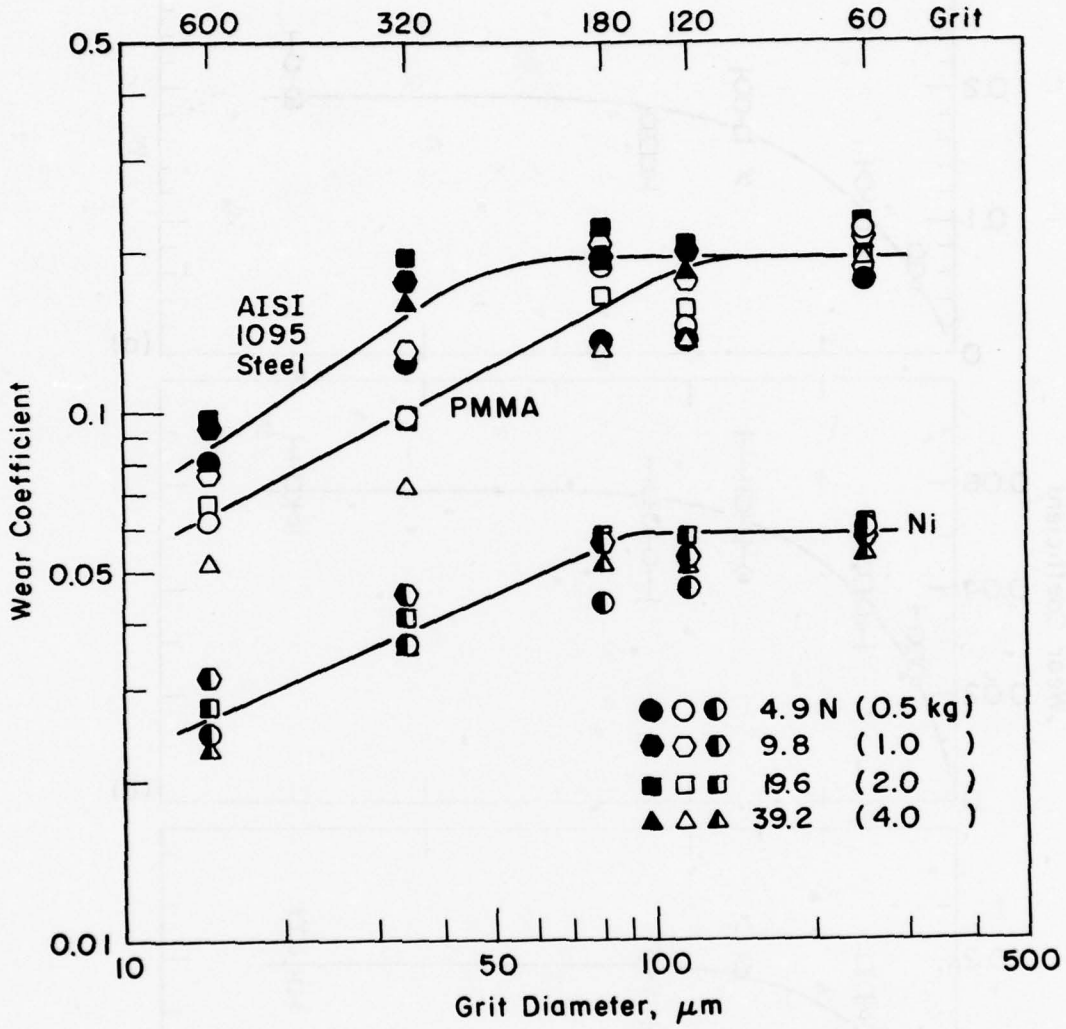

Figure 7: Logarithm of wear coefficient as a function of the logarithm of abrasive grit diameter.

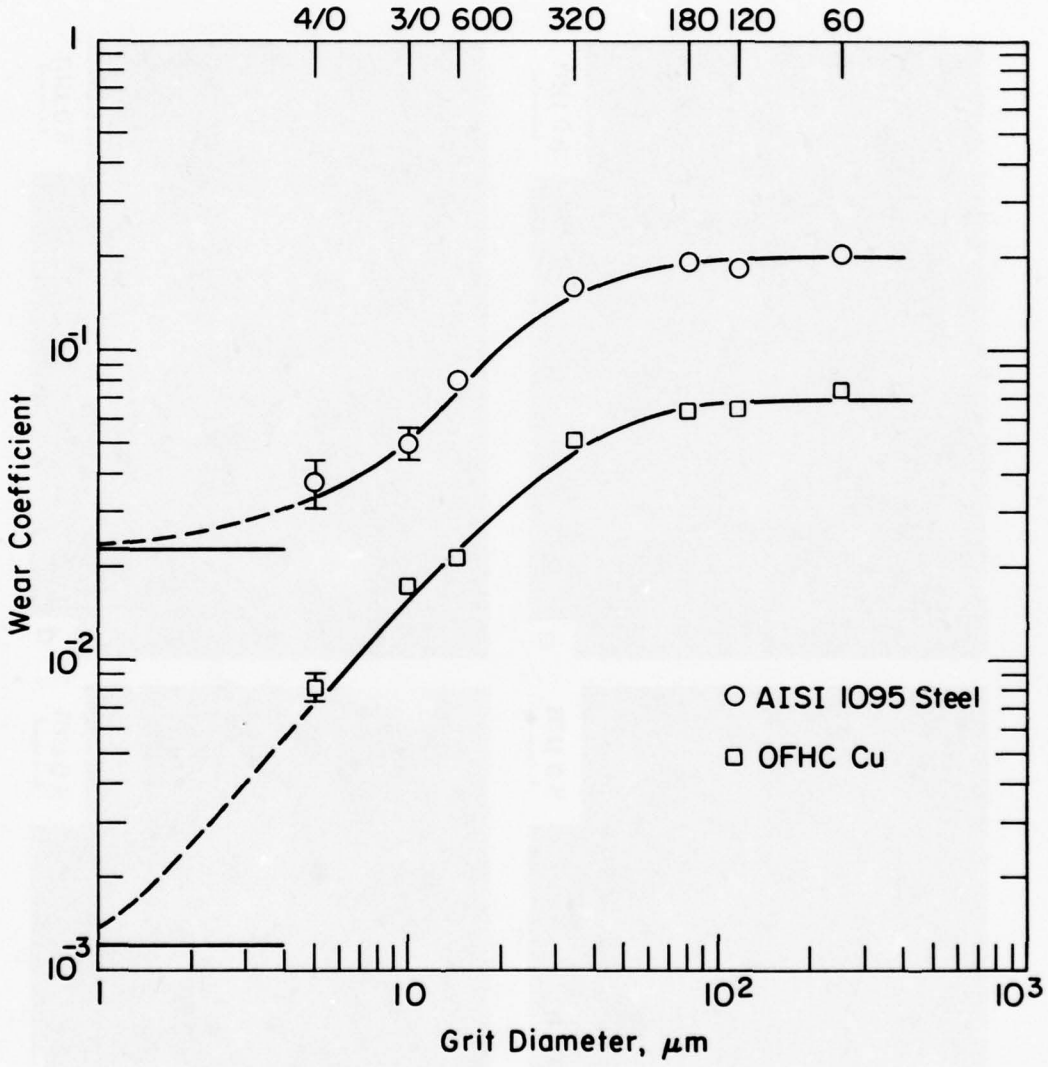

Figure 8: Wear coefficient as a function of the abrasive grit diameter up to 4/0 paper. The normal load was 39.2 N. Horizontal lines on the left represent the sliding wear coefficient.

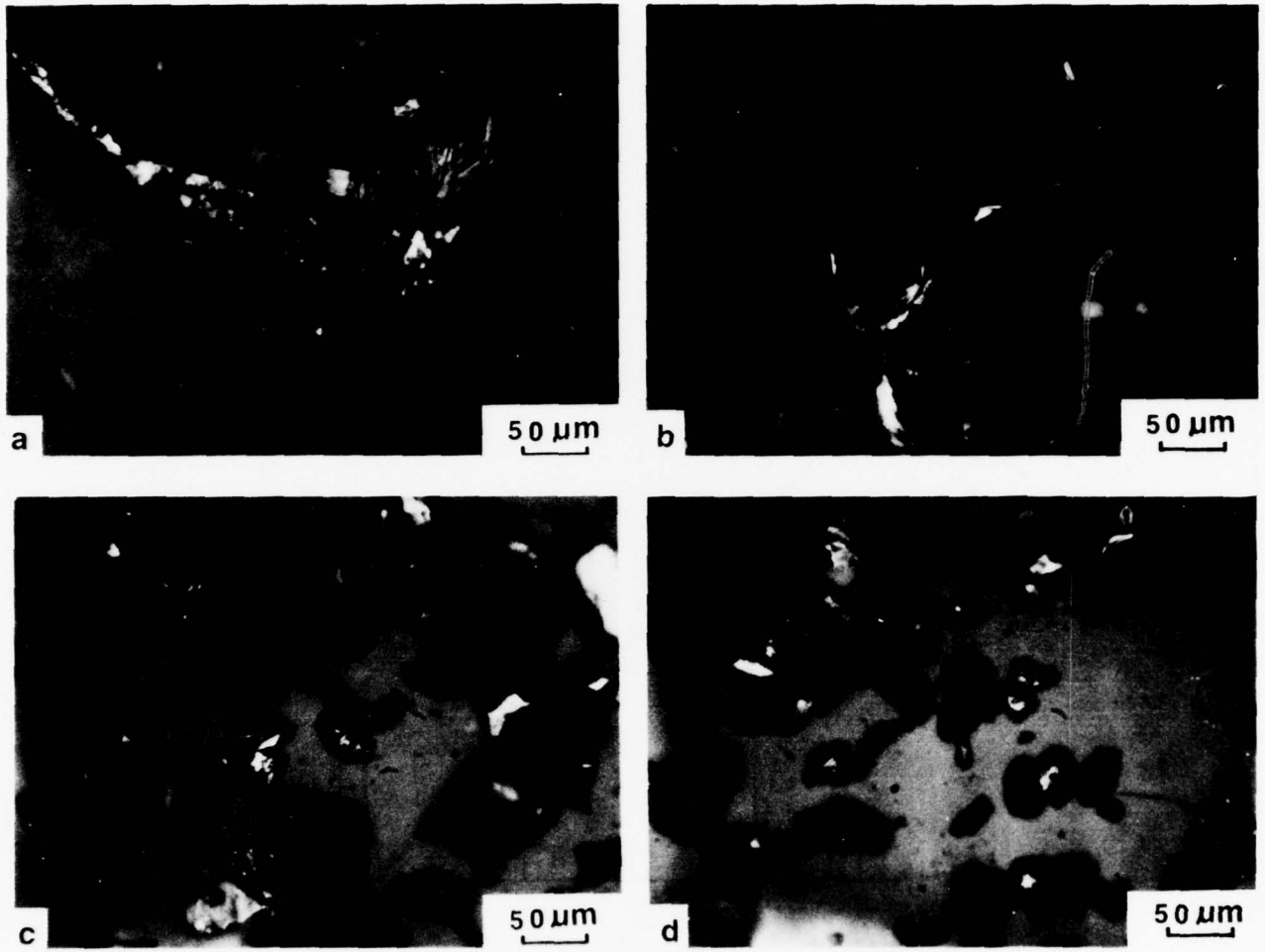

Figure 9: Abrasive wear particles of OFHC copper for different grit sizes: (a) 60, (b) 120, (c) 180 (d) 320 grit. Experimental conditions are same as in Figure 8.

and their sizes vary with grit diameter. For finer grits wear particles generated during abrasion were attached to the abrasive surface; these are shown in Figure 10.

Metallographic examination of the surface and the subsurface of worn specimens was conducted to investigate the mechanism. Figure 11 shows that the surfaces of worn specimens are entirely covered with many grooves. It can be seen from the figure that large plastic deformation of groove materials by plowing took place as a result of abrasion. It clearly shows the variation of the number of grooves and their widths with grit diameter.

Optical and scanning electron micrographs of the subsurface, shown in Figures 12&13, clearly indicate that large subsurface deformation took place as a result of abrasion. For the coarser grits the deformation zone is clearly observable, but for the finer it is hardly observable probably because it is too shallow.

B. Number of Grooves and Their Widths

Figure 14 shows the scanning electron micrographs of the surface of the abrasive. It can be seen that the shapes and orientations of the abrasive particles are irregular. They are azimuthally and randomly oriented pyramids rather than cones with a wide range of included angles. From the figure the total number of abrasive particles was counted. For similar packing condition, it would be expected that if the grains are similar in shape, the total number of particles would vary inversely as the square of the mean grain diameter. Results for the variation of the number of abrasive particles per unit area with grit diameter are shown in Figure 15,

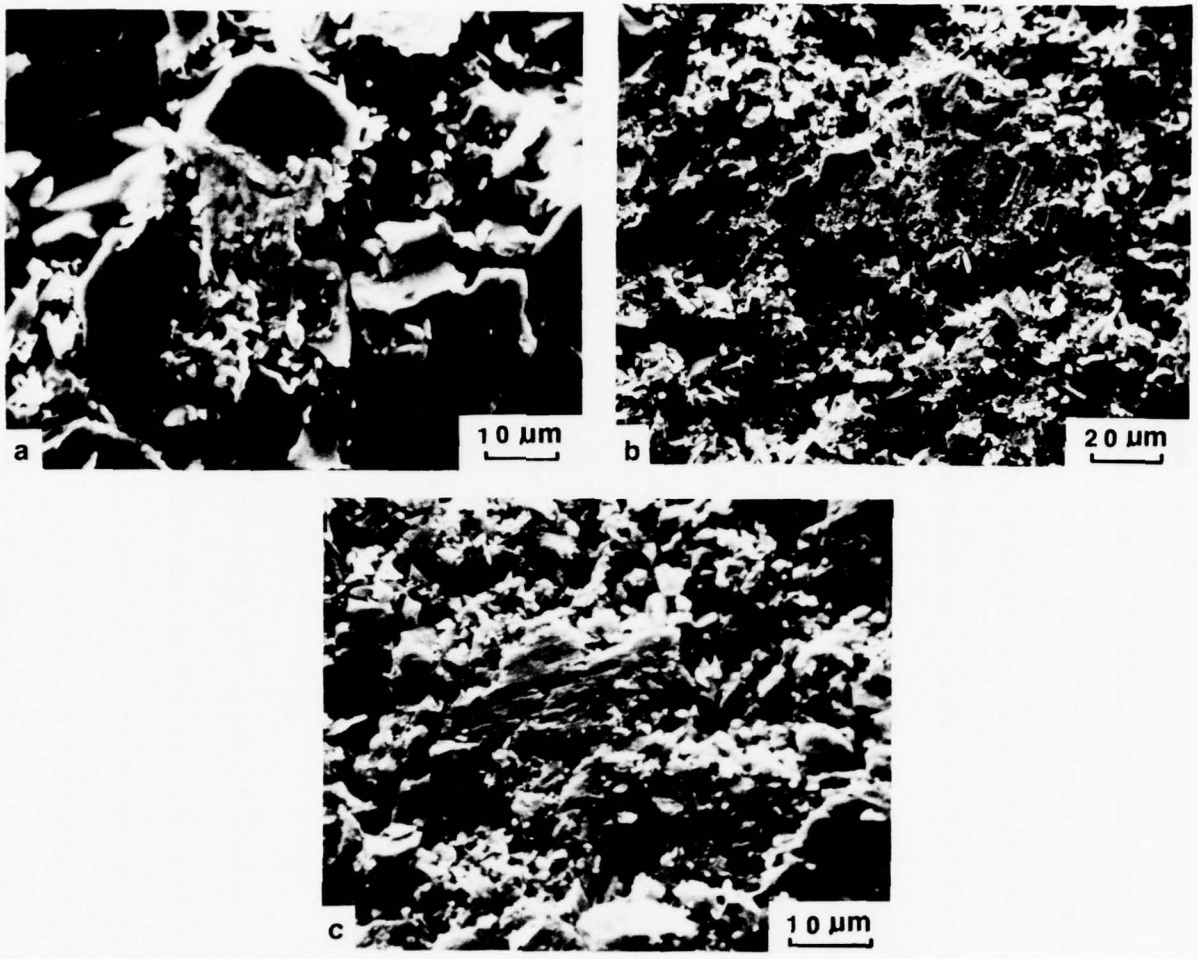

Figure 10: Abrasive Wear particles of OFHC copper attached to the abrasive surface for fine grits: (a) 600, (b) 3/0 (c) 4/0. Experimental conditions are same as in Figure 8.

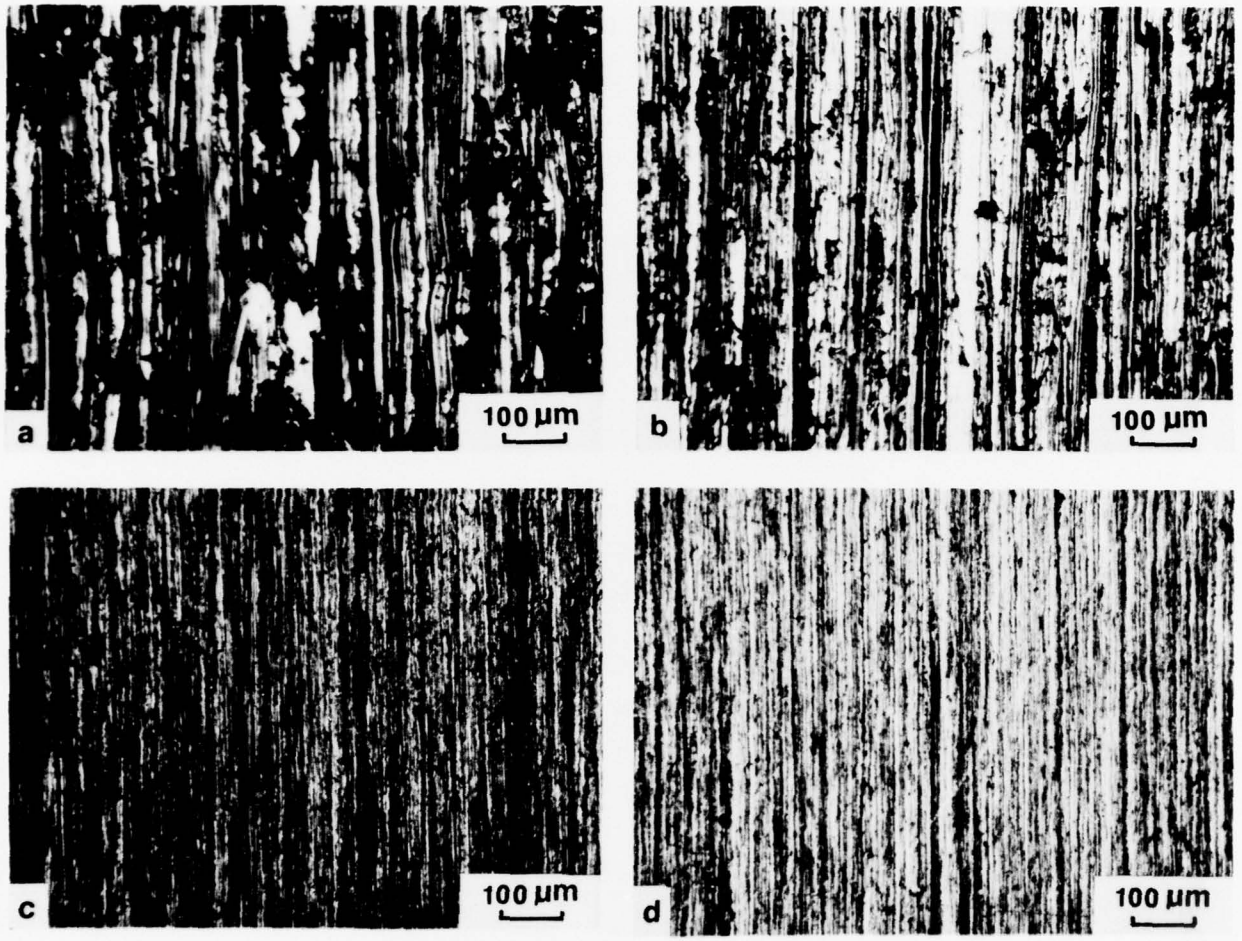

Figure 11: Surfaces of worn OFHC copper specimen for different grits: (a) 60, (b) 180 (c) 600 (d) 4/0. Experimental conditions are same as in Figure 8.

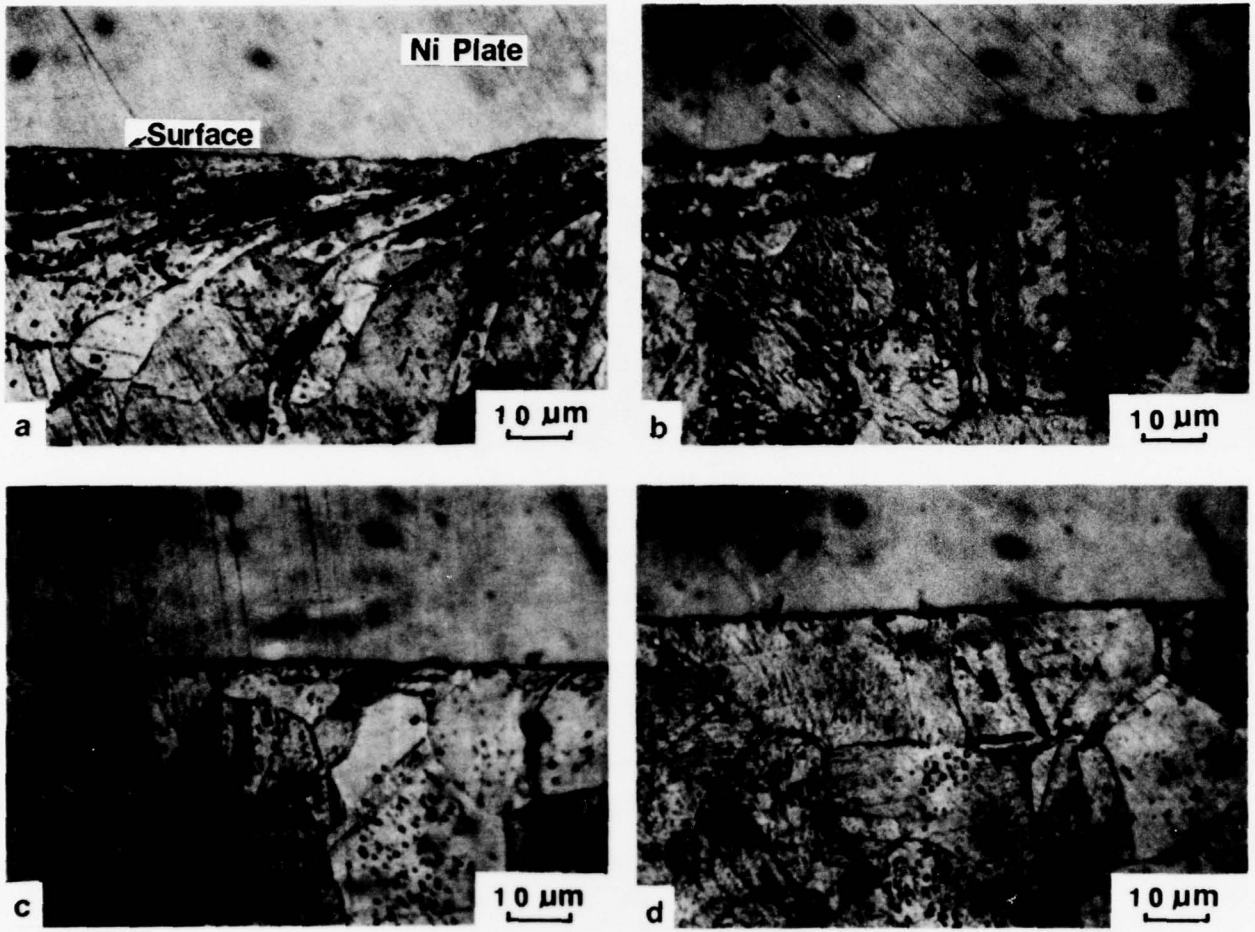

Figure 12: Optical micrographs of the OFHC copper subsurface for different grits: (a) 60 (b) 180, (c) 320 (d) 600 grit. Experimental conditions are same as in Figure 8.

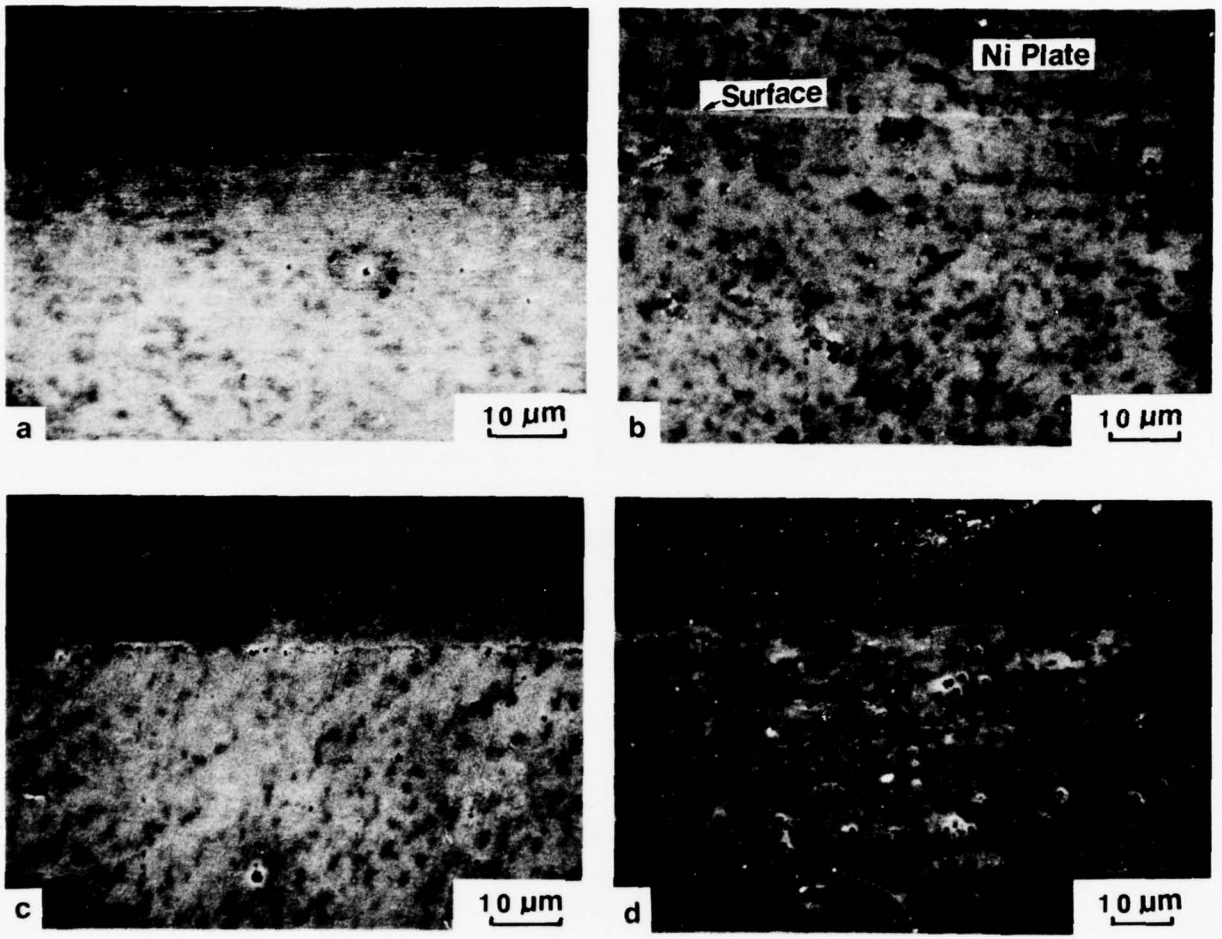

Figure 13: Scanning electron micrographs of the AISI 1095 steel subsurface for different grits: (a) 120, (b) 600, (c) 3/0 (d) 4/0. Experimental conditions are same as in Figure 8.

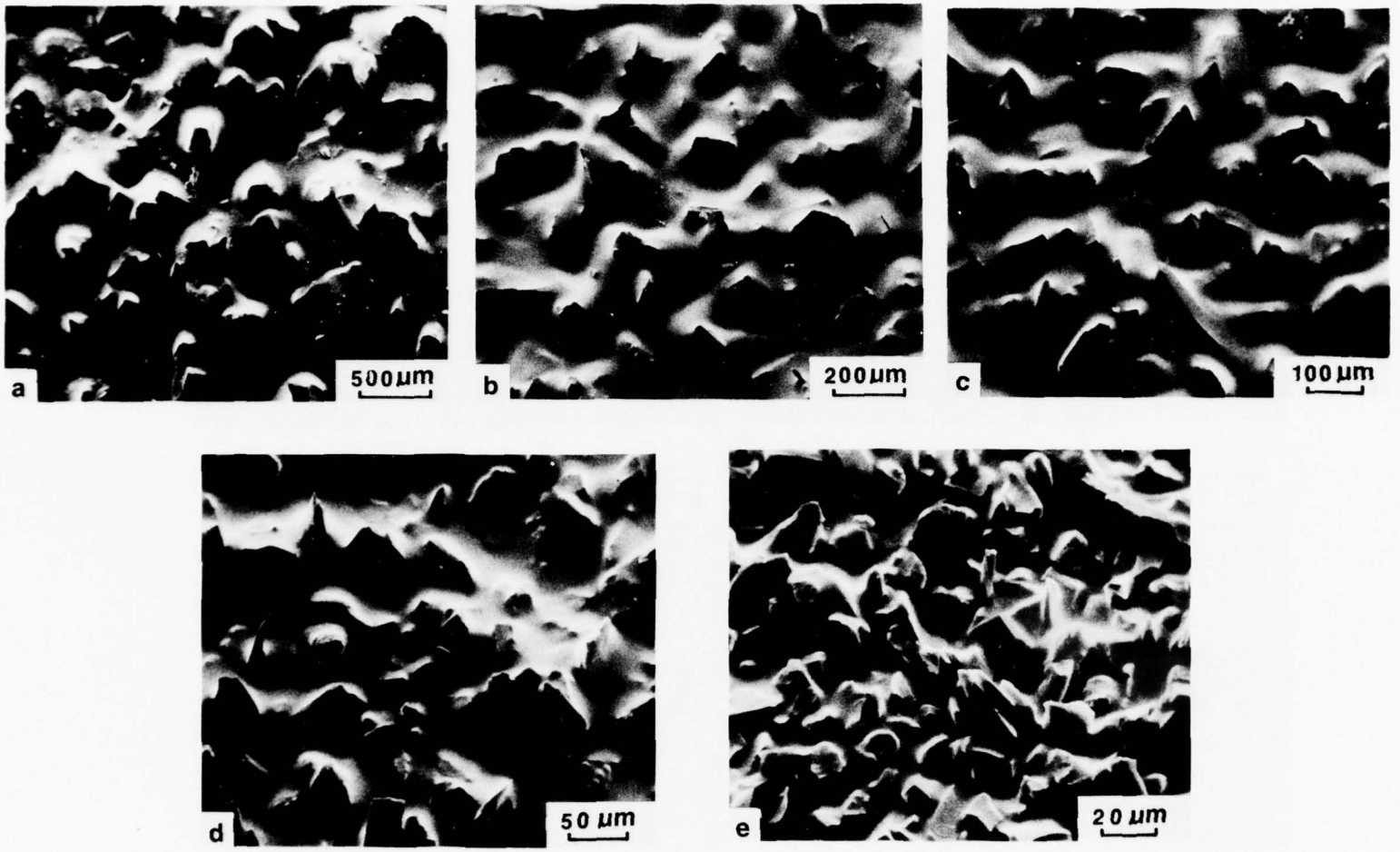

Figure 14: Scanning electron micrographs of the abrasive surface: (a) 60, (b) 120, (c) 180, (d) 320 (e) 600 grit.

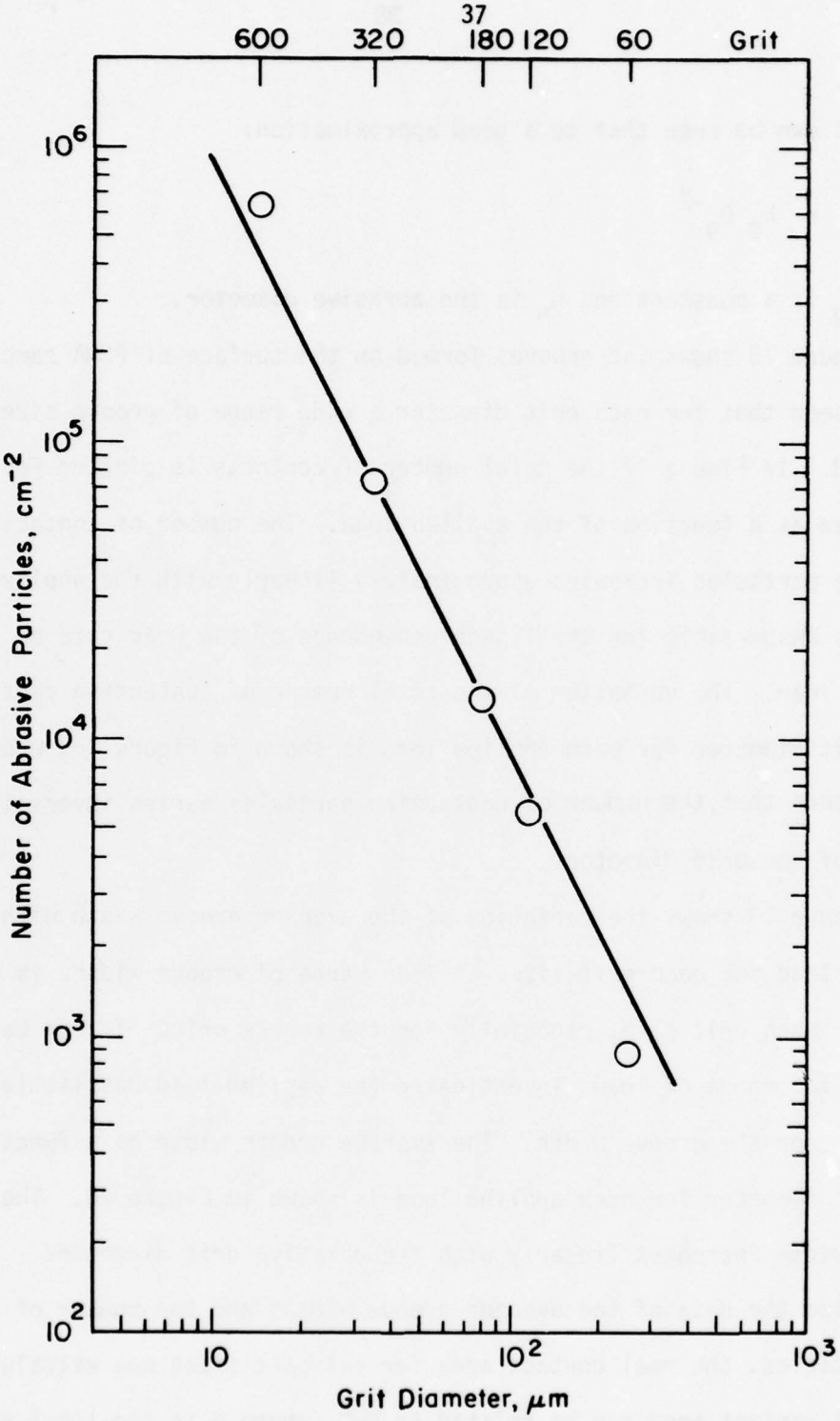

Figure 15: Number of abrasive particles per unit area of the abrasive surface as a function of the grit diameter.

where it can be seen that to a good approximation:

$$N_t = k_g D_g^{-2} \quad (1)$$

where k_g is a constant and D_g is the abrasive diameter.

Figure 16 shows the grooves formed on the surface of PMMA sample. It can be seen that for each grit diameter a wide range of groove sizes is obtained. In Figure 17 the total number of contacts is plotted for each grit size as a function of the applied load. The number of contacting abrasive particles increases approximately linearly with the applied load, which is responsible for the linear dependence of the wear rate on the applied load. The variation of the total number of contacting particles with grit diameter for each applied load is shown in Figure 18, where it can be seen that the number of contacting particles varies inversely as the square of the grit diameter.

Figure 19 shows the variation of the average groove width with the applied load for each grit size. A wide range of groove widths is observable for each grit size, especially for the coarse grit. It can be seen that in the range of loads investigated the applied load has little influence on the groove width. The average groove width as a function of the grit diameter for each applied load is shown in Figure 20. The average groove width increases linearly with the abrasive grit diameter.

Using the data of the average groove widths and the number of contacting particles, the real contact area for all grit sizes was calcalulated. The real contact area can be related to Nw^2, where N is the total number of contacts and w is the average groove width. Results for the variation of

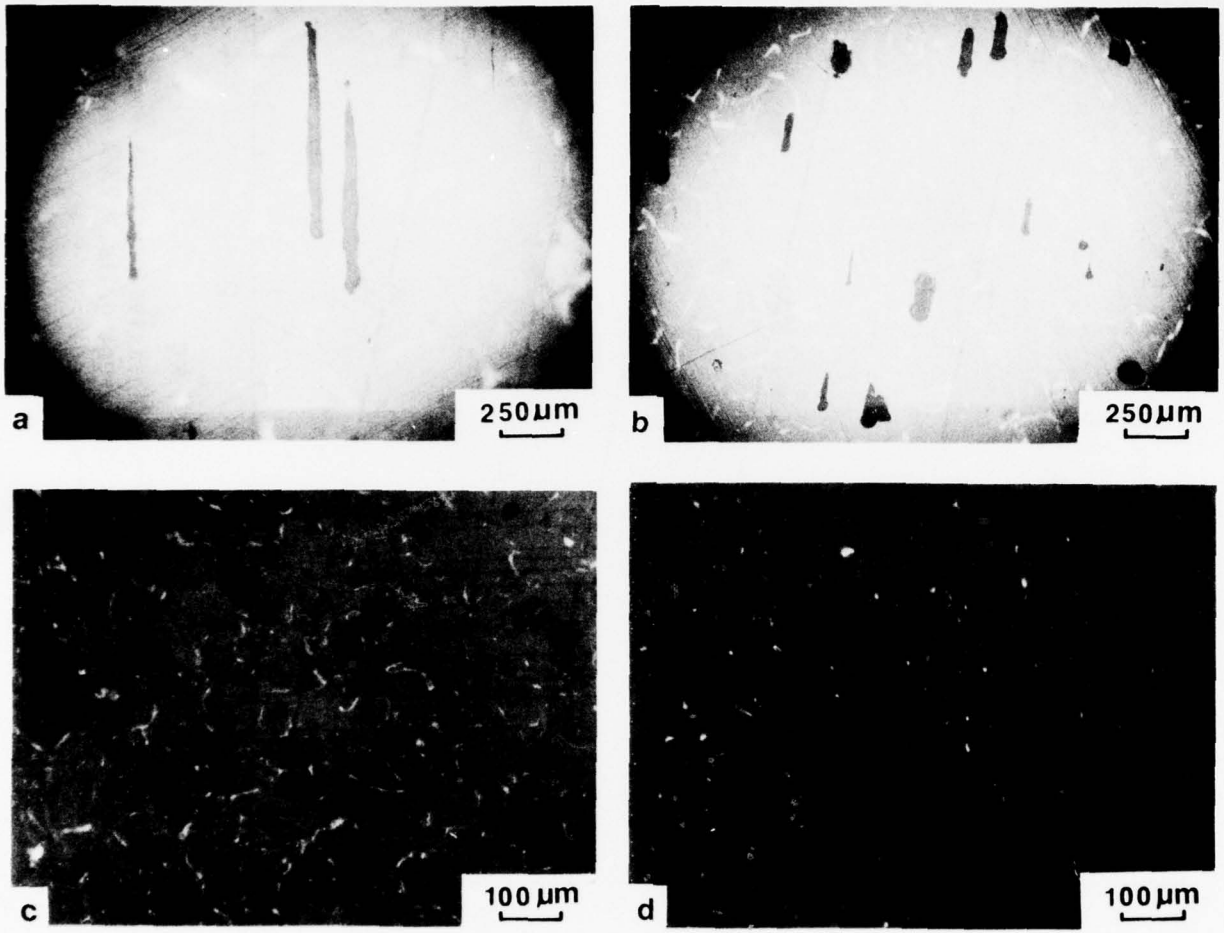

Figure 16: Grooves formed on the surface of PMMA specimen: (a) 60 grit, 4.9 N, (b) 120 grit, 19.6 N, (c) 320 grit, 39.2 N (d) 600 grit, 19.6 N.

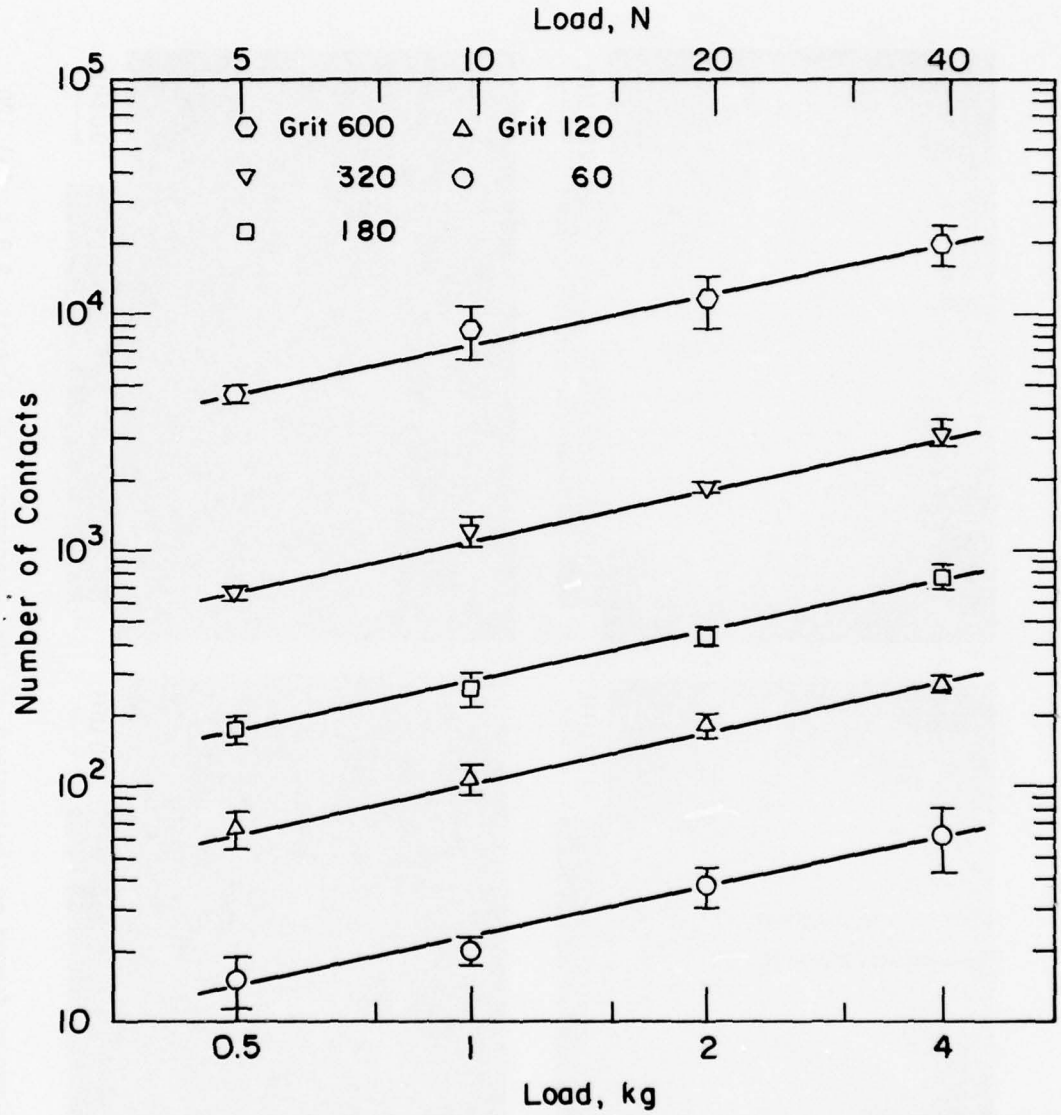

Figure 17: Number of contacting abrasive particles versus applied normal loads for different grits. PMMA specimen of 6.35 mm diameter was used.

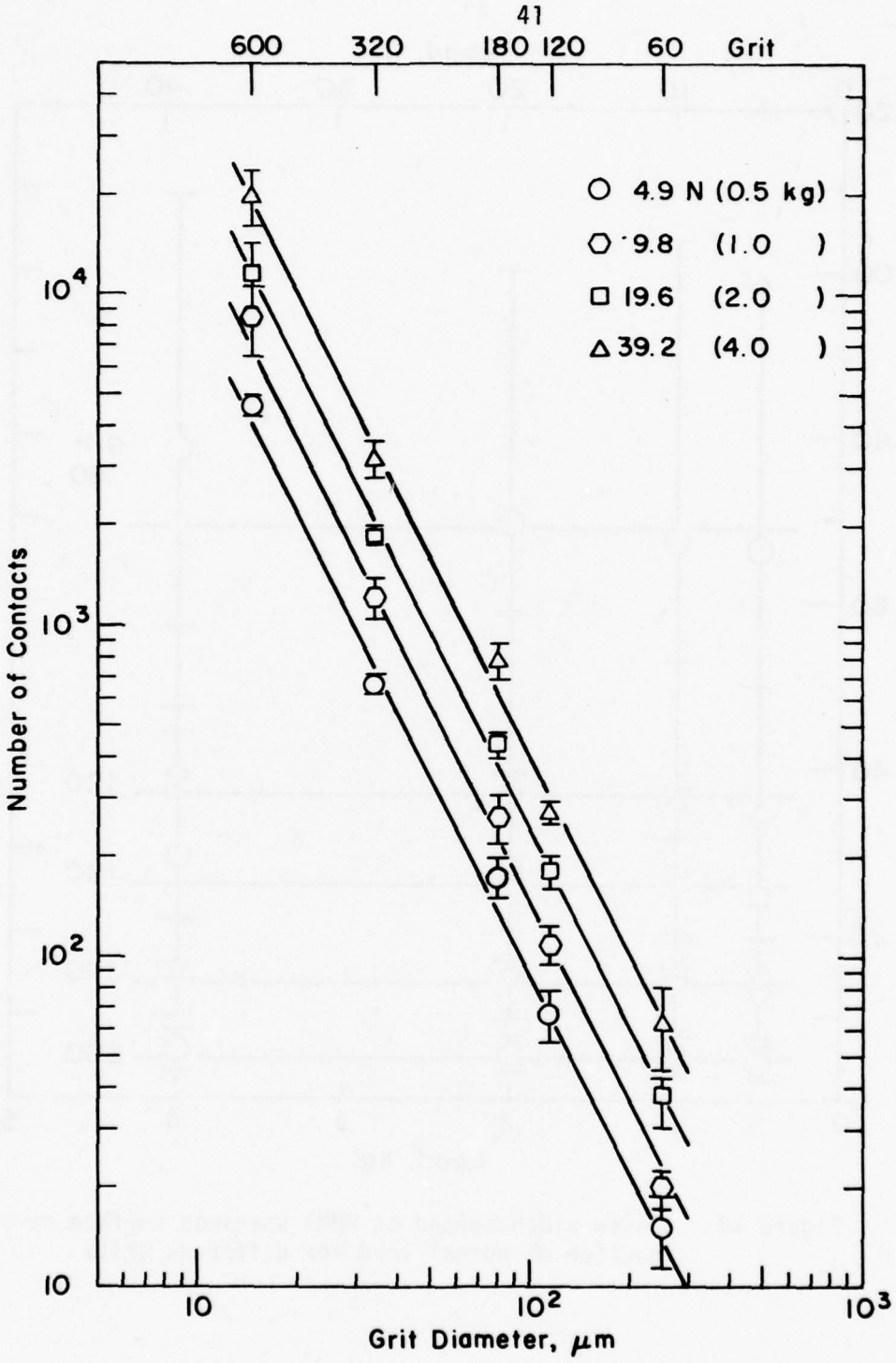

Figure 18: Number of contacting particles as a function of the grit diameter for different normal loads. PMMA specimen of 6.35 mm diameter was used.

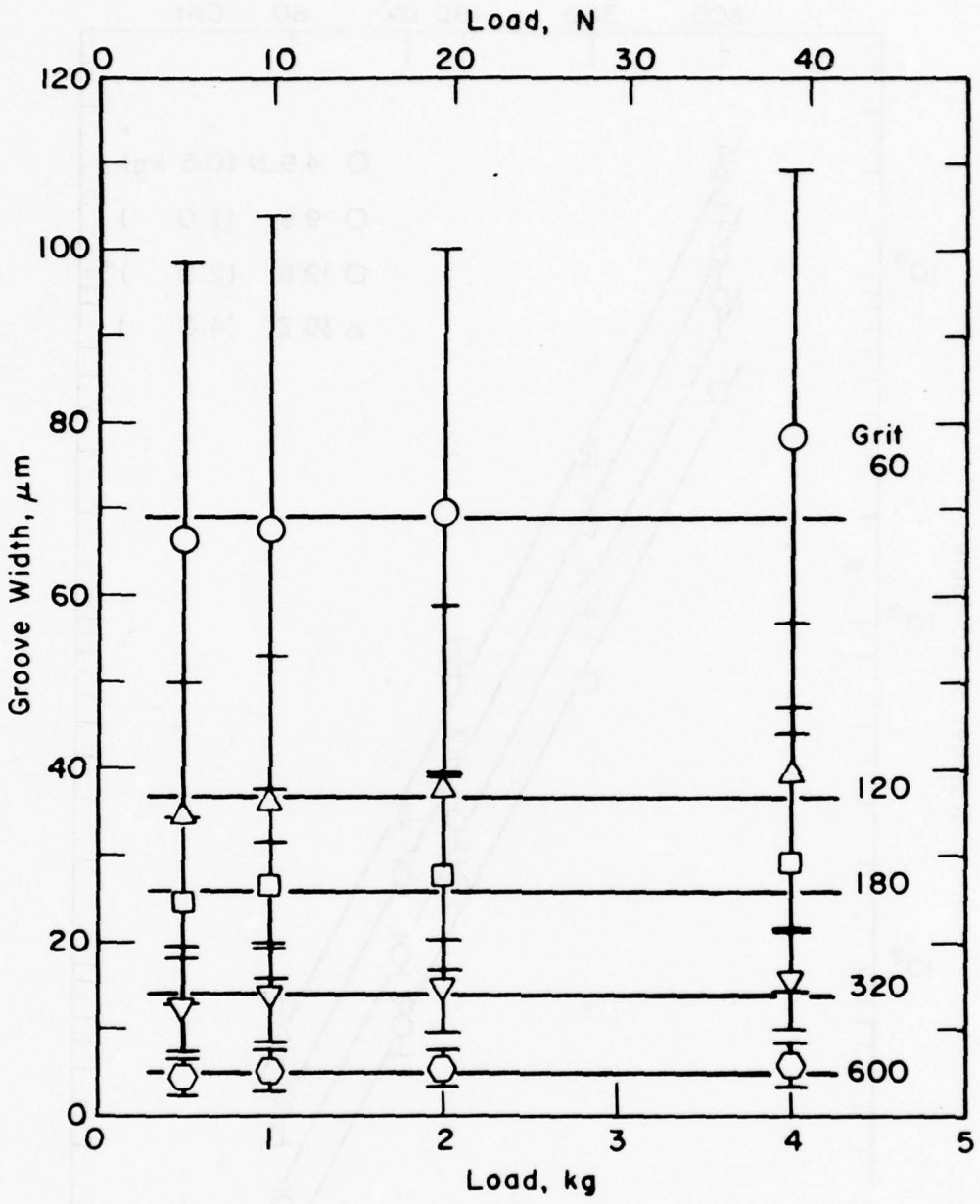

Figure 19: Groove width formed on PMMA specimen surface as a function of normal load for different grits.

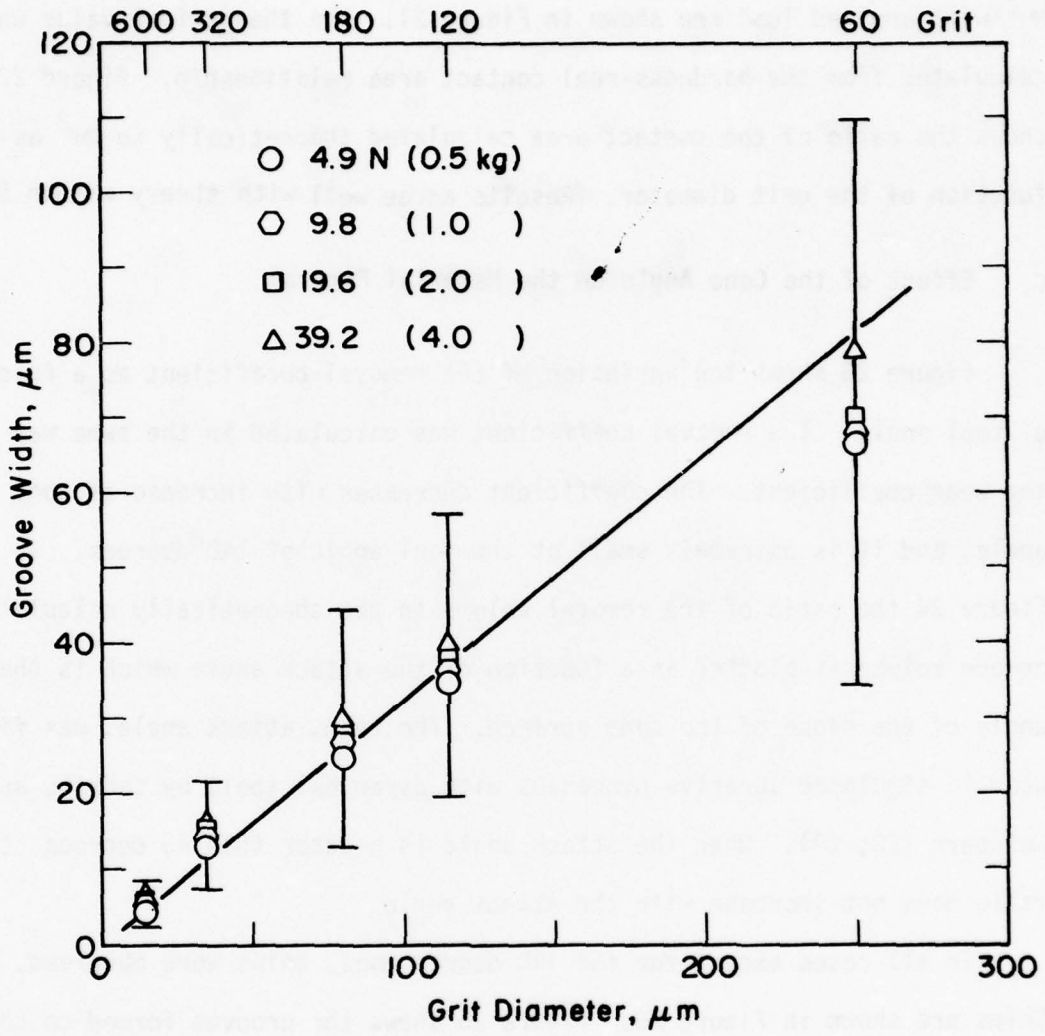

Figure 20: Groove width formed on PMMA specimen versus abrasive grit diameter.

Nw^2 with applied load are shown in Figure 21. The theoretical value was calculated from the hardness-real contact area relationship. Figure 22 shows the ratio of the contact area calculated theoretically to Nw^2 as a function of the grit diameter. Results agree well with theory within 50%.

C. Effect of the Cone Angle on the Material Removal

Figure 23 shows the variation of the removal coefficient as a function of tool angle. The removal coefficient was calculated in the same way as the wear coefficient. The coefficient decreases with increase of tool angle, and it is extremely small at the tool angle of 140 degrees. In Figure 24 the ratio of the removal volume to the theoretically calculated groove volume is plotted as a function of the attack angle which is the angle of the slope of the cone surface. The term, attack angle, was first used in simulated abrasive processes with pyramidal tools by Sedriks and Mulhearn (28, 29). When the attack angle is greater than 45 degrees, the ratio does not increase with the attack angle.

In all cases except for the 140 degree tool, chips were observed. Chips are shown in Figure 25. Figure 26 shows the grooves formed on the specimens.

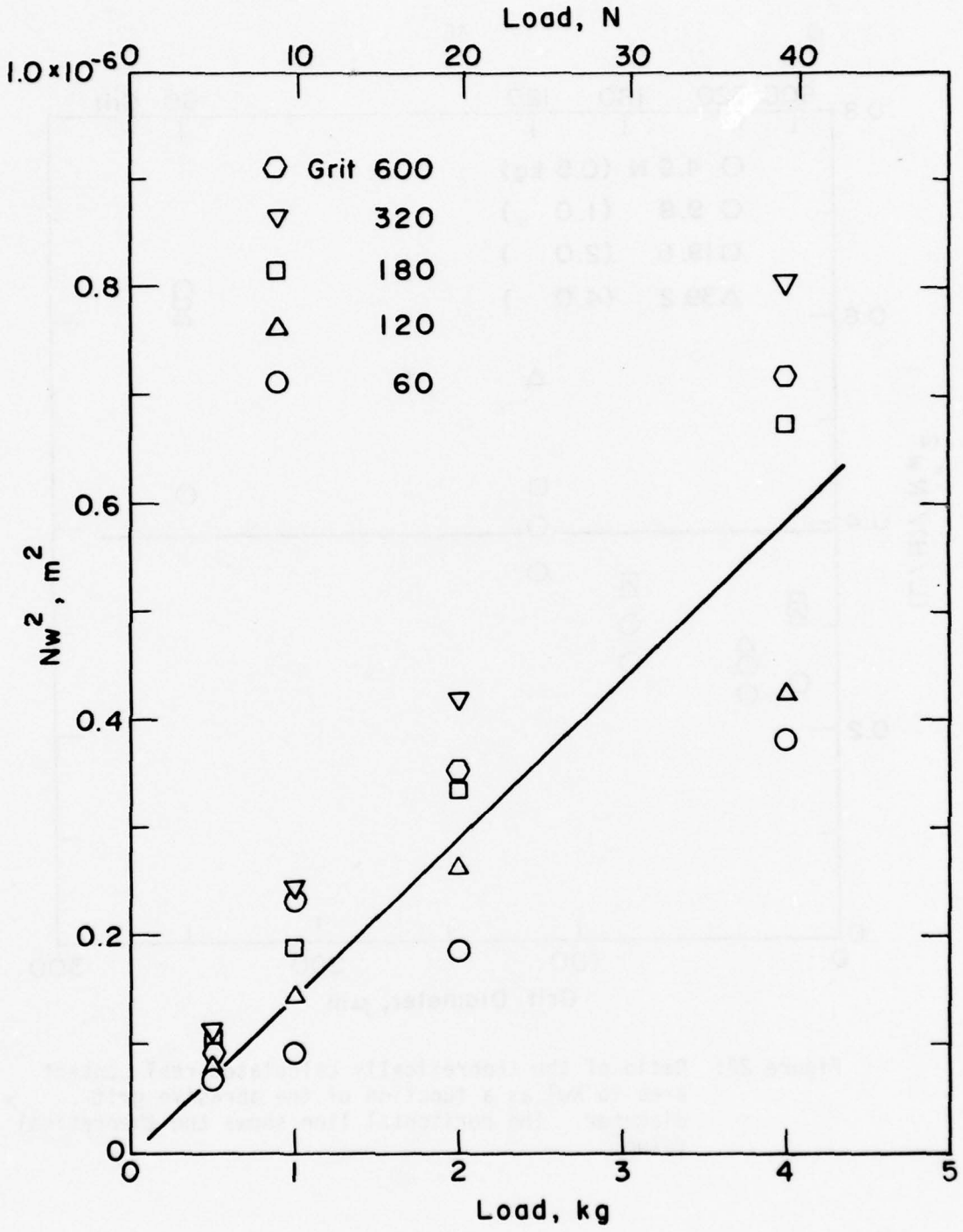

Figure 21: Number of contacting particles times the square of the average groove width as a function of the applied normal load (Nw^2 is proportional to the real contact area).

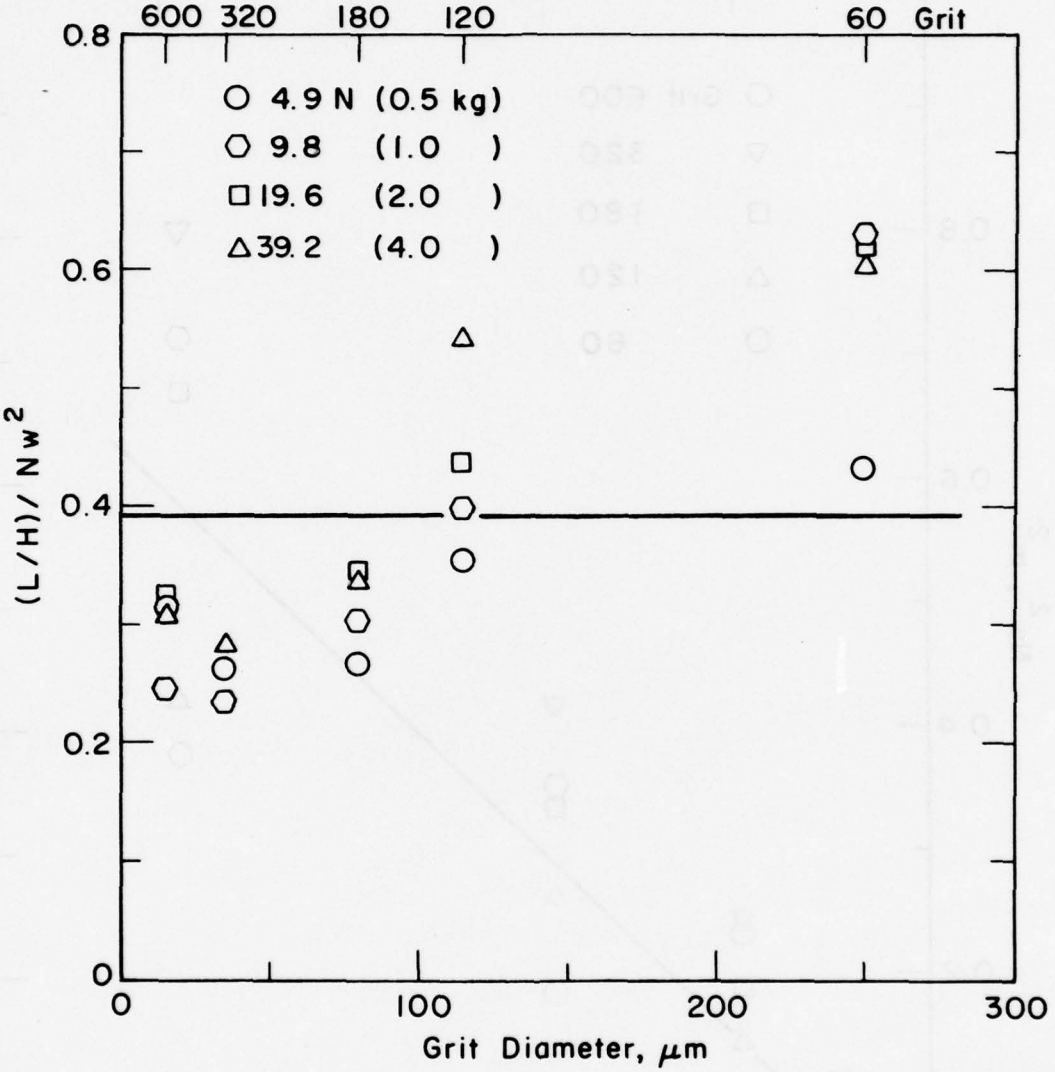

Figure 22: Ratio of the theoretically calculated real contact area to Nw^2 as a function of the abrasive grit diameter. The horizontal line shows the theoretical value.

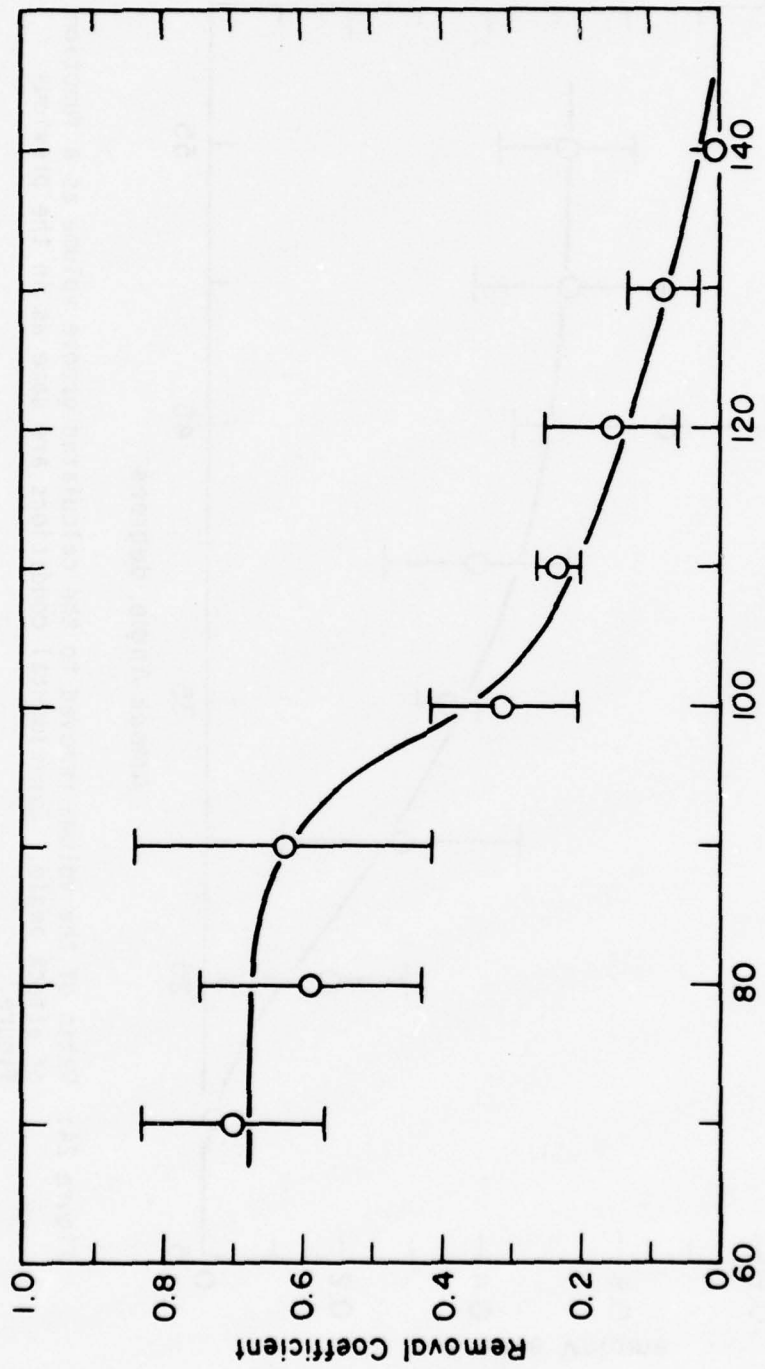

Figure 23: Removal coefficient as a function of conical tool angle in cutting tests of AISI 1095 steel. The applied load was 4.4 N.

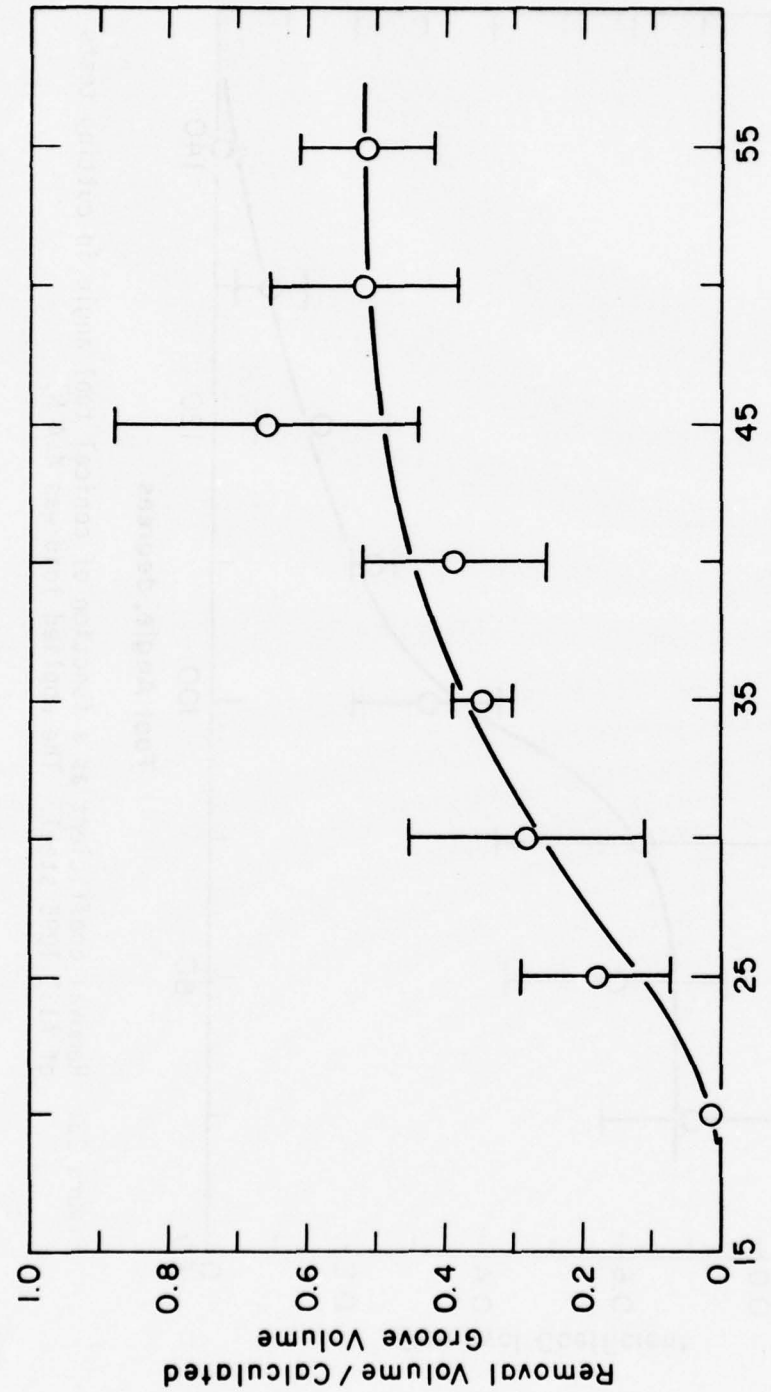

Figure 24: Ratio of the volume removed to the calculated groove volume as a function of attack angle. Experimental conditions are same as in the previous figure.

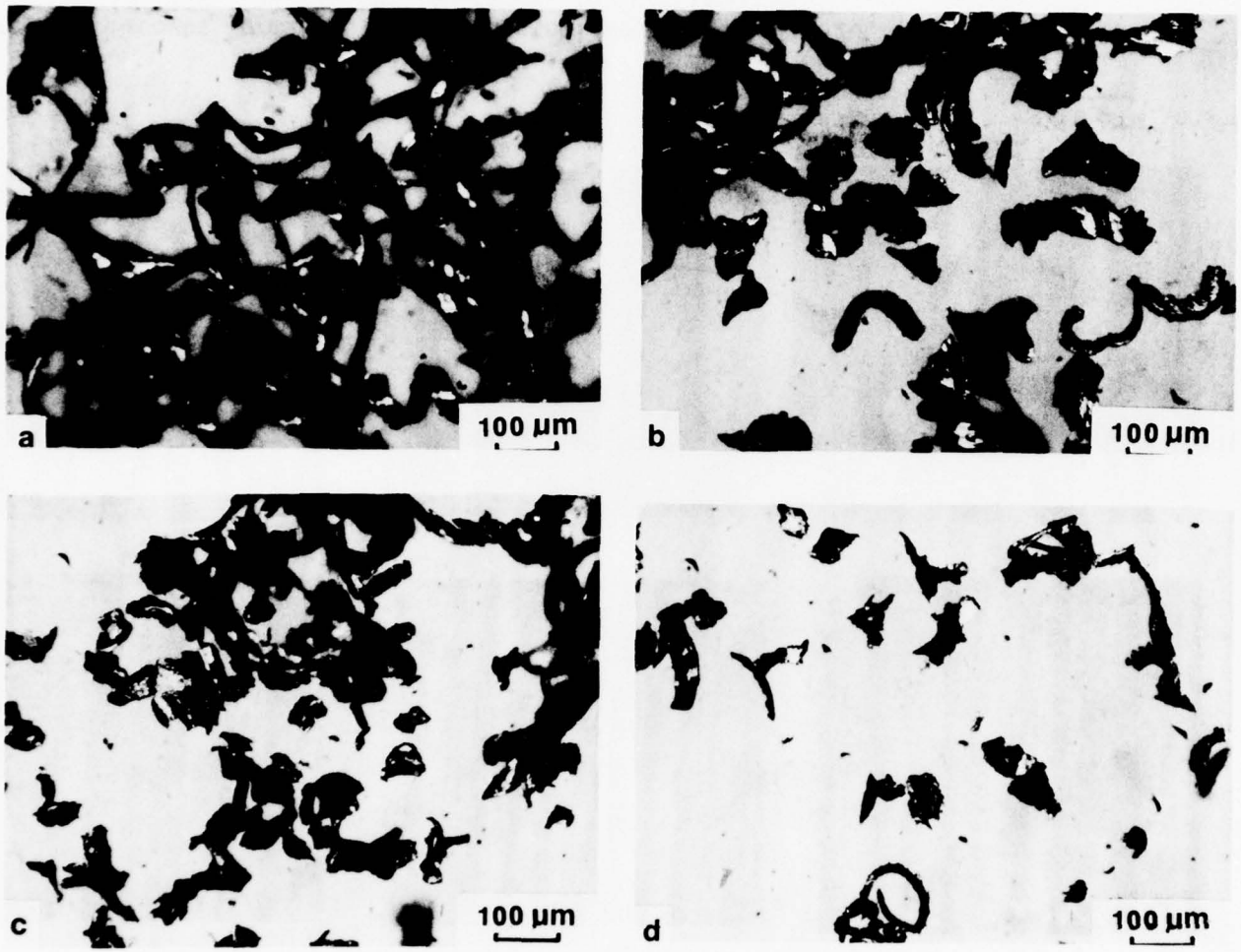

Figure 25: Micrographs of AISI 1095 steel chips: (a) 70, (b) 90, (c) 110 (d) 130-degree conical tool.

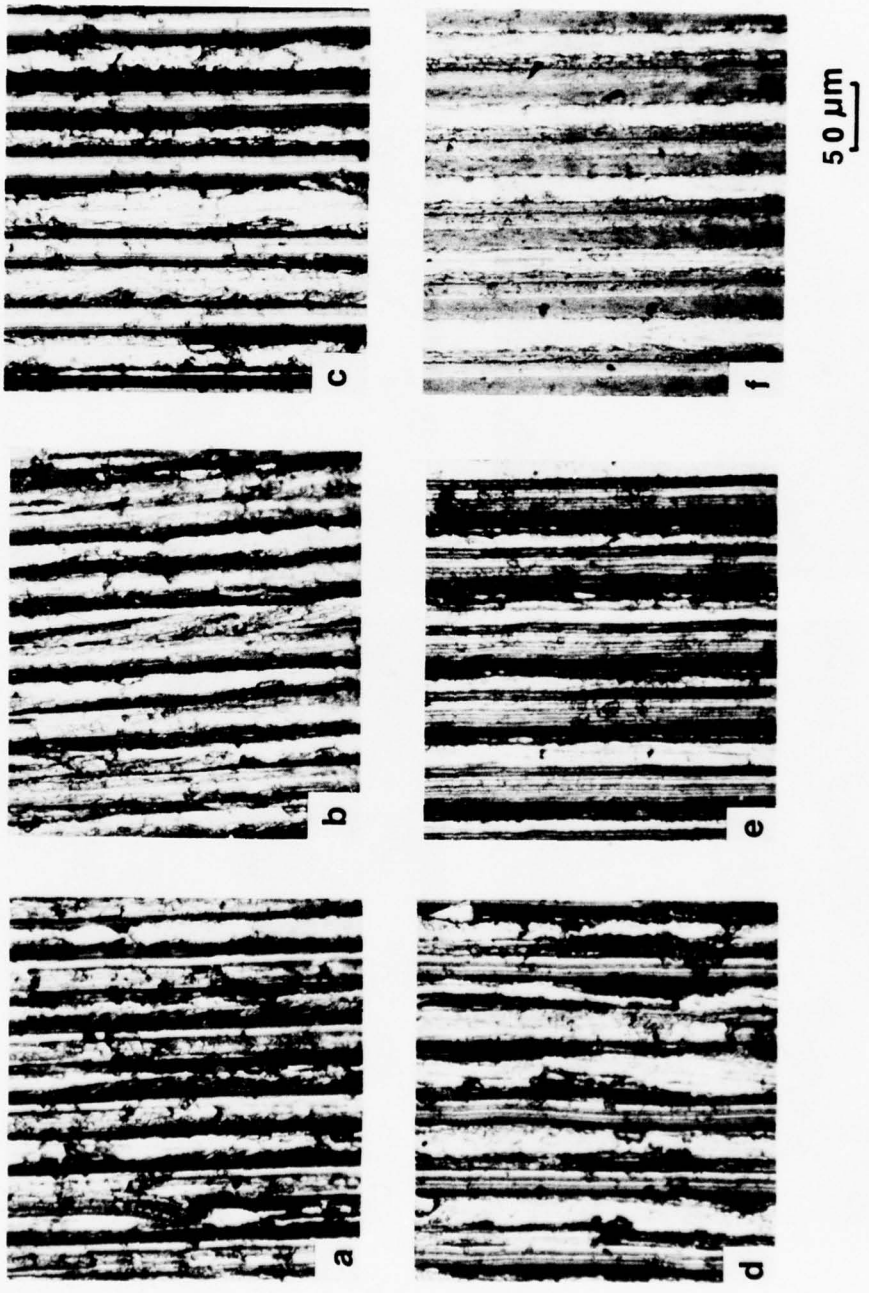

Figure 26: Grooves formed on AISI 1095 steel specimens: (a) 70, (b) 90, (c) 100, (d) 110, (e) 120 (f) 140-degree conical tool.

IV. DISCUSSION

A. Friction Coefficient

Micrographs of the worn surface shown in Figure 11 clearly indicate that plowing is dominant during abrasion. Even for the finest abrasive (4/0), the surface of the abraded sample is entirely covered with a large number of fine grooves. Therefore, the plowing component of friction plays a dominant role in abrasion.

Results of theoretical analyses and experiments with spheres, cones and pyramids (11, 30-38) show that the plowing component is strongly dependent on the shape of the asperity. For a spherical model of asperity, theoretically calculated values of the friction coefficient range from 0.1 to 1.2 as can be seen from Figure 27. Experimental values simulating abrasion with spheres (30, 37) agree with theory. Figure 20 shows that the ratio of the groove width on the PMMA specimen to the abrasive grit diameter is about 0.3. For the value of w/D_g the friction coefficient should be approximately 0.24 for a spherical particle (Figure 27). But the observed values of the friction coefficient in this work are 0.5-0.7 (Figure 4), which agree fairly well with others (10, 11, 39). Therefore, the abrasive particles cannot be modeled as spheres; they are angular as clearly seen from Figure 14.

If it is assumed that the abrasive particle has a conical shape, the plowing component of friction for the idealized model (23) is expressed as

$$\mu_p = \frac{\tan \theta}{\pi} \qquad (2)$$

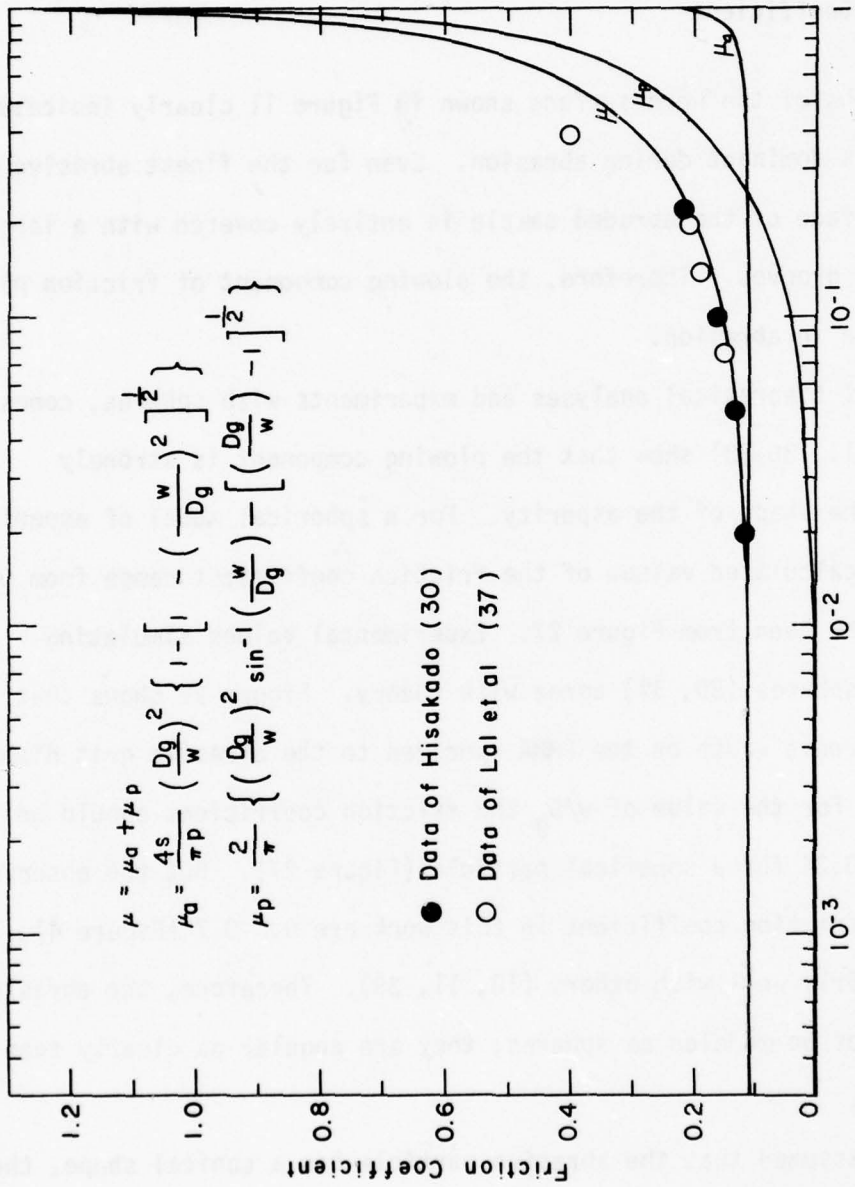

Figure 27: Friction coefficient as a function of the ratio of groove width to diameter of sphere (from Reference 11).

where θ is the slope angle of the cone surface. But the results of cutting experiments do not obey this idealized theory even when the adhesion component is considered together (Figure 28). Modified theories by Hisakado (30) and Goddard and Wilman (11) show fair agreement for θ values of 25-40 degrees. The Hisakado equation is expressed as

$$\mu = \frac{\tan\theta + \frac{\pi}{4}\mu_a (\sec\theta + 1)}{\frac{\pi}{2} - \mu_a \tan\theta} \tag{3}$$

and the Goddard and Wilman is

$$\mu = \frac{2}{\pi}\left[\tan\theta + \frac{s}{p}\sec\theta\right] \tag{4}$$

where s is the shear strength and p is the flow pressure of the material. For the range of θ = 25-40 degrees, the friction coefficient varies from 0.5 to 0.7 approximately. These values agree well with μ in abrasion tests (Figure 4). Therefore, it can be assumed that abrasive particles are approximately conical in shape with this range of slope angles.

For geometrically similar particles, the theoretical models predict that the friction coefficient must be constant for all grit diameters. But the experimental results (Figure 4) show that initially the friction coefficient slightly increases as the grit size is increased up to about 80 μm, which approximately coincides with the critical grit diameter, and later levels out and becomes essentially constant. The variation of the friction coefficient with grit diameter is similar to that of the wear rate with grit diameter (see Figure 5).

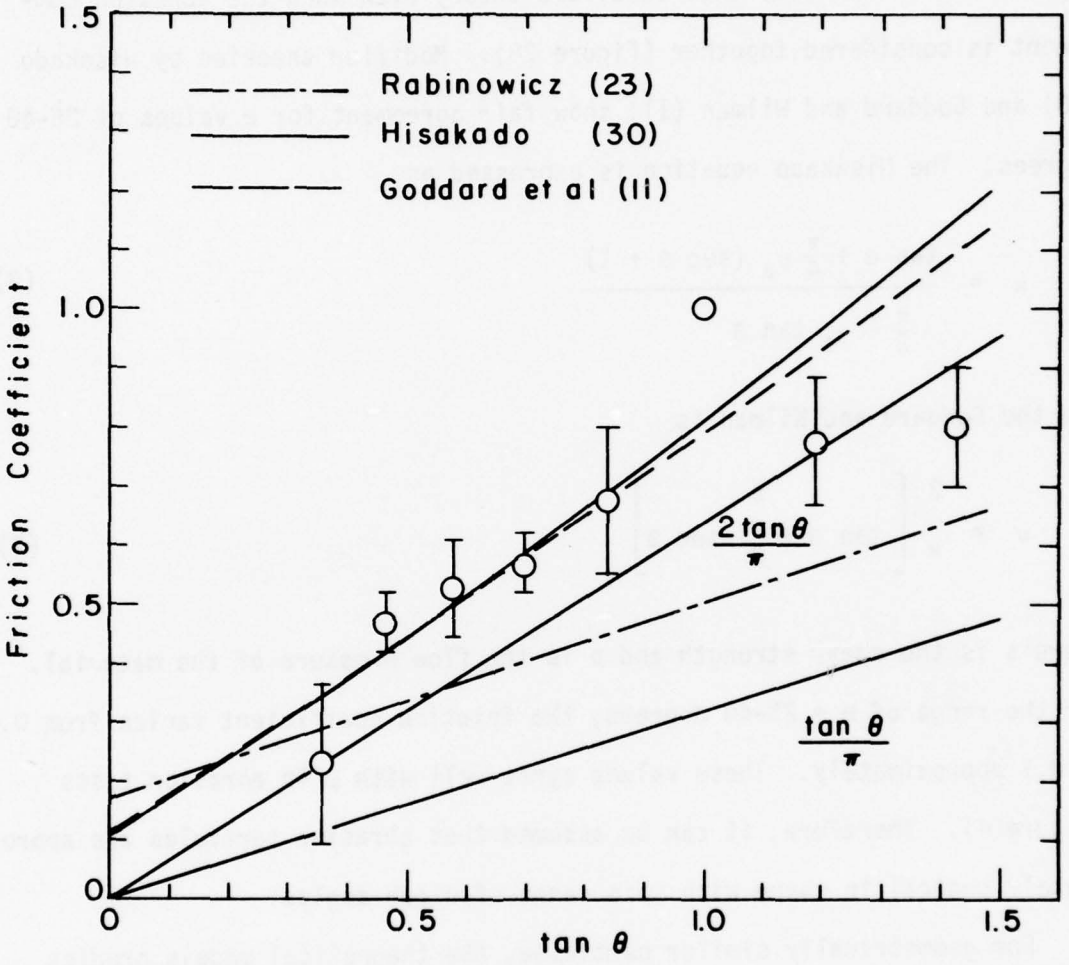

Figure 28: Friction coefficient as a function of the slope of the cone surface in cutting tests of AISI 1095 steel.

Much attention has not been paid to this grit size effect in friction coefficient. Goddard, Harker and Wilman (9) proposed that with finer grit only a limited front region of the specimen contacts the abrasive particles effectively and the remaining rear part of the face contacts metal which has been worn away from the front region. Therefore, they concluded that the friction coefficient depends on the specimen size for the finer grits and showed that for 4/0 abrasive paper the friction coefficient for a small specimen (0.18 cm) is larger by a factor of 2.5 than that for a large specimen (2 cm). But even for the smaller specimen 20% of variation, which is about the same amount of variation as in this study (Figure 4), still persists. This implies that there should be other reason in addition to clogging. Spurr and Newcomb (39) attributed the increase in friction coefficient with grit size to increasing plowing component. But they did not give any explanation why the plowing component increases.

Theoretical simple models of particle such as sphere and cone cannot explain the grit size effect because the friction coefficient is constant for all geometrically similar particles as mentioned above. If abrasive particles are conical in shape with hemispherical tip, then the friction coefficient for this can be calculated by combining sphere and cone. The plowing component μ_p is expressed as

$$\mu_p = \frac{2}{\pi}\left\{\left(\frac{w}{2r}\right)^{-2} \sin^{-1}\frac{w}{2r} - \left[\left(\frac{w}{2r}\right)^{-2} - 1\right]^{\frac{1}{2}}\right\} \qquad (5)$$

when $w \leq 2r \sin\theta$, and

$$\mu_p = \frac{2 \tan \theta}{\pi} \left[1 - \frac{4 (\tan \theta - \theta)}{\tan \theta} \left(\frac{w}{r} \right)^{-2} \right] \qquad (6)$$

when $w \geq 2r \sin \theta$. Figure 29 shows the friction coefficient of this combined model as a function of w/r, the ratio of the groove width to the tip radius. The adhesion component was estimated by considering the limiting cases of cone and sphere. If r is about 1-5 μm, the ratio w/r is about 1-5 for 600 grit and 3-15 for 320 grit (Figure 19), falling on the transition region. Therefore, by assuming that abrasive particles have this shape the size effect can be explained. With decrease of grit diameter, the width of contact decreases as shown in Figure 20, and so does the ratio w/r.

Therefore, it can be concluded that the increasing dullness of the particle due to decrease of the depth of penetration is the main reason for the decrease of μ with grit diameter in abrasion. From Figure 29 it can be also clearly seen that the decrease of μ with w/r is mainly due to the plowing component μ_p.

As far as the tip radius r is concerned, it is not possible to measure r exactly, and no one has ever specified this. From Figure 29 it can be clearly seen that the above discussion depends on the exact value of r. The grit tip radius is assumed to be of the order of that of diamond conical tools used in cutting tests.

B. Wear Coefficient

The observed values of the wear coefficient for the coarse grit are

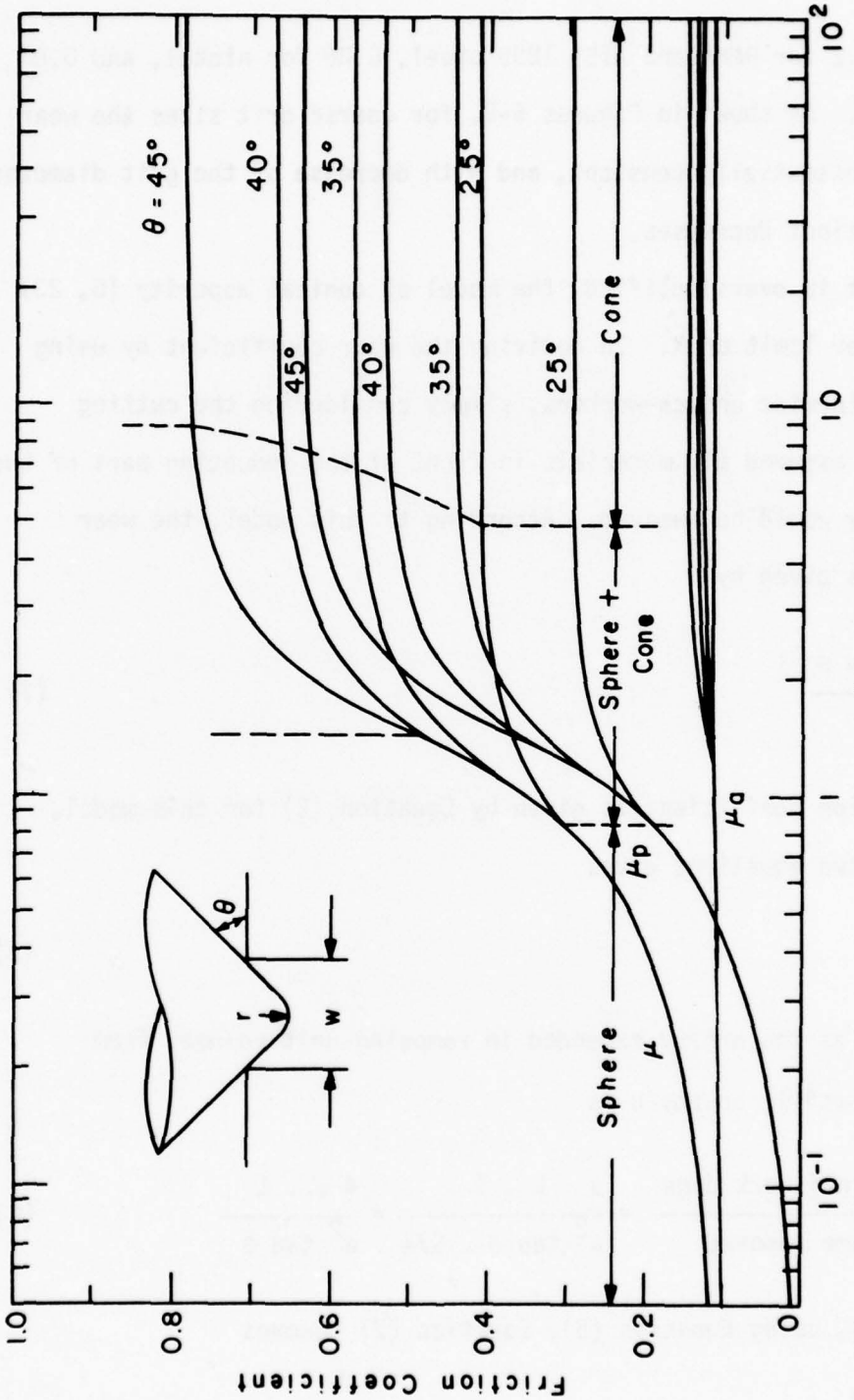

Figure 29: Friction coefficient as a function of the ratio of the groove width to the tip radius of conical particle for different cone angles.

approximately 0.2 for PMMA and AISI 1095 steel, 0.06 for nickel, and 0.07 for OFHC copper. As shown in Figures 6-8, for coarse grit sizes the wear coefficient is essentially constant, and with decrease of the grit diameter the wear coefficient decreases.

Although it is oversimplified, the model of conical asperity (6, 23) provides an upper limit on K. In deriving the wear coefficient by using this model, Rabinowicz and co-workers, simply considering the cutting mechanism only, assumed all materials in front of the indenting part of the conical asperity would be removed. According to this model, the wear coefficient K is given by

$$K = \frac{3 \tan \theta}{\pi} \tag{7}$$

Since the friction coefficient is given by Equation (2) for this model, equating these two equations gives

$$K = 3\mu \tag{8}$$

If u is defined as the energy expended in removing unit volume, from Figure 30 the specific energy u is

$$u = \frac{\text{External work done}}{\text{Volume removed}} = \frac{\mu \cdot L \cdot S}{w^2 \tan \theta \cdot S/4} = \frac{4 \mu \cdot L}{w^2 \tan \theta} \tag{9}$$

Since $L = \pi w^2 H/4$, using Equation (5), Equation (2) becomes

$$u = \frac{\mu \pi H}{\tan \theta} = H \tag{10}$$

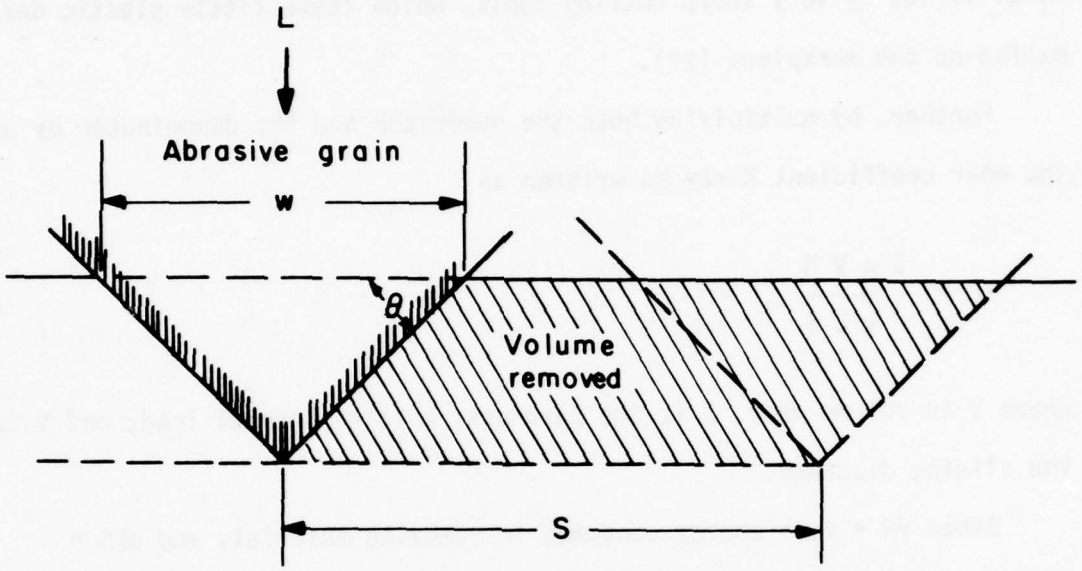

Figure 30: Idealized abrasion model in which a cone removes material from a surface.

which means the specific energy u is equal to the hardness of the material removed for the rigid plastic model. Indeed, this is the case when the metal is cut by very sharp cutting tools, which leave little plastic deformation on the workpiece (27).

Further, by multiplying both the numerator and the denominator by μ, the wear coefficient K may be written as

$$K = \frac{3 \mu V H}{\mu L S} \tag{11}$$

where V is volume wear, H is the hardness, L is the normal load, and S is the sliding distance.

Since $VH = Vu$ = energy consumed in removing material, and μLS = external work done, from Equations (8) and (11),it can be seen that the ratio of these energies is 1. This means that for the rigid plastic model the external work done is completely expended in removing material.

But the results of cutting tests do not obey Equations (7) and (8) as shown in Figures 31 and 32. For $\mu = 0.6$ θ is about 35 degrees (Figure 28) and K is 0.23 (Figure 23), but Equation (7) gives K = 0.67. Therefore, it can be concluded that although the rigid plastic analysis forms a basis its results are not strictly valid for abrasion.

Contrary to general belief, abrasion is not a simple cutting process. As shown in the micrographs of the surface (Figure 11) and the subsurface (Figure 12), large plastic deformation occurs at and below the surface during abrasion. Due to this large plastic deformation, consisting of plowing and subsurface deformation, only a small fraction of the energy input is

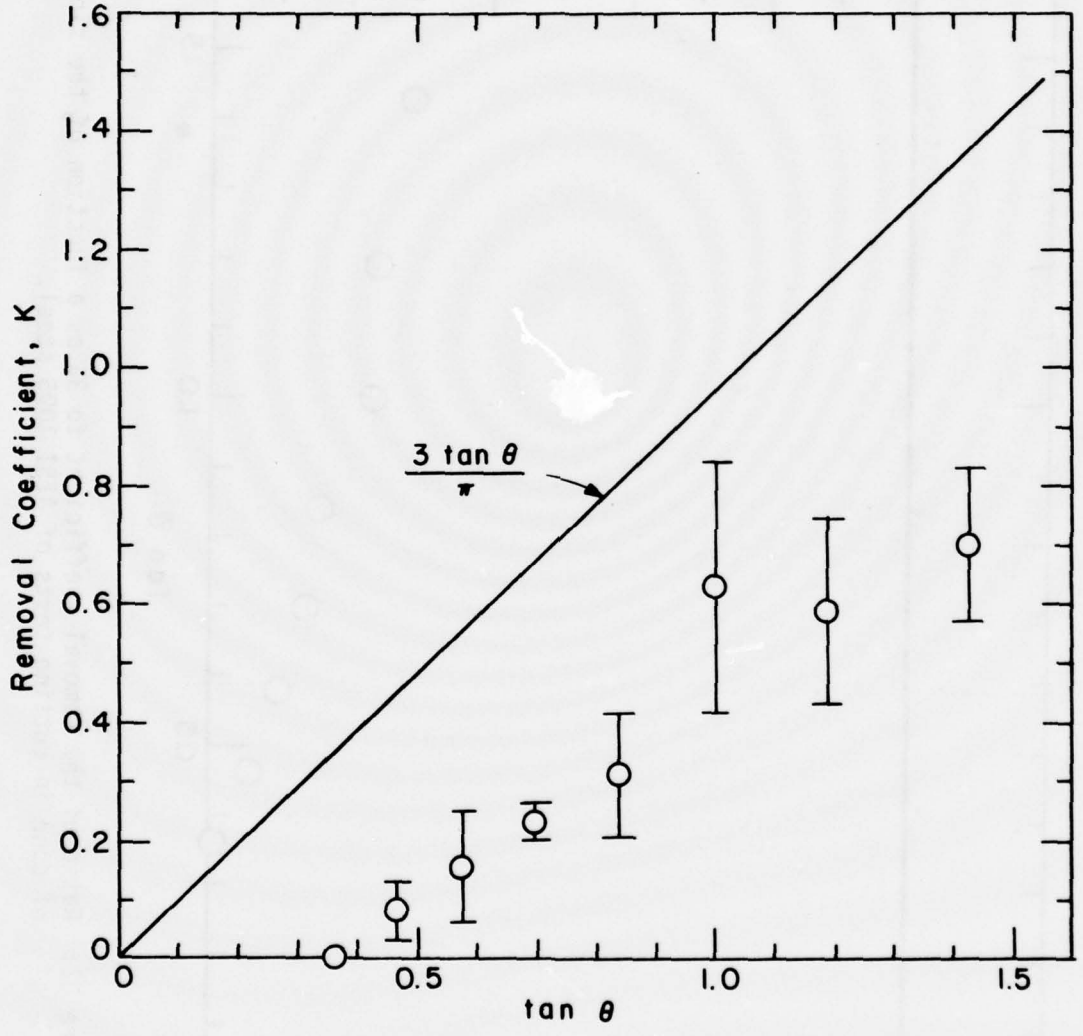

Figure 31: Removal coefficient as a function of the slope of the cone in cutting tests of AISI 1095 steel.

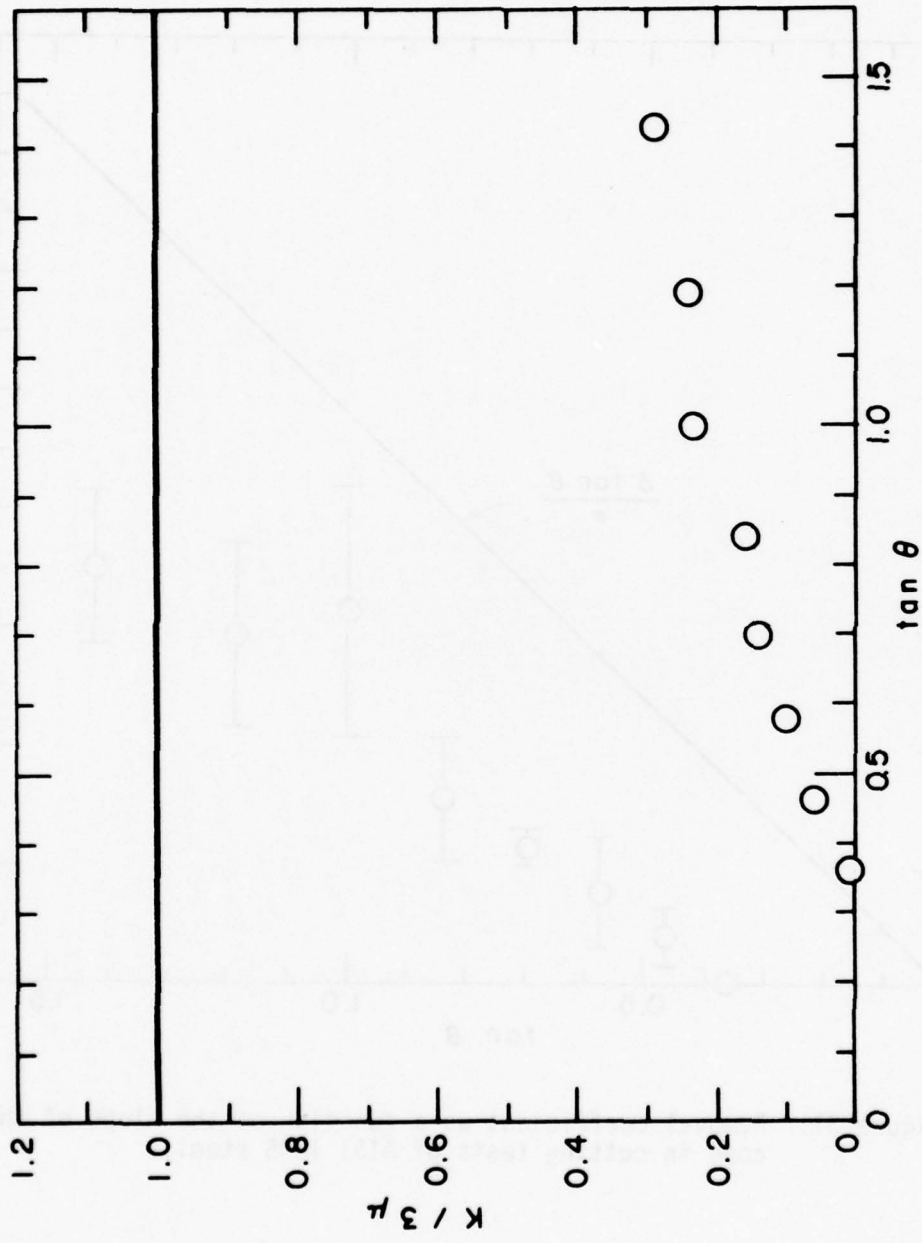

Figure 32: Ratio of the removal coefficient to 3μ as a function of the slope of cone in cutting tests of AISI 1095 steel.

expended in cutting. As for plowing component, it can be seen from Figure 24 that a conical asperity has a certain cutting efficiency defined as the ratio of removed volume to calculated groove volume in the figure. This indicates that not all material in front of the intenting part is removed in the form of chips. Instead, a large fraction of the material is plowed into ridges. Therefore, this plowing is responsible for the deviation of K from the idealized model. For θ = 35 degrees, K should be 0.25 instead of 0.67 by multiplying the cutting efficiency of about 0.4 (Figure 24). Subsurface deformation is also responsible for the deviation of K (Figure 12).

The wear coefficient not only depends on the geometry of abrasive particle but also on such material properties as hardness, toughness and work-hardening property. Table II shows the abrasive wear resistance, defined as the inverse of wear rate, of materials tested. In general, hard materials have superior abrasive wear resistance. From the table, it can be clearly seen that the wear resistance is not strictly proportional to the hardness of the materials tested. The wear resistance of heat treated AISI 1095 steel is only slighly larger than that of nickel, while the hardness values of the two are different by a factor of five. This is due to the dependence of the wear resistance of materials on the microstructure and the different work-hardening behavior by heat treatment (40-45) even for the same hardness. The lower abrasion resistance of PMMA is probably due to its brittle nature (46).

Figure 33 shows the dependence of wear coefficient on ductility of materials. As discussed the flow pattern of material around abrasive

TABLE II: ABRASION RESISTANCE OF MATERIALS TESTED

MATERIAL	HARDNESS (Kg/mm^2)	WEAR RATE (m^3/m)	ABRASION RESISTANCE (m/m^3)
PMMA	17.5	1.49×10^{-8}	7×10^{7}
OFHC Cu	44.0	2.23×10^{-9}	45×10^{7}
Ni	88.5	8.06×10^{-10}	124×10^{7}
AISI 1095 Steel	472.0	5.84×10^{-10}	171×10^{7}

* Applied Load = 4 kg

Abrasive Size = 60 grit

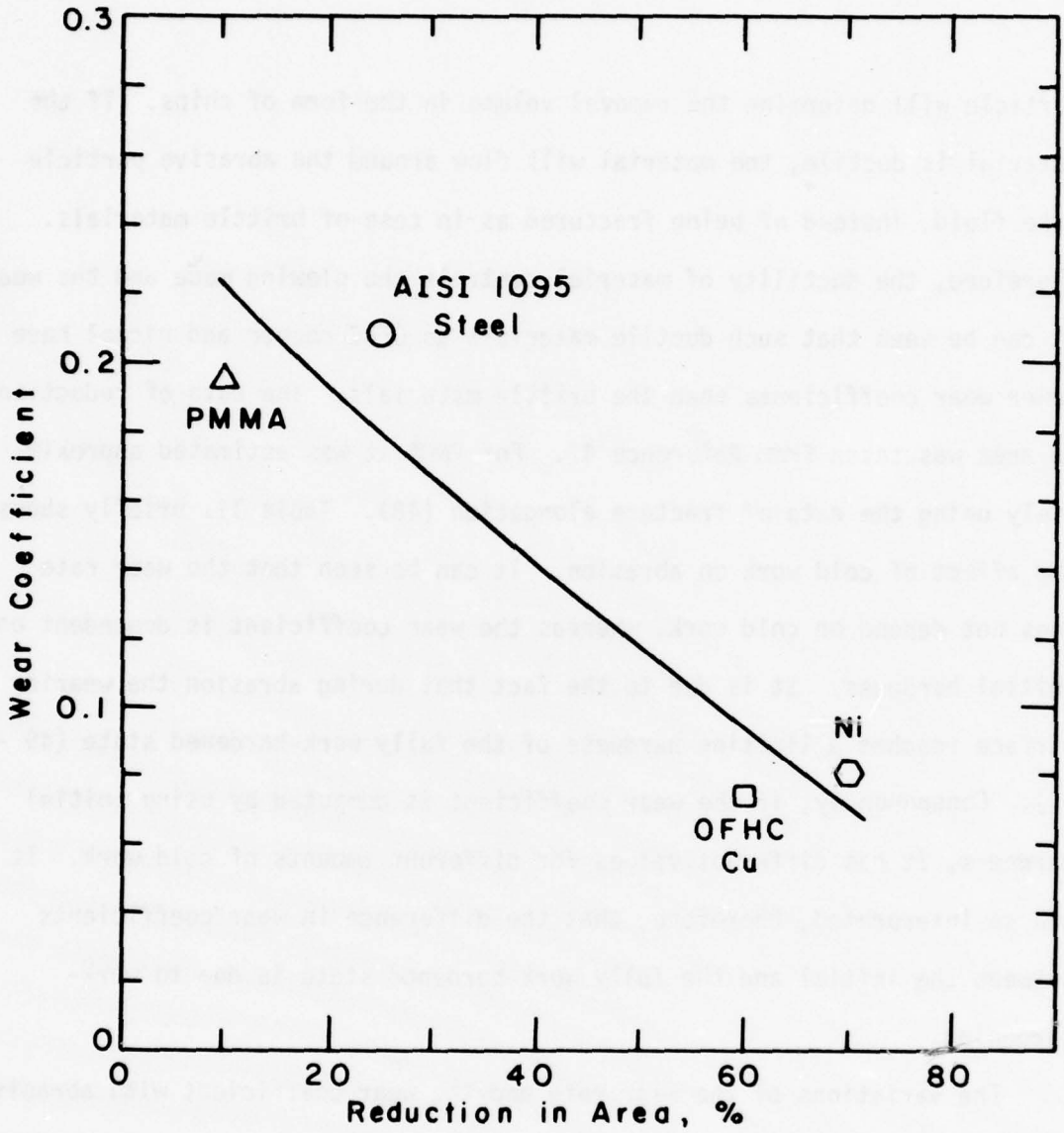

Figure 33: Wear coefficient as a function of reduction in area of materials tested for 60 grit. Applied load was 39.2 N.

particle will determine the removal volume in the form of chips. If the material is ductile, the material will flow around the abrasive particle like fluid, instead of being fractured as in case of brittle materials. Therefore, the ductility of material controls the plowing mode and the wear. It can be seen that such ductile materials as OFHC copper and nickel have lower wear coefficients than the brittle materials. The data of reduction in area was taken from Reference 47. For PMMA it was estimated approximately using the data of fracture elongation (48). Table III briefly shows the effect of cold work on abrasion. It can be seen that the wear rate does not depend on cold work, whereas the wear coefficient is dependent on initial hardness. It is due to the fact that during abrasion the wearing surface reaches a limiting hardness of the fully work-hardened state (49 - 51). Consequently, if the wear coefficient is computed by using initial hardness, it has different values for different amounts of cold work. It can be interpreted, therefore, that the difference in wear coefficients between the initial and the fully work-hardened state is due to work-hardening.

The variations of the wear rate and the wear coefficient with abrasive grit diameter are similar for all materials examined; between 600 and 60 grit they vary by a factor of about 3, slightly depending on materials (Table IV). It seems that there is no systematic dependence of that factor on the hardness of material. As for the grit size dependence of the abrasion behavior of material, many explanations have been forwarded.

The clogging of the interstices between the finer abrasive grits by wear debris (10, 15), the pickup of abrasive particles by wearing surface

TABLE III: EFFECT OF COLD WORK ON ABRASION

CONDITION	HARDNESS (kg/mm^2)	WEAR RATE (m^3/m)	WEAR COEFFICIENT	HARDNESS AFTER TEST
Annealed	88.5	8.07×10^{-10}	0.053	~ 240
Fully Cold Worked	242.0	8.66×10^{-10}	0.157	~ 242

* Material = Ni

Applied Load = 4 kg

Abrasive Size = 60 grit

TABLE IV: RATIO OF WEAR COEFFICIENTS BETWEEN 60 AND 600 GRIT

MATERIAL	HARDNESS (kg/mm^2)	LOAD (kg) 0.5	1	2	4
PMMA	17.5	3.5	2.9	2.9	3.8
OFHC Cu	44.0	---	---	---	3.4
Ni	88.5	2.4	1.9	2.2	2.4
AISI 1095 Steel	472.0	2.2	2.3	2.4	2.6

(17) and the deterioration of the abrasive with continued use (16) have been given as possible reasons for the size effect. But by making the specimen contact the fresh surface of the abrasive as conducted in this study, those factors can be minimized. Therefore, they are only partly responsible for the size effect as shown in the study of the effect of sample size (14).

Mulhearn and Samuels (8) suggested that for the fine abrasive the proportion of acicular particles is much larger and, therefore, marked cracking is present even in the unused condition. But from the micrographs of the abrasive surface (Figure 14) it is hard to conclude that is the case.

The elastic contact hypothesis proposed by Larsen-Basse (18) is based on measurements of the number of grooves and their widths for several grit sizes. The real contact area estimated by using these values up to 0.4 kg agrees very well with theory. While for loads above 0.4 kg it shows marked deviation. For a load of 1.8 kg the sum of the squares of the groove width is about 50% greater for 60 grit and 75% less for 600 grit than the corresponding values for 120, 180 and 320 grits. Combining this fact with Kragelskii's criterion (19), he postulated that many fine grits have only elastic contact with the surface. But the results of the present study (Figure 21) show that the estimated real contact area agrees within $\pm$ 50% with the theory. It is less for 60 grit and greater for 600 grit than the theoretical value. In this study the sliding distance is of the order of the average contacting grit spacing, while in Larsen-Basse's (18) study the sliding distance is approximately 1 mm, which is very large.

Therefore, the possibility of the interaction between grooves and the underestimation of the number of grooves for the fine grits cannot be ruled out.

Malkin and co-workers (20-22) have been trying to explain the size effect in abrasion from the grinding viewpoint. It was argued that the relatively flexible backing of the coated abrasive allows some of grains to come into elastic contact with the specimen surface at a load per particle less than that required to cause plowing or cutting. They concluded that this type of sliding and the increase of plowing energy with decrease of cutting depth, as clearly seen in the experiments with spherical tools, are responsible for the size effect. But this is true only when the cutting depth is varied for a given grit size. Calculations by using the results of the number of contacting particles (Figure 18) and the groove widths (Figure 20) show that even for the spherical grit model the grooves are geometrically similar for all grit size, which is contrary to the illustration of Larsen-Basse (12), who considered only one grit.

As discussed above the theories proposed in the past can explain the grit size effect only partly or some of them cannot explain it clearly because of incorrect assumptions. From now on the possible reason will be discussed.

Kragelskii (19) has proposed that, when a spherical asperity of radius R slides on a metal surface and indents it to a depth h, various types of asperity - surface interaction occur, depending on h/R. In the case of ferrous metals, for $h/R < 0.01$ only elastic deformation takes place; for $0.01 < h/R < 0.1$ plastic displacement, and when $h/R > 0.1$ cutting occurs.

According to Shaw's interpretation (25) of K, the wear coefficient is proportional to the ratio of the volume worn away to the plastically deformed volume below the indenter. The removal volume is determined by groove area, and plastically deformed volume by the area of contact since it is proportional to the cross-sectional area of plastic deformation. Therefore, the geometric parameter h/R characterizes the particle-surface interaction for a spherical indenter. For an arbitrary geometry of particles the ratio of the groove area to the contact area characterizes the interaction, therefore, the wear coefficient K.

If the abrasive particle is conical in shape with grit tip radius r, the groove area A_g can be calculated as a function of the groove width w. For $w \geq 2r \sin\theta$, the groove area Ag is

$$A_g = \frac{w^2 \tan\theta}{4}\left[1 - \frac{4(\tan\theta - \theta)}{\tan\theta}\left(\frac{w}{r}\right)^{-2}\right] \tag{12}$$

and for $w \leq 2r \sin\theta$,

$$A_g = w^2\left\{\left(\frac{w}{r}\right)^{-2}\sin^{-1}\frac{w}{2r} - \frac{1}{2}\left(\frac{w}{r}\right)^{-1}\left[1 - \left(\frac{w}{2r}\right)^2\right]^{\frac{1}{2}}\right\} \tag{13}$$

From Equation (10) it can be seen that if $w/r \to \infty$, then $A_g \to w^2 \tan\theta/4$. In this case the particle essentially acts like a cone, and here the expression $w^2 \tan\theta/4$ is equal to the exact groove area formed by a cone. From the measurement point of view, the ratio w/r is rather direct parameter than the Kragelskii's parameter h/R, because it is easier to measure w than h and w directly determines the real contact area. For the finest

grit h is of the order of 1 μm or less in abrasion.

Figure 34 shows the variation of A_g/w^2 as a function of w/r for slope angles 25-45 degrees. Variation of the mechanical interaction between the particle and the specimen by Kragelskii's criterion is also shown in the figure. The tip radius of the diamond conical tool used in simulated cutting tests was about 5 μm, which is comparable with the radius of very sharp tools used in turning operation (52). Therefore, if it is assumed that the tip shape and size of abrasive particles are more or less the same as those of the diamond tools, then the radius of the abrasive particle tip is of the order of a few microns, say 1 to 5 μm. Because the measured average groove widths on PMMA specimen are about 5 μm for 600 grit, 15 μm for 320 grit and 70 μm for 60 grit (Figure 19), the ratio w/r is about 1 to 5 for 600 grit and 3 to 15 for 320 grit, which fall on the transition region, and 14 to 70 for 60 grit, falling on the region of cone. For the change of these w/r values, the ratio A_g/w^2 varies by a factor of 2 or so, depending on θ, from 600 to 60 grit.

As discussed above not all groove volume is removed in the form of chips. The fraction of this removal volume is dependent on the geometry of the particle-specimen contact as implied by Kragelskii's criterion. Experimental results of cutting tests with spherical tools (20) show that the removal fraction depends on the ratio h/R. At present no rigorous solution for the removal fraction exists. Combining Kragelskii's criterion with experimental results for sphere (20) and for cone (Figure 24), the removal fraction can be approximately estimated. By multiplying the groove area by this fraction, the removal volume, therefore, the wear coefficient K can be

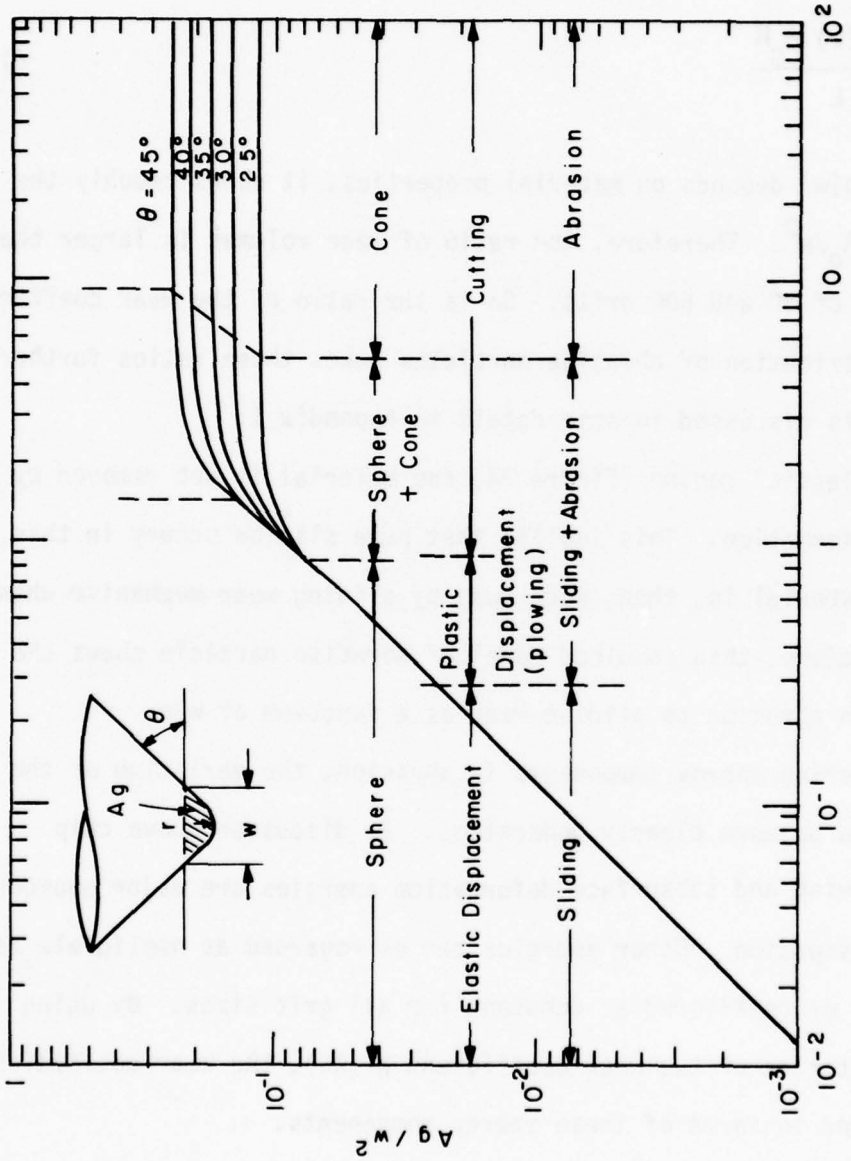

Figure 34: Ratio of the groove area to the square of the groove width as a function of the ratio of the groove width to the grit tip radius of conical particle.

obtained. If g(w) is defined as this removal fraction function, the wear coefficient K can be expressed as

$$K = \frac{3\, g(w)\, A_g H}{L} \qquad (14)$$

Although g(w) depends on material properties, it shows roughly the same trend as A_g/w^2. Therefore, the ratio of wear volumes is larger than that of A_g/w^2, of 60 and 600 grits. So is the ratio of the wear coefficients. The height distribution of abrasive particles makes these ratios further larger. This is discussed in some detail in Appendix I.

In the "elastic" region (Figure 34) the material is not removed by a single groove formation. This implies that pure sliding occurs in this region. The material is, then, worn away by sliding wear mechanism when $w/r \to 0$. Therefore, this combined model of abrasive particle shows the transition from abrasion to sliding wear as a function of w/r.

By considering energy components in abrasion, the variation of the wear coefficient can be more clearly understood. As discussed above chip formation, plowing and subsurface deformation energies are major sources of the energy dissipation. Other energies can be regarded as negligible as in metal cutting, or considered as constant for all grit sizes. By using Suh's interpretation of the wear coefficient K (26), the wear coefficient can be expressed in terms of these energy components.

As the friction coefficient is nearly independent of the grit size, the total external work done can be regarded as constant for all grit sizes. Therefore, the external work done W_e is

$$W_e = \mu LS = W_c + W_p + W_s \tag{15}$$

where W_c is the cutting energy, W_p is the plowing energy and W_s is the subsurface deformation energy. By taking $3\mu \simeq O(1)$ in Equation (11), the wear coefficient K has been interpreted as (27).

$$K \simeq \frac{VH}{\mu LS} \simeq \frac{V_u}{\mu LS} = \frac{\text{Work done to generate chips}}{\text{Total external work done}} \tag{16}$$

Since $Vu = W_c$, the wear coefficient K is

$$K \simeq \frac{W_c}{W_c + W_p + W_s} \tag{17}$$

Therefore, the relative amount of each energy component determines the wear coefficient K.

Actual abrasion process is a combination of cutting and sliding processes as discussed above. Although no exact solution for the state of stress and strain in abrasion exists, the approximate solution for an elastic-perfectly plastic plane in sliding obtained by Jahanmir and Suh (53) can provide the method of estimation of the subsurface deformation energy. When a material is subjected to cyclic loading, it can accumulate plastic strain, which is quite substantial in sliding. By applying the method of Suh and Sridharan (54) to the case of abrasion, it shows that subsurface deformation energy calculated is independent of abrasive grit sizes if grooves are similar for all grits (Appendix II). For this

assumption from Equation (15) it can be seen that $W_c + W_p \simeq$ constant.

All materials plowed ahead of the abrasive particle do not become loose wear particles. Only a fraction of the plowed material is removed. Therefore, wear attributable to plowing can be explained in terms of the fraction of the material removed after being plowed. For a conical particle with hemispherical tip, the removal fraction function g(w) vs. w has approximately the same shape as A_g/w^2. Since w is proportional to the grit diameter D_g (Figure 20) and g(w) decreases with decreased w, the plowing energy W_p will increase with decrease of D_g, and, therefore, the cutting energy W_c will decrease. This is shown schematically in Figure 35. Accordingly, the wear coefficient K will decrease with decreased grit diameter as can be seen from Equation (17).

For the extremely small grits, the wear is essentially controlled by the sliding wear mechanism as can be seen from Figure 34 since $w/r \to 0$. Assuming that sliding wear is controlled by the delamination mechanism (55), the wear occurs as a result of several sequential (or independent, if there are pre-existing subsurface cracks) processes, namely subsurface deformation, crack nucleation and crack propagation. Analysis of subsurface deformation and crack nucleation by Jahanmir and Suh (53) has shown that deformation and crack nucleation around hard particles take very short time. Therefore, the crack propagation will control the sliding wear. By applying the analysis of crack propagation (56) to the liming case of $D_g \to 0$ in abrasion (Appendix III), it can be seen that $K \sim D_g^{\frac{m}{2}}$, where m is the constant in crack growth equation. Although this does not predict exact variation of K, it provides a qualitative explanation. It is conceivable that the

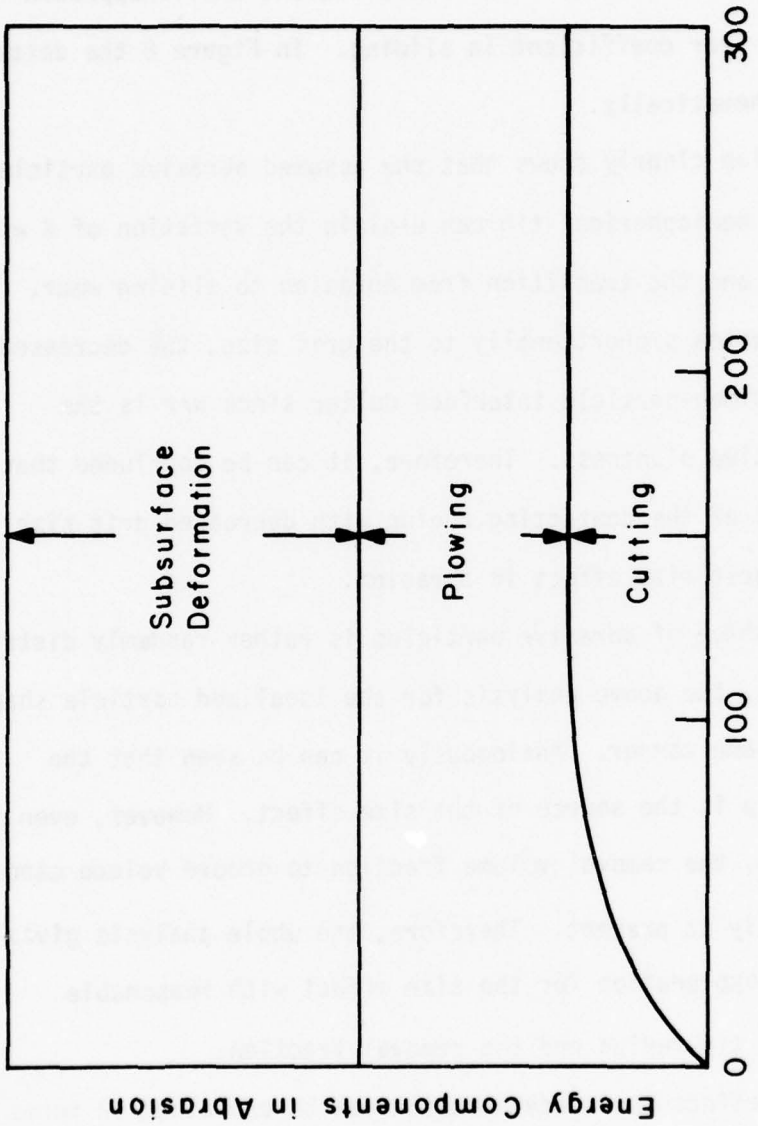

Figure 35: Schematic of energy components in abrasion.

abrasive wear cannot be less than the sliding wear under identical experimental conditions. Therefore, the wear coefficient K will approach asymptotically the wear coefficient in sliding. In Figure 8 the dotted lines show this schematically.

Above discussion clearly shows that the assumed abrasive particle shape of cone with hemispherical tip can explain the variation of K with the grit diameter, and the transition from abrasion to sliding wear. As the groove width varies proportionally to the grit size, the decreased grit size makes the specimen-particle interface duller since w/r is the indication of relative bluntness. Therefore, it can be concluded that the increasing dullness of the contacting region with decreased grit size is the source of the grit size effect in abrasion.

Although the shape of abrasive particles is rather randomly distributed pyramids than cones, the above analysis for the idealized particle shape is applicable in the same manner. Analogously it can be seen that the relatively blunt tip is the source of the size effect. However, even for the idealized shape, the removal volume fraction to groove volume cannot be determined rigorously at present. Therefore, the whole analysis gives an order of magnitude explanation for the size effect with reasonable assumptions for the tip radius and the removal fraction.

The grit size effect in 3-body abrasion can be explained in terms of the relative bluntness of abrasive grits. As can be seen from the expression for K, i.e. Equation (7), small values of K imply the decrease of the slope angle θ, which implicitly means the increasing bluntness of the particle geometry with decreased grit size. Since abrasive particles spend

most of the time in rolling in 3-body abrasion, much more energy goes into plastic deformation. Therefore, the transition from abrasion to sliding wear will occur more rapidly than in 2-body abrasion.

Further, the relative hardness between abrasive and specimen will control the position of transition region as a function of grit size. As shown by Richardson (2), the wear resistance of the material increases when its hardness exceed about 80% of the abrasive hardness. If the hardness of the wearing material is comparable with the abrasive hardness, it is no longer controlled by abrasion mechanism. For a given load, the particles cannot indent deep, and, therefore, the contacting geometry becomes duller even for coarse grits. Therefore, increasing hardness of material or decreasing hardness of the abrasive will accelerate the transition from abrasion to delamination wear.

The abrasion behavior of materials with grit size is of practical interest in terms of wear prevention related to the wear mechanism. One of the applications is the filtration of lubrication systems. By proper filter design the wear caused by loose particles in fluid system can be minimized. These particles are either from outside or oxidized wear debris from sliding surfaces. In case of oxidized wear particles, the wear can be further reduced by proper designing of materials. Usually the hard particles in the matrix are more detrimental when they are worn away and become loose. By controlling the hard particle size far below the critical size of about 80 μm, the wear can be reduced. In most multiphase material the hard particle size is about 1 μm, but in composite it is of the order of 10 μm. Furthermore, by reducing the size less than 1 μm, the wear mode can

be changed to sliding wear. Then the wear minimization techniques in delamination theory (57) will provide better solution. Therefore, choosing proper hard phase size in composite material wear can be further minimized by combining those techniques.

V. CONCLUSIONS

As a result of this study the following conclusions can be drawn:

1. The idealized rigid plasticity models of abrasive wear using simple geometries are not strictly valid. The wear coefficient predicted by those theories is of the order of unity whereas the experimentally measured values are in the range 10^{-2} - 10^{-1}.
2. The reason for that disagreement between theory and experiment is due to the fact that only a very small fraction of the external work done is consumed in removing the material by simple cutting process. Large fraction of the work is dissipated by plowing, subsurface deformation, etc.
3. According to the classical theories, for a given load the wear rate is dependent on the hardness of the material only. However, results of this study show that the wear rate is dependent not only on hardness but on ductility also.
4. Previous theories of grit size effect in abrasive wear such as clogging, elastic contact, etc. are not fully valid.
5. The increase in the relative bluntness of the indenting part of abrasive particle with decreased diameter is the major cause for the dependence of friction coefficient and wear coefficient on the grit size. An idealized model of abrasive particle as cone with hemispherical tip explains the variation of friction coefficient with grit diameters, and qualitatively shows the transition from cutting mode to sliding mode.

6. The grit size effect in abrasion can be used to advantage in designing filters for lubrication systems and materials for abrasion and sliding wear resistance.

REFERENCES

1. D. Tabor, The Hardness of Metals, Clarendon Press, 1951.

2. R.C.D. Richardson, "The Wear of Metals by Relatively Soft Abrasives," Wear, 11(1968), 245-275.

3. B.W.E. Avient and H. Wilman, "New Features of the Abrasion Process Shown by Soft Metals; The Nature of Mechanical Polishing," Brit. J. Appl. Phys., 13(1962), 521-526.

4. G.K. Nathan and W.J.D. Jones, "The Empirical Relationship Between Abrasive Wear and the Applied Conditions," Wear, 9(1966), 300-309.

5. J. Larsen-Basse and P.A. Tanouye, "Strain Rate Effects in Low Speed Two-Body Abrasion," Wear of Materials, 1977, The Int. Conf. on Wear of Materials, St. Louis, Missouri, 1977.

6. E. Rabinowicz, L.A. Dunn and P.G. Russell, "A Study of Abrasive Wear Under Three-Body Conditions," Wear, 4(1961), 345-355.

7. E. Rabinowicz and A. Mutis, "Effect of Abrasive Particle Size on Wear," Wear, 8(1965), 381-390.

8. T.O. Mulhearn and L.E. Samuels, "The Abrasion of Metals: A Model of the Process," Wear, 5(1962), 478-498.

9. J. Goddard, H.J. Harker and H. Wilman, "A Theory of the Abrasion of Solids Such as Metals," Nature, 184(1959), 333-335.

10. B.W.E. Avient, J. Goddard and H. Wilman, "An Experimental Study of Friction and Wear During Abrasion of Metals," Proc. Roy. Soc. (London), A258(1960), 159-179.

11. J. Goddard and H. Wilman, "A Theory of Friction and Wear During the Abrasion of Metals," Wear, 5(1962), 114-135.

12. J. Larsen-Basse, "Influence of Grit Diameter and Specimen Size on Wear During Sliding Abrasion," Wear, 12(1968), 35-53.

13. J. Larsen-Basse, "Some Effects of Specimen Size on Abrasive Wear," Wear, 19(1972), 27-35.

14. E. Rabinowicz, "Practical Uses of the Surface Energy Criterion," Wear, 7(1964), 9-22.

15. M.A. Moore and R.M. Douthwaite, "Plastic Deformation Below Worn Surfaces," Met. Trans., 7A(1976), 1833-1839.

16. S.W. Date and S. Malkin, "Effects of Grit Size on Abrasion with Coated Abrasives," Wear, 40(1976), 223-235.

17. R.W. Johnson, "A Study of the Pickup of Abrasive Particles During Abrasion of Annealed Aluminum on Silicon Carbide Abrasive Papers," Wear, 16(1970), 351-358.

18. J. Larsen-Basse, "Influence of Grit Size on the Groove Formation During Sliding Abrasion," Wear, 11(1968), 213-222.

19. I.V. Kragelskii, Friction and Wear, Butterworths, London, 1965.

20. S. Malkin, K.L. Wiggins, M. Osman and R.W. Smalling, "Size Effects in Abrasive Processes," Proc. 13th Int. Mach. Tool Des. Res. Conf., Birmingham, 1972, Macmillan, London, 1973.

21. S. Malkin and N. Joseph, "Minimum Energy in Abrasive Processes," Wear, 32(1975), 15-23.

22. S. Malkin, "Specific Energy and Mechanisms in Abrasive Processes," Proc. 3rd North American Metalworking Res. Conf., Pittsburgh, 1975, 453-465.

23. E. Rabinowicz, Friction and Wear of Materials, Wiley, New York, 1965.

24. M.C. Shaw, "Fundamentals of Wear," CIRP Ann., 19(1971), 533-543.

25. M.C. Shaw, "Dimensional Analysis for Wear Systems," Wear, 43(1977), 263-266.

26. N.P. Suh, "Scientific and Technical Problems in Erosive Wear," Presented at Institute on Scientific Problems Relevant to Coal Utilization, West Virginia University.

27. N.H. Cook, Manufacturing Analysis, Addison-Wesley, Reading, 1966.

28. A.J. Sedriks and T.O. Mulhearn, "Mechanics of Cutting and Rubbing in Simulated Abrasive Processes," Wear, 6(1963), 457-466.

29. A.J. Sedriks and T.O. Mulhearn, "The Effect of Work-Hardening on the Mechanics of Cutting in Simulated Abrasive Processes," Wear, 7(1964), 451-459.

30. T. Hisakado, "On the Mechanism of Contact Between Solid Surfaces," Bull. JSME, 13(1970), 129-139.

31. T. Tsukizoe and T. Sakamoto, "On the Geometrical Shape of Scratched Groove in Friction Process," Bull. JSME, 17(1974), 1637-1644.

32. T. Tsukizoe and T. Sakamoto, "Friction in Scratching Without Metal Transfer," Bull. JSME, 18(1975), 65-72.

33. A. Broese van Groenou, N. Maan and J.D.B. Veldkamp, "Scratching Experiments on Various Ceramic Materials," Philips Res. Rep., 30(1975), 320-359.

34. N. Maan and A. Broese van Groenou, "Low Speed Scratch Experiments on Steels," Wear, 42(1977), 365-390.

35. D. Graham and R.M. Baul, "An Investigation into the Mode of Metal Removal in the Grinding Process," Wear, 19(1972), 301-314.

36. N. Gane and J. Skinner, "The Friction and Scratch Deformation of Metals on a Micro Scale," Wear, 24(1973), 207-217.

37. G.K. Lal and M.C. Shaw, "Experiments with Spherical Tools," Wear, 29(1974), 153-161.

38. S.K. Dean and E.D. Doyle, "Significance of Grit Morphology in Fine Abrasion," Wear, 35(1975), 123-129.

39. R.T. Spurr and T.P. Newcomb, "The Friction and Wear of Various Materials Sliding Against Unlubricated Surfaces of Different Types and Degrees of Roughness," Proc. Conf. Lubrication and Wear, Instn. Mech. Engrs., London, 269-275.

40. M.M. Khrushchov and M.A. Babichev, "The Effect of Heat Treatment and Work Hardening on the Resistance to Abrasive Wear of Some Alloy Steels," Friction and Wear in Machinery, ASME, 19(1964), 1-15.

41. M.M. Khrushchov and M.A. Babichev, "Resistance to Abrasive Wear of Structurally Inhomogeneous Materials," Friction and Wear in Machinery, ASME, 12(1960), 5-24.

42. M.M. Khrushchov and M.A. Babichev, "Abrasive-Wear Resistance and the Modulus of Elasticity of Heat-Treated Steels," Friction and Wear in Machinery, ASME, 17(1965), 9-18.

43. J. Larsen-Basse, "The Abrasion Resistance of Some Hardened and Tempered Carbon Steels," Trans. AIME, 236(1966), 1461-1466.

44. J. Larsen-Basse, "Abrasion Resistance of Some S.A.P.-Type Alloys at Room Temperature," Wear, 12(1968), 357-368.

45. J. Larsen-Basse and K.G. Mathew, "Influence of Structure on the Abrasion Resistance of a 1040 Steel," Wear, 14(1969), 199-206.

46. A. Selwood, "The Abrasion of Materials by Carborundum Paper," Wear, 4(1961), 311-318.

47. D.F. Miner and J.B. Seastone, Handbook of Engineering Materials, John Wiley, 1955.

48. F.A. McClintock and A.S. Argon, Mechanical Behavior of Materials, Addison-Wesley, 1966.

49. M.M. Khrushchov and M.A. Babichev, "An Investigation of the Wear of Metals and Alloys by Rubbing on an Abrasive Surface," Friction and Wear in Machinery, ASME, 11(1956), 1-12.

50. M.M. Khrushchov, "Resistance of Metals to Wear by Abrasion, as Related to Hardness," Proc. Conf. Lub. Wear, Inst. Mech. Engrs., London, 1957, 655-659.

51. R.C.D. Richardson, "The Maximum Hardness of Strained Surfaces and the Abrasive Wear of Metals and Alloys," Wear, 10(1967), 353-382.

52. P. Albrecht, "New Developments in the Theory of the Metal-Cutting Process, Part I, The Ploughing Process in Metal-Cutting," J. Engng. for Industry, Trans. ASME, 82(1960), 348-358.

53. S. Jahanmir and N.P. Suh, "Mechanics of Subsurface Void Nucleation in Delamination Wear," Wear, 44(1977), 17-38.

54. N.P. Suh and P. Sridharan, "Relationship Between the Coefficient of Friction and the Wear Rate of Metals," Wear, 34(1975), 291-299.

55. N.P. Suh, "An Overview of the Delamination Theory of Wear," Wear, 44(1977), 1-16.

56. J.R. Fleming and N.P. Suh, "Mechanics of Crack Propagation in Delamination Wear," Wear, 44(1977), 39-56.

57. N.P. Suh, N. Saka and S. Jahanmir, "Implications of the Delamination Theory on Wear Minimization," Wear, 44(1977), 127-134.

APPENDIX I

EFFECT OF THE GRIT TIP AND THE HEIGHT DISTRIBUTION

The shape of the abrasive particles (Figure 14), and the groove width (Figure 20) apparently show that grooves are geometrically similar. However, as shown in text the relative sharpness of the grit tip will influence the groove geometry and, therefore, geometrical similarity is not realized. In a microscopic sense the grit tip is relatively dull when the depth of cut is extremely small. Since the heights of the abrasive particles are distributed over a wide range, there are particles whose depths of cut are less than a critical depth where the relative sharpness starts to affect the wear rate even for the coarse grits.

If the heights of the abrasive particles are normally distributed (Figure I-1), then we have

$$f(u) = \frac{1}{(2\pi)^{\frac{1}{2}}\sigma} \exp\left\{-\frac{1}{2}\left(\frac{u}{\sigma}\right)^2\right\} \qquad \text{(I-1)}$$

where

$f(u)$ = probability density

u = distance from median line

σ = standard deviation

The standard deviation σ, and the maximum height u_m can be assumed to be approximately proportional to the abrasive grit size D_g(I-1). And the total number of abrasive particles within the apparent contact area is inversely proportional to the grit diameter (Figure 15). Therefore,

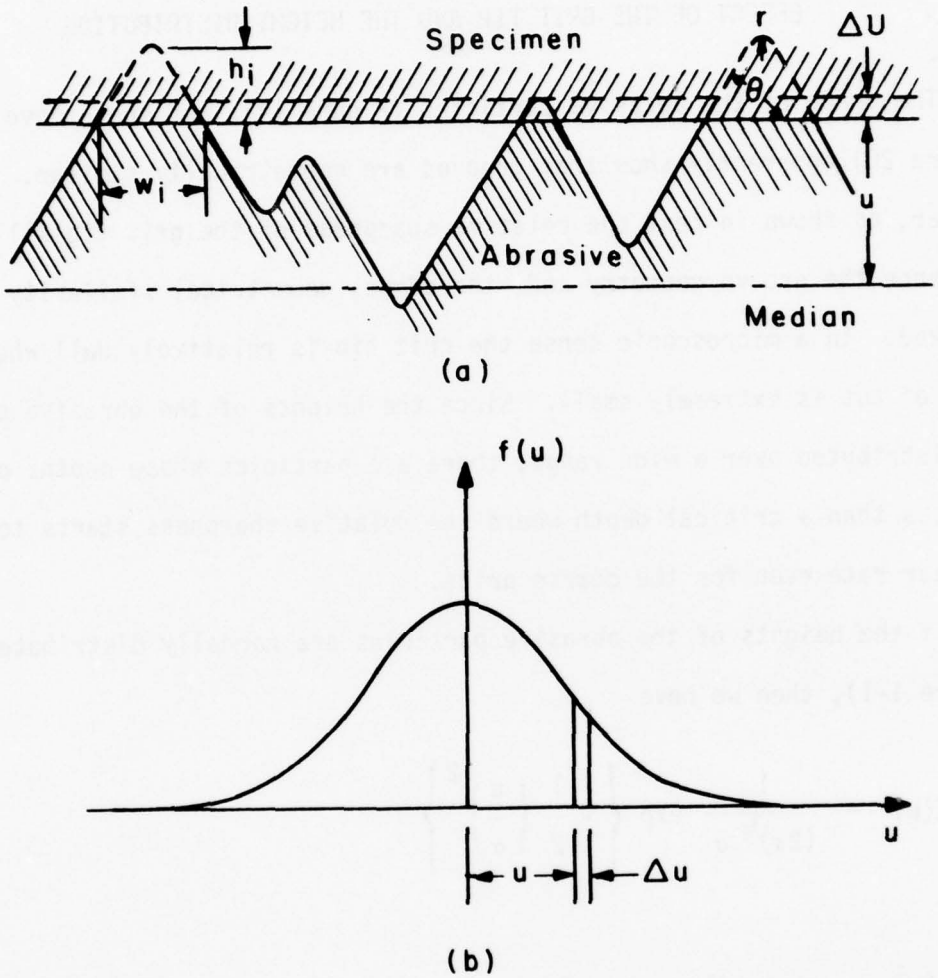

Figure I-1 Abrasive surface: (a) schematic of abrasive surface pressed by specimen, (b) height distribution curve.

$$\sigma = k_1 D_g$$
$$u_m = k_2 D_g \qquad \text{(I-2)}$$
$$N_t = k_3 D_g^{-2}$$

The number of contacting particles whose heights are between u and u_m is

$$N(u) = N_t \int_u^{u_m} f(u)\, du \qquad \text{(I-3)}$$

Assuming that the particles are conical in shape with a slope angle of θ, we have the expression for the real contact area,

$$A(u) = N_t \pi \int_u^{u_m} \left(\frac{u_1 - u}{\tan \theta} \right)^2 f(u_1)\, du_1 \qquad \text{(I-4)}$$

It can be assumed that the penetrating depth is approximately proportional to the grit diameter (I-2). Therefore, the penetrating depth, $u_m - u$, is related to D_g as

$$u_m - u = C D_g \qquad \text{(I-5)}$$

Using Equation (I-5), we get expression for $-\frac{dN}{du}$ from Equation (I-3)

$$-\frac{dN}{du} = \frac{k_3}{(2\pi)^{\frac{1}{2}} k_1 D_g^3} \exp\left\{ -\frac{1}{2} \left(\frac{k_2 - C}{k_1} \right)^2 \right\} = C_1 D_g^{-3} \qquad \text{(I-6)}$$

where

$$C_1 = \frac{k_3}{(2\pi)^{\frac{1}{2}} k_1} \exp\left\{-\frac{1}{2}\left(\frac{k_2 - C}{k_1}\right)^2\right\}$$

This means that for a given increase of penetrating depth Δu, the increase of newly penetrating particles is inversely proportional to D_g^3.

If Δu_c is the depth of penetration where the grit tip radius begins to influence the groove geometry, from Equation (I-6) the number of penetrating particles whose depths of penetration are less than Δu_c is

$$\Delta N = k_4 D_g^{-3} \tag{I-7}$$

and experimental results (Figure 18) show that the total number of penetrating particles, N, is

$$N = k_5 D_g^{-2} \tag{I-8}$$

Using Equations (10) and (11), the total groove area ΣAg_i is

$$\Sigma Ag_i = \sum_{w_i \geq 2r\sin\theta} \frac{w_i^2 \tan\theta}{4}\left[1 - \frac{4(\tan\theta - \theta)}{\tan\theta}\left(\frac{w_i}{r}\right)^{-2}\right] + \sum_{w_i < 2r\sin\theta} w_i^2\left\{\left(\frac{w_i}{r}\right)^{-2} \sin^{-1}\frac{w_i}{2r} - \frac{1}{2}\left(\frac{w_i}{r}\right)^{-1}\left[1 - \left(\frac{w_i}{2r}\right)^2\right]^{\frac{1}{2}}\right\} \tag{I-9}$$

Results of cutting experiments (Figure 24) and limited cutting data (I-2) show that the ratio of removal volume to groove volume is dependent on w and

θ. If g(w) is defined as the removal fraction function for a given θ and r (Figure I-2), the removal volume V in sliding distance S is

$$\frac{V}{S} = \Sigma\, g(w_i)\, Ag_i \tag{I-10}$$

From Figure 34 it can be assumed that beyond a certain value of w/r (about 5) the particle acts essentially like a cone and below it like a combination of cone and sphere. For $w/r < 0.8$, it is a sphere. Therefore, from Equation (I-10) the wear rate becomes

$$\frac{V}{S} = \sum_{\text{cone}}^{N-\Delta N} [g(w_i)\, Ag_i] + \sum_{\text{cone + sphere}}^{\Delta N1} [g(w_i)\, Ag_i]$$

$$+ \sum_{\text{sphere}}^{\Delta N2} [g(w_i)\, Ag_i] \tag{I-11}$$

where $\Delta N = \Delta N1 + \Delta N2$. Further, Equation (I-11) can be written as

$$\frac{V}{S} = \sum_{\text{cone}}^{N} \left[g(w_i)\, Ag_i\right]_{\text{cone}} - \sum_{\text{cone + sphere}}^{\Delta N1} \left\{ \left[g(w_i)\right]_{\text{cone}} - \left[g(w_i)\right]_{\text{cone + sphere}} \right\} Ag_i$$

$$- \sum_{\text{sphere}}^{\Delta N2} \left\{ \left[g(w_i)\right]_{\text{cone}} - \left[g(w_i)\right]_{\text{sphere}} \right\} Ag_i \tag{I-12}$$

In this equation, the second term on the right represents the decrease of wear rate due to the combined shape in the transition region, and the third due to sphere. For 600 and 320 grit it was shown in the text that w/r

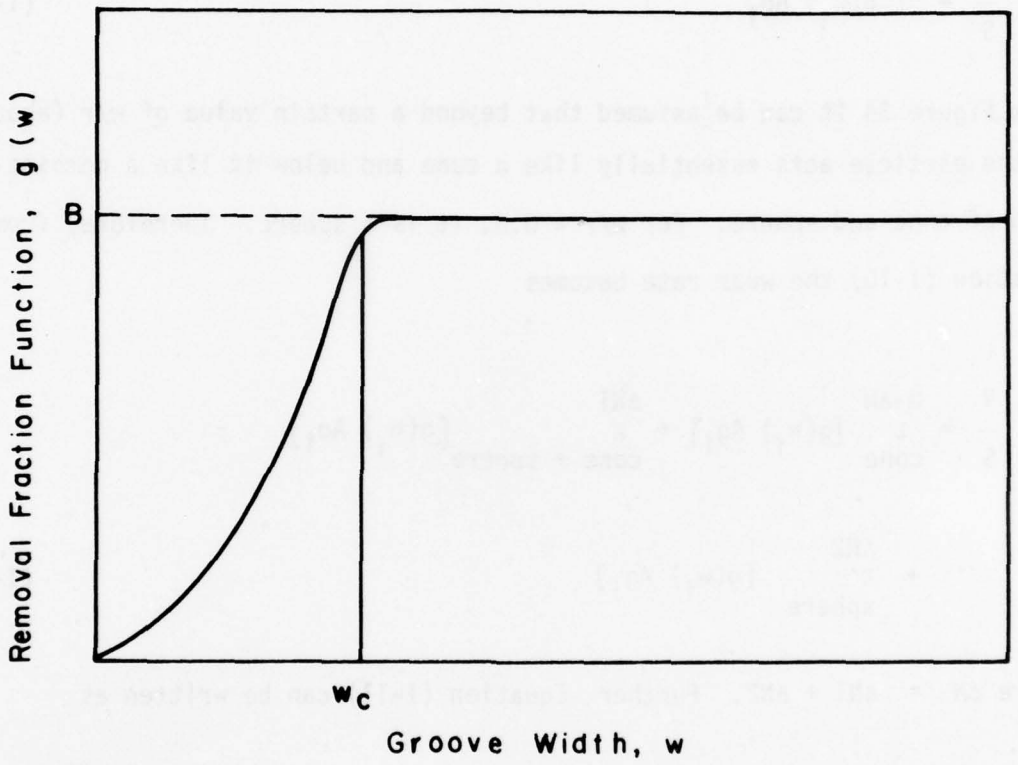

Figure I-2 Schematic of removal fraction function g(w) as a function of groove width.

values fall on the transition region i.e., cone + sphere. But a large number of contacts are in sphere region for these grits due to the height distribution of abrasive particles as can be seen from Equation (I-7). Therefore, not only the average geometry of abrasive particles but also the height distribution makes the wear rate decrease with decreased grit size.

APPENDIX I - REFERENCES

I-1. T. Tsukizoe and T. Hisakado, "On the Mechanism of Contact Between Metal Surfaces - The Penetrating Depth and the Average Clearance," J. Bas. Engng., Trans. ASME, 87(1965), 666-674.

I-2. S. Malkin, K.L. Wiggins, M. Osman and R.W. Smalling, "Size Effects in Abrasive Processes," Proc. 13th. Int. Mach. Tool Des. Res. Conf., Birmingham, 1972, Macmillan, London, 1973.

AD-A060 120 MASSACHUSETTS INST OF TECH CAMBRIDGE LAB FOR MFG AND--ETC F/G 11/11
EFFECT OF ABRASIVE GRIT SIZE ON ABRASIVE WEAR.(U)
JUN 78 N P SUH, N SAKA, H SIN N00014-76-C-0068

UNCLASSIFIED NL

2 OF 2
AD A060120

END
DATE FILMED
12 78
DDC

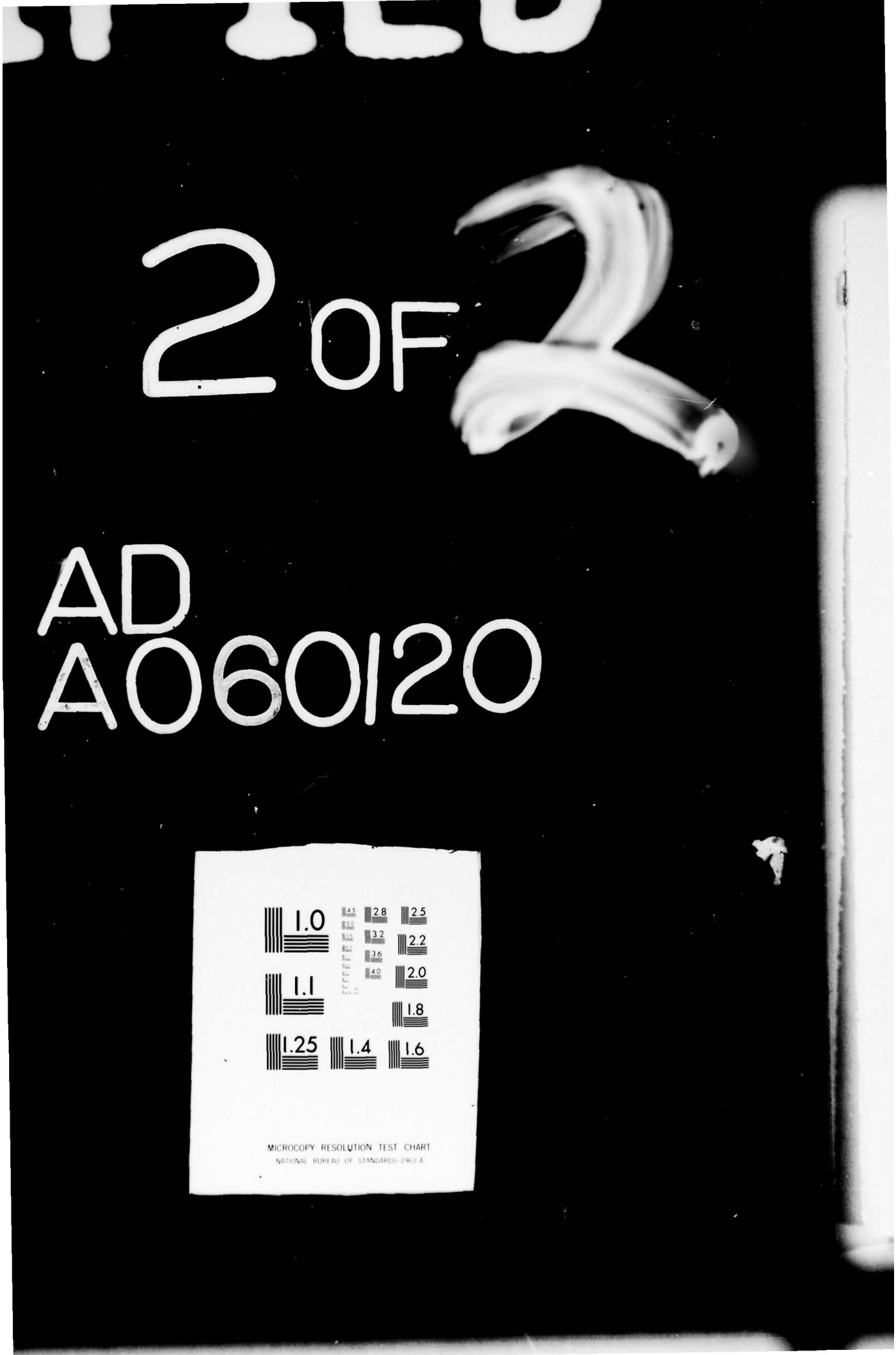
2 OF 2
AD
A060120
1.0
1.1
1.25
1.4
1.6
2.8
2.5
3.2
2.2
3.6
2.0
4.0
1.8
MICROCOPY RESOLUTION TEST CHART
NATIONAL BUREAU OF STANDARDS 1963-A

APPENDIX II

SUBSURFACE DEFORMATION BY CYCLIC LOADING

In sliding the plastic strain is accumulated in several cycles, each cycle corresponding to the passage of one asperity. The deformation energy of the material element in the plastically deformed layer during the ith cycle is

$$dE_i = \left[\bar{\tau}\, d(\bar{\gamma}_i)\right] dy \tag{II-1}$$

where $\bar{\tau}$ is the equivalent stress and $\bar{\gamma}_i$ is the equivalent strain the material undergoes. If the specimen slides a distance S and undergoes N_f loading cycles, then the total equivalent plastic strain $\bar{\gamma}$ is

$$\bar{\gamma} = \sum_{i=1}^{N_f} \Delta\, \bar{\gamma}_i \tag{II-2}$$

where $\Delta\, \bar{\gamma}_i$ is the net plastic strain generated during the ith cycle. Therefore, the total plastic work done W_s is

$$W_s = \frac{\pi}{4} D^2 \sum_{i=1}^{N_f} \int_o^{\infty} \int_o^{\bar{\gamma}_i} \bar{\tau}\, d(\bar{\gamma}_i)\, dy \tag{II-3}$$

where D is the specimen diameter.

As a first approximation to the problem one may assume that (II-1)

$$\bar{\tau} = k \tag{II-4}$$

where k is the shear yield stress. Substituting this into Equation (II-3), the latter may be written as

$$W_s = \frac{\pi}{4} D^2 \sum_{i=1}^{N_f} \int_o^\infty \int_o^{\bar{\gamma}_i} k \, d(\bar{\gamma}_i) \, dy$$

$$= \frac{\pi}{4} D^2 \sum_{i=1}^{N_f} \int_o^\infty k \, \bar{\gamma}_i \, dy \qquad \text{(II-5)}$$

Let the ratio m_i of the total equivalent strain $\bar{\gamma}_i$ to the net plastic strain per cycle $\Delta \bar{\gamma}_i$ be defined as

$$m_i = \frac{\bar{\gamma}_i}{\Delta \bar{\gamma}_i} \qquad \text{(II-6)}$$

and as a first approximation let $m_i = m$, where m is a constant independent of y and also independent of i. Substituting Equation (II-6) into Equation (II-5), we obtain

$$W_s = \frac{\pi}{4} D^2 \, m N_f \int_o^\infty k \, \Delta \bar{\gamma} \, dy$$

$$= \frac{\pi}{4} D^2 \, a \, m N_f \int_o^\infty k \, \Delta \bar{\gamma} \, d\left(\frac{y}{a}\right) \qquad \text{(II-7)}$$

where a is the half width of contact.

From Figure II-1, it can be seen that $\int_o^\infty \Delta \bar{\gamma} \, d\left(\frac{y}{a}\right)$ is determined for a given μ. If it is denoted by I_o, then Equation (II-7) becomes

$$W_s = \frac{\pi}{4} D^2 a m N_f k I_o \qquad \text{(II-8)}$$

From the relationship between the real contact area A_c and the number of contacting particles N_c, the number of cycles N_f is

$$N_f \simeq \frac{S}{D} (N_c)^{\frac{1}{2}}$$

$$= \frac{S}{aD} \left(\frac{A_c}{4k_p} \right)^{\frac{1}{2}} \qquad \text{(II-9)}$$

where k_p is a constant depending on the shape of contacting area. Substituting Equation (II-9) into Equation (II-8) gives

$$\frac{W_s}{S} = \frac{\pi}{8} Dkm I_o \left(\frac{A_c}{k_p} \right)^{\frac{1}{2}} \qquad \text{(II-10)}$$

which means that the work done per unit sliding distance by cyclic plastic deformation is independent of the grit size.

A numerical example may be given using the abrasion data in the text, the relationship $p_o = 4H/\pi$ and Figure II-1. For OFHC copper under the applied normal load of 39.2N, the friction coefficient is approximately 0.5. Using $G = 4.5 \times 10^{10}$ N/m^2 and assuming $m = 70$, the subsurface deformation energy W_s is about 40J, while the total external work done W_e is 80J. Therefore, about 50% of external work done is expended in the subsurface deformation in this calculation. This is rather qualitative since it is for

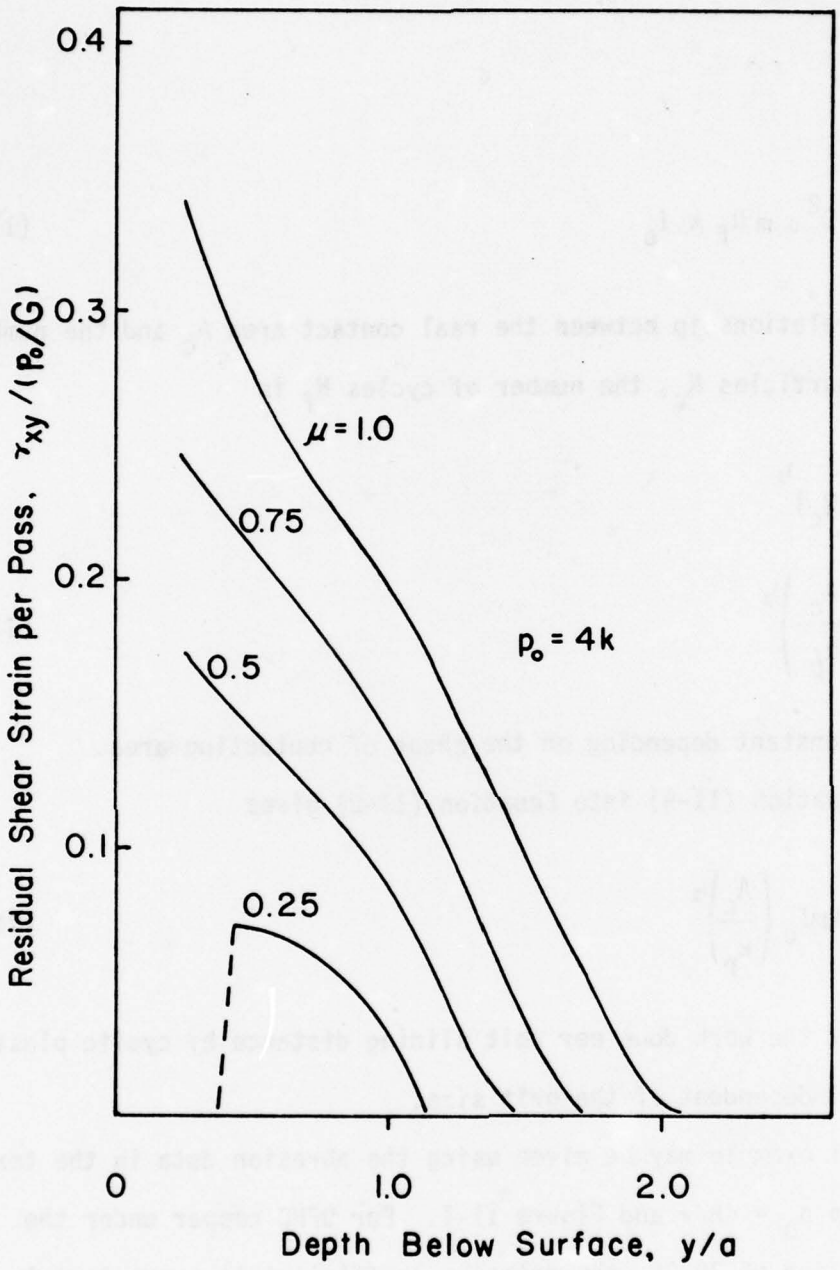

Figure II-1 The steady state residual shear strain per pass, for different friction coefficients, normalized with respect to the maximum applied normal stress $p_o = 4k$, divided by the shear modulus G (Reference II-2).

the idealized sliding case and the assumed m value. But the fraction of the subsurface deformation energy is comparable with that of Moore and Douthwaite (II-3).

APPENDIX II - REFERENCES

II-1. N.P. Suh and P. Sridharan, "Relationship Between the Coefficient of Friction and the Wear Rate of Metals," Wear, 34(1975), 291-299.

II-2. S. Jahanmir and N.P. Suh, "Mechanics of Subsurface Void Nucleation in Delamination Wear," Wear, 44(1977), 17-38.

II-3. M.A. Moore and R.M. Douthwaite, "Plastic Deformation Below Worn Surfaces," Met. Trans., 7A(1976), 1833-1839.

APPENDIX III

CALCULATION OF WEAR COEFFICIENT BY CRACK PROPAGATION ANALYSIS FOR THE CASE OF EXTREMELY SMALL GRIT SIZE

The crack extension, dC, per contacting particle passage can be expressed as a power function of the change in stress intensity factor, Δk, and two material constants β and m as in fatigue crack growth (III-1)

$$\frac{dC}{dN} = \beta (\Delta k)^m \tag{III-1}$$

When the tip of the crack in the tensile region, k is a function of the average normal contact stress σ_n, the coefficient of friction μ, the length of crack in the tensile region, and the depth of the crack below the surface.

As shown by Fleming and Suh (III-2), the maximum k occurs when the crack lies at some constant critical depth d, and when some constant critical effective crack length C_e is in the tensile region. Thus, Δk associated with the maximum k is

$$\Delta k = k(\sigma_n, \mu, d, C_e) \tag{III-2}$$

Substituting Equation (III-2) into Equation (III-1) and integrating the result gives

$$C = \beta [k(\sigma_n, \mu, d, C_e)]^m \; N + C_e \tag{III-3}$$

If η is defined as the number of contacts per unit length and S is the sliding distance, then $N = \eta S$ or

$$C = \beta[k(\sigma_n, \mu, d, C_e)]^m \eta S + C_e \qquad \text{(III-4)}$$

The real contact area is approximately proportional to the applied load (Figure 21), and the increase of real area of contact is due to an increase in the number of contacts (Figures 17, 19). Therefore, the number of contacts is essentially proportional to the normal load L.

$$\eta = \alpha L \qquad \text{(III-5)}$$

Thus, Equation (III-4) becomes

$$C = \alpha\beta[k(\sigma_n, \mu, d, C_e)]^m LS + C_e \qquad \text{(III-6)}$$

The worn volume V_1 below one wear track produced by a row of particles is $C \cdot d$ times some crack breadth which is assumed to be of the order of C_e(III-2), and multiplied by ϕ which is a function of the spacing between crack nucleation sites and the probability of their joining. But it is reasonable to assume that crack breadth b is of the order of the average spacing λ of contacting abrasive particles. If we let $b = \zeta\lambda$ as a first approximation, the total wear volume V is given by $V = C \cdot d \cdot \lambda N_w$, where N_w is the number of wear tracks. Since λN_w is the dimension of the specimen, D, the wear volume V can, therefore, be expressed as $V = \phi \cdot C \cdot d \cdot D$, or

$$V = \phi \{\alpha\beta [k(\sigma_n, \mu, d, C_e)]^m LS + C_e\} d D \qquad \text{(III-7)}$$

In the case of abrasion, individual contacting particle acts like an indenter, and experimental results (Figures 21, 22) show that the hardness-real contact area relationship is well obeyed. Therefore, it is quite reasonable to assume that σ_n is equal to the hardness. Equation (III-7) may be re-written as

$$V = \phi\{\alpha\beta [k (H, \mu, d, C_e)]^m LS + C_e \} d D \qquad \text{(III-8)}$$

Normalizing k by σ_n and the square root of the half contact length a to get a dimensionless $\bar{k}$, Fleming and Suh (III-2) evaluated the constants d and C_e, and k as a function of friction coefficient μ. The results are shown in Figures III-1, III-2 and III-3. From the results it can be seen that for a given μ, the normalized stress intensity factor, $k\pi/P_o\sqrt{a}$, the normalized critical depth, d/a, and the normalized critical length, C_e/a, have constant values with upper and lower bounds. Therefore, d, C_e and k can be determined, if μ is known.

From the hardness and applied load relationship, the real contact area A_c is approximately

$$A_c = \frac{L}{H} = N_c k_p w^2 \qquad \text{(III-9)}$$

where N_c is the number of contacting particles, w is the contact length which is equal to 2a, and k_p is a constant depending on the shape of the

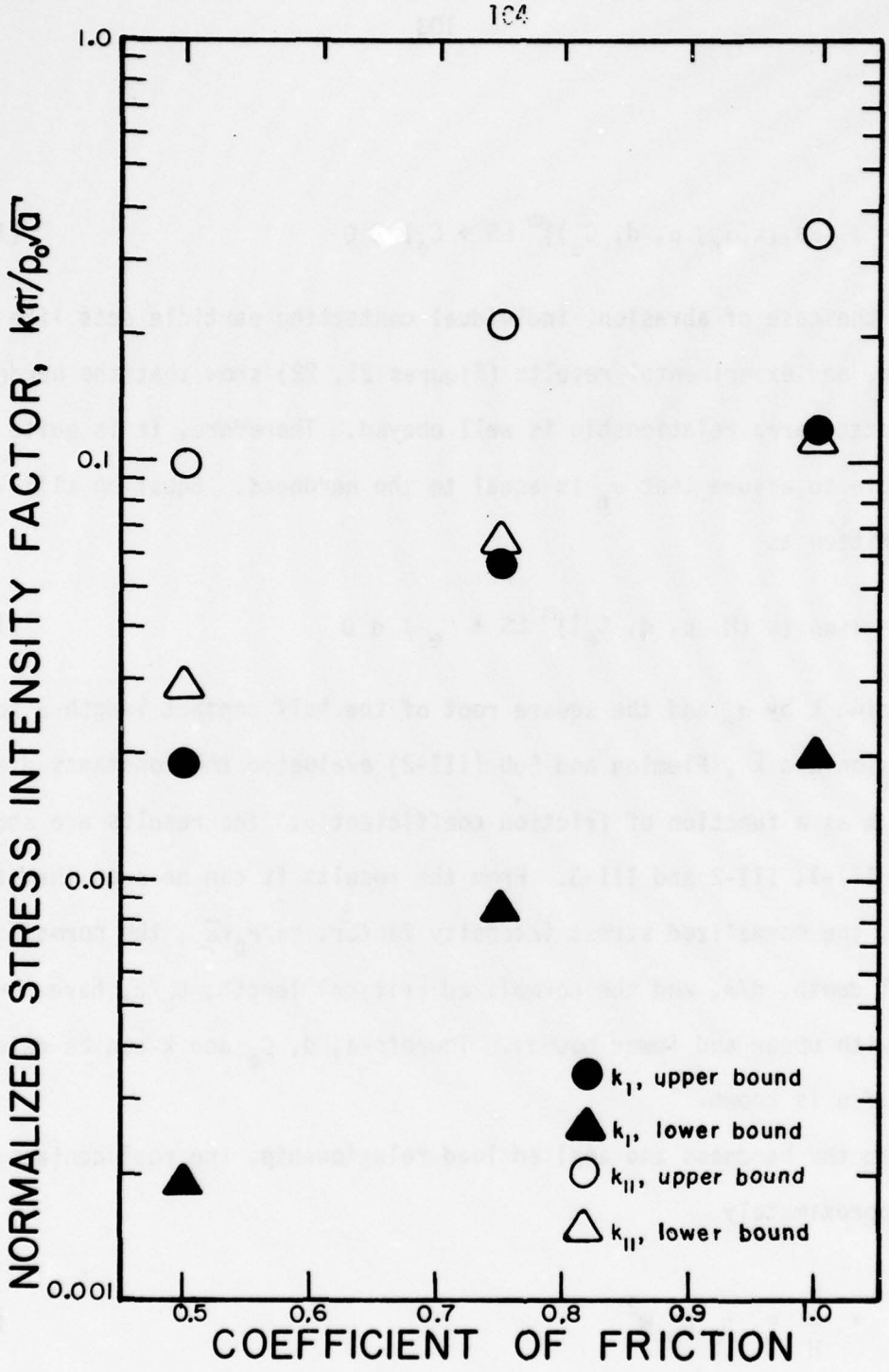

Figure III-1 Normalized stress intensity factor as functions of coefficient of friction (Reference III-2).

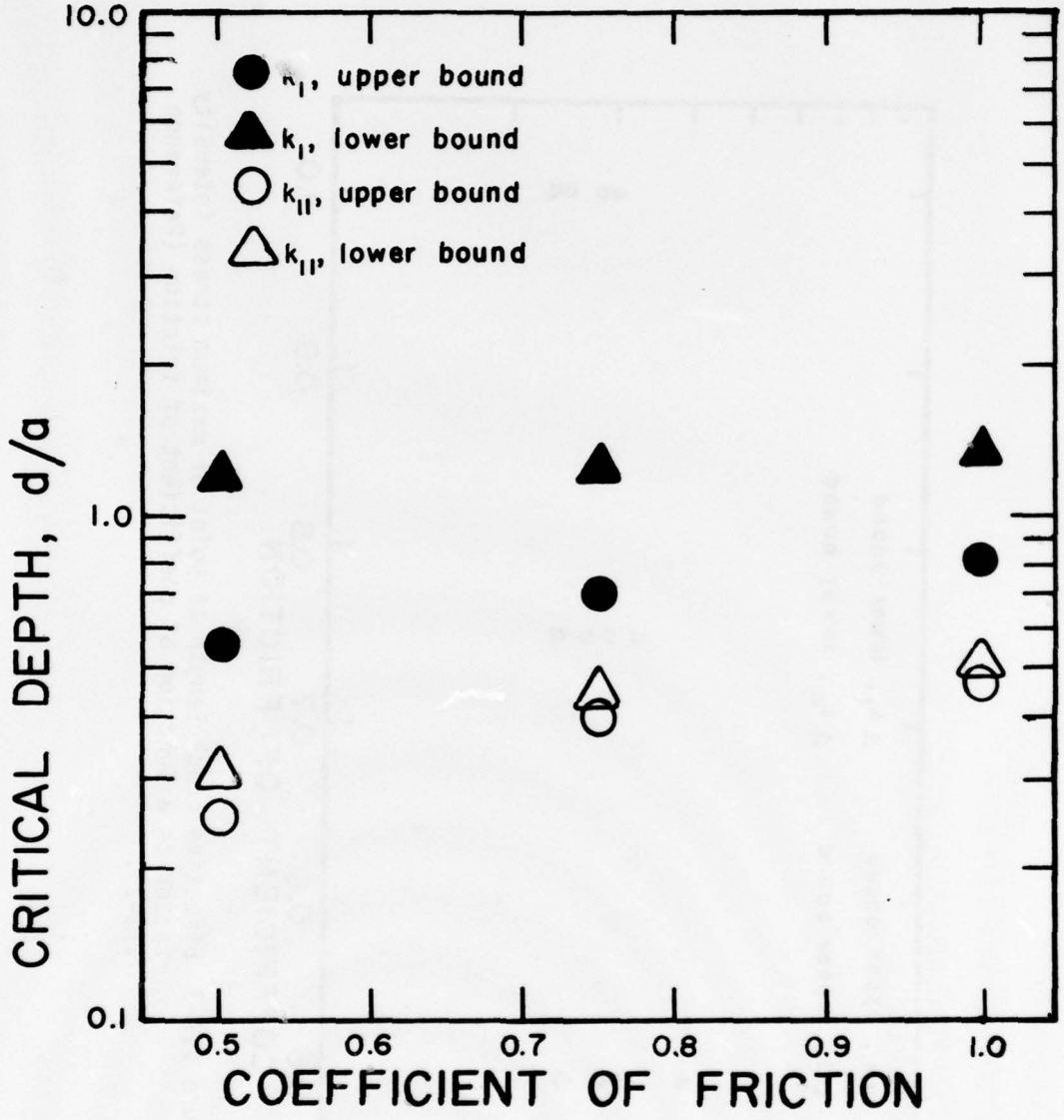

Figure III-2 Critical depth (depth of propagation of the most favored crack) as a function of coefficient of friction (Reference III-2).

Figure III-3 Effective crack length at point of maximum stress intensity factor as a function of coefficient of friction (Reference III-2).

contact area. As shown in Figure 21, the contact length is directly proportional to the abrasive grit diameter.

$$a = \delta D_g \tag{III-10}$$

And the number of cycles N is dependent on the distribution of contacts. For randomly distributed case it is approximately given as

$$N = \frac{S}{D} (N_c)^{\frac{1}{2}} \tag{III-11}$$

and from Figure III-3, it can be assumed $d = \nu D_g$ for a given μ.

By equating Equations (III-5) and (III-11), the expression for α is obtained as

$$\alpha = \frac{1}{L D D_g} \left(\frac{L}{4\delta^2 k_p H} \right)^{\frac{1}{2}} \tag{III-12}$$

Substituting expressions for α, a, d and k into Equation (III-8) gives the expression for the wear volume V

$$V = \phi \left\{ \frac{\beta S}{2D} \left(\frac{L}{k_p H} \right)^{\frac{1}{2}} \left(\frac{\bar{k} P_o}{\pi} \right)^m (\delta D_g)^{\frac{m}{2}} - 1 + C_e \right\} \nu D_g D \tag{III-13}$$

The wear rate is expressed as

$$\frac{V}{S} = \frac{\phi \left\{ \frac{\beta S}{2D} \left(\frac{L}{k_p H} \right)^{\frac{1}{2}} \left(\frac{k P_o}{\pi} \right)^m (\delta D_g)^{\frac{m}{2}} - 1 + C_e \right\} \nu D_g D}{S} \tag{III-14}$$

and the wear coefficient K is

$$K = \frac{3\phi H\left\{\frac{\beta S}{2D}\left(\frac{L}{k_p H}\right)^{\frac{1}{2}}\left(\frac{\bar{k}\,P_o}{\pi}\right)^m \left(\delta D_g\right)^{\frac{m}{2}-1} + C_e\right\} \nu\, D_g\, D}{LS} \qquad \text{(III-15)}$$

This equation shows that K varies as $D_g^{m/2}$.

A numerical example may be given using experimental results and fatigue crack growth data. For D_g = 5 μm, the friction coefficient μ is about 0.5 (Figure 4) and $\delta \simeq 0.1$ (Figure 20). For μ = 0.5, following values are obtained.

$0.001 < \bar{k} < 0.1$ (Figure III-1)

$0.025 < \nu < 0.1$ (Figure III-2)

$2.5 < C_e/a < 4.0$ (Figure III-3).

Fatigue crack growth data for materials is limited and only for mode I is available. For alloy steel, m = 3 and $\Delta k \simeq 5$ MN/m$^{3/2}$ for dC/dN = 10^{-6} mm/pass (III-3). Using experimental conditions in abrasion for AISI 1095 steel and assuming $\phi = 10^3$, the wear coefficient K is 10^{-4} - 10^{-6}, which is lower than the wear coefficient of 10^{-2} in abrasion. This is probably due to the fact that the crack propagation mechanism is more complicated than the mode I mechanism. At present no other data is available than mode I. Another reason to this is that the analysis itself provides the order of magnitude solution. It needs modification by combining the function ϕ, but no rigorous solution of ϕ is available presently. Although the analysis cannot provide the exact solution, it still shows the wear coefficient K varies as $D_g^{m/2}$.

APPENDIX III - REFERENCES

III-1. P.C. Paris and F. Erdogan, "A Critical Analysis of Crack Propagation Laws," J. Bas. Engng., Trans. ASME, 85(1963), 528-534.

III-2. J.R. Fleming and N.P. Suh, "Mechanics of Crack Propagation in Delamination Wear," Wear, 44(1977), 39-56.

III-3. L.P. Pook, "Fatigue Crack Growth Data for Various Materials Deduced from the Fatigue Lives of Precracked Plates," Stress Analysis and Growth of Cracks, Proc. of the 1971 National Symposium on Fracture Mechanics, Part 1, STP 513, ASTM.

Distribution List

	Number of Copies
Aero Material Department Naval Air Development Center Jahnsville, Warminster, Pennsylvania 18974 Attn: Code 30-7, M. J. Devine	1
Air Force Aero Propulsion Laboratory AFAPL/SFL Wright Patterson Air Force Base, Ohio 45433 Attn: Mr. C. Hudson	1
Air Force Materials Laboratory Wright-Patterson Air Force Base Dayton, Ohio 45433 Attn: Mr. F. Brooks	1
Defense Documentation Center Building 5 Cameron Station Alexandria, Virginia 22314	12
National Bureau of Standards Department of Commerce Washington, D.C. 20234 Attn: Dr. E. Passaglia Attn: Dr. W. Ruff	1 1
National Science Foundation Engineering Mechanics Division 1800 G Street Washington, D.C. Attn: M. S. Ojalvo	1
Naval Air Engineering Center Group Support, Equipment Division Lakehurst, New Jersey 08733 Attn: Code 92724, P. Senholzi	1
Naval Air Systems Command Washington, D.C. 20361 Attn: B. Poppert, Code 340E	1
Director, Naval Research Laboratory Washington, D.C. 20375 Attn: Technical Information Division Code 6170, Dr. L. Jarvis	6

	Number of Copies
Naval Research Laboratory Washington, D.C. 20375 Attn: R.C. Bowers, Code 6170	1
Naval Sea Systems Commands Code SEA 04321H Washington, D.C. 20362 Attn: Mr. M. Hoobchack	1
Naval Ship Research and Development Laboratory Annapolis, Maryland 21402 Attn: Mr. N. Glassman Attn: Mr. W. Smith	1 1
Assistant Chief for Technology Office of Naval Research, Code 200 800 N. Quincy Street Arlington, Virginia 22217	1
Office of Naval Research 800 N. Quincy Street Arlington, VA 22217 Attn: S. Dordoff, Code 438	1
Office of Naval Research 800 N. Quincy Street Arlington, VA 22217 Attn: Code 411-6, R. Miller	6
Office of Naval Research 800 N. Quincy Street Arlington, VA 22217 Attn: Code 411, D. Lauver	1
Professor T. H. Alden Department of Metallurgy University of British Columbia Vancouver, B. C. Canada	1
W. J. Anderson NASA-Lewis Research Center 21000 Brookpark Road Cleveland, Ohio 44135	1

	Number of Copies
Dr. George S. Ansell Department of Materials Science Rensselaer Polytechnic Institute Troy, New York 12181	1
Professor A. S. Argon Department of Mechanical Engineering Massachusetts Institute of Technology Cambridge, Massachusetts 02139	1
Professor M. F. Ashby University Engineering Department Cambridge University Trumpington Street Cambridge CB2 1PZ England	1
Professor John A. Bailey North Carolina State Univerity Hillsborough Street Raleigh, North Carolina 27607	1
Professor F. T. Barwell University College of Swansea Singleton Park Swansea, Wales SA2 8PP	1
Dr. John M. Batch Director Battelle Columbus Laboratories 505 King Avenue Columbus, Ohio 43201	1
A. Beerbower Esso Research and Engineering Company P.O. Box 51 Linden, New Jersey 07036	1
Dr. R. T. Begley, Manager Metallurgy and Metals Processing Westinghouse Electric Corporation Research and Development Center Beulah Road Pittsburgh, Pennsylvania 15235	1

	Number of Copies
Professor Arden L. Bement Department of Materials Science and Engineering Massachusetts Instute of Technology Cambridge, Massachusetts 02139	1
Dr. B. Bethune University of Manchester Institute of Science and Technology P.O. Box 88 Manchester M60 1QD England	1
E.E. Bisson 20786 Eastwood Avenue Fairview Park, Ohio 44126	1
J.E. Booker Sibley School of Mechanical Engineering Cornell University Ithaca, New York 14850	1
Mr. R.W. Bramham Procurement Executive, Ministry of Defense Royal Aircraft Establishment Materials Department Farnborough Hants GU14 5TD England	1
Dr. B.J. Briscoe Department of Chemical Engineering Imperial College Prince Consort Road, London SW7 2BY England	1
D.A. Buckley NASA-Lewis Research Center 21000 Brookpark Road Cleveland, Ohio 44135	1
Professor Bernard Budiansky Divison of Engineering and Applied Physics Harvard University 313 Pierce Hall Cambridge, Massachusetts 02138	1

Number of Copies

Dr. R. F. Bunshah
UCLA - Materials Department
6532 Boelter Hall, UCLA
Los Angeles, California 90024 — 1

Professor R.A. Burton
Department of Mechanical Engineering
and Astronautical Sciences
Northwestern University
Evanston, Illinois 60201 — 1

Dr. Spencer H. Bush
Battelle
Pacific Northwest Laboratories
Battelle Boulevard
Richland, Washington 99352 — 1

Professor Alistair Cameron
Imperial College of Science and Technology
Department of Mechanical Engineering
Exhibition Road
London SW7 2BX
England — 1

Dr. J.D. Campbell
Department of Engineering Science
University of Oxford
Parks Road
Oxford OX1 3PJ
England — 1

W. Campbell
Wear Sciences Inc.
32 Sutherland Drive
Scotia, New York 12302 — 1

Professor H.S. Cheng
Department of Mechanical Engineering
and Astronautical Sciences
Northwestern University
Evanston, Illinois 60201 — 1

Mr. Paul Chuttlebottom
University of Lancaster
Department of Physics
Bailrigg, Lancaster
England — 1

Number of Copies

Dr. A.H. Clauer
Metal Science Section
Battelle
Columbus Laboratories
505 King Avenue
Columbus, Ohio 43201 1

Professor Morris Cohen
Department of Materials Science and Engineering
Room 13-5046
Massachusetts Institute of Technology
Cambridge, Massachusetts 02139 1

V.N. Constantinescu
Institute of Fluid Mechanics
Academy of the Socialist Republic Rumania
Bucharest, Rumania 1

Professor N.H. Cook
Department of Mechanical Engineering
Massachusetts Insitute of Technology
Cambridge, Massachusetts 02139 1

P.K. Das
John Deere Waterloo Tractor Works
Waterloo, Iowa 50704 1

Dr. J.H. Dautzenberg
Mechanical Engineering Materials Laboratory
University of Technology
Eindhoven, Netherlands 1

Dr. L.A. Davis
Materials Research Center
Allied Chemical Corporation
Morristown, New Jersey 07960 1

Dr. Raymond F. Decker
Director of R&D
Inco Inc.
1 New York Plaza
New York, New York 10004 1

	Number of Copies
Mr. Edward Ditto Manufacturing Development General Motors Technical Center Warren, Michigan 48090	1
Dean D. Drucker College of Engineering University of Illinois Urbana, Illinois	1
Mr. John H. Dumbletar University of Cincinnati Department of Materials Science and Metallurgical Engineering 498 Rhodes Hall Cincinnati, Ohio 45221	1
N.S. Eiss, Jr. Virginia Polytechnic Institute Mechanical Engineering Blacksburg, Virginia 24060	1
Professor J.D. Embury Department of Metallurgy & Materials Science McMaster University Hamilton, Ontario Canada	1
R. Fein Fundamental Research Section Research and Technical Department Texaco Research Center Beacon, New York 12508	1
Dr. Michael Field Metcut Research Associates Inc. 3980 Rosslyn Drive Cincinnati, Ohio 45209	1
Professor I. Finnie Department of Mechanical Engineering University of California Berkeley, California 94720	1
Professor R.F. Firestone Metallurgical and Materials Engineering 848 Benedum Hall University of Pittsburgh Pittsburgh, Pennsylvania 15213	1

Number of Copies

Dr. Donald G. Flom
General Electric Research and Development Center
P.O. Box 8
Schenectady, New York 12302 — 1

Dr. Arthur E. Foche
University of Cincinnati
Cincinnati, Ohio 45221 — 1

Dr. I.E. French
Defense Standards Laboratories
P.O. Box 50
Ascot Vale, Victoria 3032
Australia — 1

Dr. Brian R.T. Frost, Director
Materials Science Division
Argonne National Laboratory
9700 South Cass Avenue
Argonne, Illinois 60439 — 1

Dr. H.J. Frost
University Engineering Department
Cambridge University
Trumpington Street
Cambridge CB2 1PZ
England — 1

M. Furey
Mechanical Engineering Department
Virginia Polytechnic and State University
Blacksburg, Virginia 24601 — 1

Dr. S. Ganesh
Project Engineer
Bendix Research Laboratories
20800 Civic Center Drive
Southfield, Michigan 48076 — 1

Professor Peter Glelisse
University of Rhode Island
Kingston, Rhode Island 02881 — 1

D. Godfrey
Chevron Research Company
P.O. Box 1627
Richmond, California 94802 — 1

	Number of Copies
Dr. Edward W. Goliber General Electric Company Carboloy Systems Department P.O. Box 237 - GPO Detroit, Michigan 48232	1
E. J. Gunter Department of Mechanical Engineering University of Virginia Charlottesville, Virginia 22091	1
Dr. H. P. Haasen Director Insitiut fur Metallphysik der Univeristat Gottingen Hospitalstrasse 12 34 Gottingen, Germany	1
Dr. George T. Hahn Metal Science Section Battelle Columbus Lab Columbus, Ohio 43210	1
Professor D. W. Haines College of Engineering University of South Carolina Columbia, South Carolina	1
Mr. N. E. W. Hartley Nuclear Physics Division Building 8 Atomic Energy Research Establishment Harwell, Berkshire, England	1
D. P. H. Hasselman Lehigh University Materials Research Center Bethlehem, Pennsylvania 18015	1
D. F. Hays Engineering Mechanics Department Research Laboratories General Motors Corporation Warren, Michigan 48090	1

	Number of Copies
Professor John P. Hirth Department of Metallurgical Engineering The Ohio State University 116 West 19th Avenue Columbus, Ohio 43210	1
Mr. Michael Hoch University of Cincinnati Department of Materials Science & Met. Engineering Cincinnati, Ohio 45221	1
Professor E. Hornbogen Ruhr-Universitat Bochum Institut fur Werkstoffe 463 Bochum-Quirenburg Postfach 2148 Bochum, Germany	1
Mr. P. L. Hurricks Rank Xerox Development Laboratory Bessemer Road Welwyn Garden City, Hertfordshire England	1
Dr. Robert I. Jaffee Technical Manager, Materials Electric Power Research Institute 3412 Hillview Avenue P.O. Box 10412 Palo Alto, California 94304	1
W. Jamaison Department of Mechanical Engineering University of Virginia Charlottesville, Virginia 22091	1
R. L. Johnson Consultant (Adjunct Prof. R. P. I.) 4503 West 224 Street Fairview Park, Ohio 44126	1
Dr. Thomas F. Jones Vice President for Research And Development Massachusetts Institute of Technology Room 3-305 Cambridge, Massachusetts 02139	1

	Number of Copies
Dr. Joseph Kalousek Associate Research Officer National Research Council Vancouver VGRIP5 British Columbia	1
Professor C. H. Kahng Michigan Technical University Mechanical Engineering - E.M. Department Houghton, Michigan 49931	1
Mr. Herbert S. Kalish Adams Carbide Corporation Market and Passaic Streets Kenilworth, New Jersey 07033	1
Professor S. Kalpakjian Department of Mechanical and Aerospace Engineering Illinois Institute of Technology Chicago, Illinois 60616	1
Mr. G. E. Kane Lehigh University Industrial Engineering Department Bethlehem, Pennsylvania 18015	1
J. J. Kauzlarich University of Virginia Thorton Hall Charlottesville, Virginia 22091	1
Dr. Bernard H. Kear Materials Engineering and Research Laboratory Pratt & Whitney Aircraft Middletown Plant Middletown, Connecticut 06457	1
Dr. Ronald Kelsey Aluminum Company of America Alcoa Research Lab Alcoa Center, Pennsylvania 15068	1
W. L. Kennicott Kennametal Inc. Latrobe, Pennsylvania 15650	1

Number of Copies

D. F. Kettlebourgh
Mechanical Engineering Department
Texas A & M University
College Station, Texas 1

Professor E. E. Klaus
Department of Chemical Engineering
Pennsylvania State University
University Park, Pennsylvania 16802 1

Dr. Ranga Komanduri
Carnegie-Mellon University
Mechanical Engineering Department
Pittsburgh, Pennsylvania 15213 1

P. M. Ku
Southwest Research Institute
P. O. Drawer 28510
San Antonio, Texas 78284 1

Mr. J. K. Lancaster
Ministry of Defense
Royal Aircraft Establishment
Materials Department
Farnborough, Hants
England 1

Professor Jorn Larsen-Basse
Department of Mechanical Engineering
University of Hawaii
2540 Dole Street
Honolulu, Hawaii 96822 1

V. H. Larson
Department of Mechanical Engineering
Cleveland State College
Cleveland, Ohio 1

Dr. Ira S. Levy
Technical Leader
Alloy Development
Battelle
Pacific Northwest Laboratories
Battelle Boulevard
Richland, Washington 99352 1

	Number of Copies
Professor F. F. Ling Department of Mechanical Engineering Rensselaer Polytechnic Institute Troy, New York 12181	1
W. E. Littmann Timken Company 1835 Dueber Avenue, S. W. Canton, Ohio 44706	1
Professor John R. Low, Jr. Department of Metallurgy and Materials Science Carnegie-Mellon University Schenley Park Pittsburgh, Pennsylvania 15213	1
Professor K. Ludema Department of Mechanical Engineering University of Michigan Ann Arbor, Michigan 48104	1
Mr. Harvey Lyons Research Associate Department of Mechanical Engineering The Ohio State University 206 West 18th Avenue Columbus, Ohio 43210	1
C. J. Maday Department of Engineering Mechanics North Carolina State Univeristy Raleigh, North Carolina 27607	1
Mr. M. Maugis Laboratorie 25H Centre National de la Recherche Scientifique Mechanique des Surface Laboratoires de Bellevue 1, Place A. Briad - 93 Bellevue France	1
Professor Frank McClintock Room 1-304C Massachusetts Institute of Technology Cambridge, Massachusetts 02139	1
Professor Charles J. McMahon, Jr. Department of Metallurgy & Materials Science University of Pennsylvania Philadelphia, Pennsylvania 19174	1

	Number of Copies
Mr. Edward McTamany Frankford Arsenal Bridge & Tacony Streets Philadelphia, Pennsylvania 19137	1
Dr. H. D. Megelberg i Hs. Siemens ZFA-WQA-WT 1 8 Munchen 70 Schertlinstr 8, Germany	1
Dr. John E. Meyer Ford Motor Company Research Laboratory Dearborn, Michigan 48120	1
Mr. D. V. Minuti Materials Engineer, Code 30-73 ARP/SLP Project Office Air Vehicle Technology Department Naval Air Development Center Warminister, Pennsylvania 18974	1
Mr. T. O. Morris Union Carbide Corporation, Nuclear Division P. O. Box Y, Building 9998, Stop 2 Oak Ridge, Tennessee 37830	1
W. R. Murphy Mobil Research and Development Corporation Central Research Division P.O. Box 1025 Princeton, New Jersey 08540	1
Mr. K. T. O'Brien Mechanical Engineering Department The University of Leeds Leeds LS2 9JT, England	1
Professor Walter S. Owen Department of Materials Science and Engineering Massachusetts Institute of Technology Cambridge, Massachusetts 02139	1
Dr. A. Palmgren AB-Svenska Kullagerfabriken Group Headquarters S41550 Gothenberg, Sweden	1

	Number of Copies
C. T. Pan Shaker Research, Inc. Latham, New York 12110	1
Professor Earl. R. Parker Department of Materials Science & Engineering University of California Hearst Mining Building Berkeley, California 94720	1
R. Parker NASA-Lewis Research Center 2100 Brookpark Road Cleveland, Ohio 44135	1
Dr. H. W. Paxton Vice President - Research U. S. Steel Corporation 600 Grant Street, Room 56-06 Pittsburgh, Pennsylvania 15230	1
Dr. F. S. Pettit Materials Engineering & Research Laboratory Pratt & Whitney Aircraft Middletown Plant Middletown, Connecticut 06457	1
R. M. Phelan Mechanical Engineering Department Cornell University Ithaca, New York 15850	1
Mr. P. St. Pierre General Electric P.O. Box 568 Worthington, Ohio 43085	1
Professor Gordon W. Powell Department of Metallurgical Engineering Ohio State University Columbus, Ohio 43210	1
Dr. C. Pritchard British Railways Research and Development Division B. R. Technical Centre London Road Derby, DE2 8UP, England	1

	Number of Copies
Professor E. Rabinowicz Department of Mechanical Engineering Massachusetts Institute of Technology Cambridge, Massachusetts 02139	1
Dr. Robert J. Reynick National Science Foundation Washington, D.C. 20550	1
Professor J. Rice Division of Engineering Brown University Providence, Rhode Island	1
Professor David A. Rigney Department of Metallurgical Engineering The Ohio State University 116 West 19th Avenue Columbus, Ohio 43210	1
Mr. Bill Roper Lehigh University Industrial Engineering Department Bethlehem, Pennsylvania 18015	1
C. N. Rowe Mobil Research & Development Corporation Box 1025 Princeton, New Jersey 08540	1
Professor R. Roy Penn State University Department of Materials Science University Park, Pennsylvania 16802	1
Dr. E. Rudy Oregon Graduate Center 19600 N. W. Walker Road Beaverton, Oregon 97005	1
Dr. E. Saibel Army Research Office P.O. Box 1221 RTP, North Carolina 27709	1
Dr. L. E. Samuels Department of Defense Materials Research Laboratories P.O. Box 50 Ascot Vale, Victoria 3032 Australia	1

	Number of Copies
J. A. Shey Department of Materials Engineering University of Illinois at Chicago Circle Box 4348 Chicago, Illinois 60680	1
D. Scott Department of Mechanical and Production Engineering Paisley College of Technology High Street, Paisley PA1 2BE England	1
A. Seireg University of Wisconsin 1513 University Avenue Madison, Wisconsin 53706	1
Professor M. C. Shaw Engineering Science Department Arizona State University Tempe, Arizona 85281	1
Professor Oleg D. Sherby Department of Materials Science & Engineering Stanford University Stanford, California 94305	1
J. J. Sherlock Maic Division Pure Carvon Company, Inc. St. Marys, Pennsylvania 15357	1
Dr. Paul G. Shewmon Division Director Materials Research National Science Foundation Washington, D.C. 20550	1
Dr. Markus O. Speidel Brown, Boveri & Company, Inc. Research Centre 5401/Baden Switzerland	1
Mr. Vonid K. Srivastava Memorial University of Newfoundland St. John's Newfoundland Canada AIC 5S7	1

	Number of Copies
Dr. Morris Steinberg Director of Technology Lockheed Aircraft Corportation Burbank, California 91503	1
Dr. F. H. Stott University of Manchester Institute of Science and Technology P.O. Box 88 Manchester M60 1QD England	1
Professor John Stringer Electric Power Research Institute 3412 Hillview Avenue P.O. Box 10412 Palo Alto, California 94304	1
M. V. Swain Martin Marietta Laboratories 1450 South Rolling Road Baltimore, Maryland 21227	1
Professor D. Tabor University of Cambridge Cavendish Laboratory Madingley Road Cambridge, CB3 0HE England	1
A. Thiruvengadam Daedalean Associates, Inc. 15110 Frederick Road Woodbine, Maryland 21797	1
Dr. G. Thomas Department of Materials Science and Engineering University of California Hearst Mining Building Berkeley, California 94720	1
Mr. Herbert F. G. Ueltz General Abrasives Company 200 College Avenue Niagra Falls, New York 14305	1
Dr. Edward van Reuth ARPA 1400 Wilson Boulevard Arlington, Virginia 22209	1

Number of Copies

Dr. Frank L. VerSnyder
Advanced Materials Research and Development Laboratory
Pratt & Whitney Aircraft
Division of United Aircraft Corporation
North Haven, Connecticut 06473 — 1

Professor K. K. Wang
Cornell University
256 Upson Hall
Ithaca, New York 14850 — 1

Professor R. B. Waterhouse
University of Nottingham
Department of Metallurgy and Materials Science
University Park, Nottingham NG7 2RD
England — 1

Mr. V. C. Westcott
Foxboro/Trans-Sonics, Inc.
P.O. Box 435
Burlington, MA 01803 — 1

Dr. B. A. Wilcox
Division of Materials Research
National Science Foundation
1800 G Street
Washington, D.C. 20550 — 1

Professor J. Wolak
Department of Mechanical Engineering
University of Washington
Seattle, Washington 98195 — 1

Dr. I. G. Wright
Metal Science Section
Battelle
Columbus Laboratories
505 King Avenue
Columbus, Ohio 43210 — 1

Mr. Russel Young
National Bureau of Standards
Mechanics Division
Institute of Basic Standards
Washington, D.C. — 1

Professor Victor F. Zackay
Department of Materials Science & Engineering
University of California
Hearst Mining Building
Berkeley, California 94720 — 1